ASSESSMENT OF SPOT 5 AND ERS-2 OBIA FOR MAPPING WETLANDS

THEO PAUW

Thesis presented in partial fulfilment of the requirements for the degree of Master of Science in the Faculty of Science at Stellenbosch University.

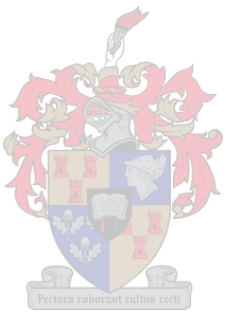

Supervisor: Dr A van Niekerk

December 2012

DECLARATION

By submitting this research report/literature review electronically, I declare that the entirety of the work contained therein is my own, original work, that I am the owner of the copyright thereof (unless to the extent explicitly otherwise stated) and that I have not previously in its entirety or in part submitted it for obtaining any qualification.

Signature:

Date:

SUMMARY

This research considered the automated remote sensing-based classification of wetland extent within the Nuwejaars and Heuningnes River systems on the Agulhas Plain. The classification process was based on meaningful image objects created through image segmentation rather than on single pixels. An expert system classifier was compared to a nearest-neighbour supervised classifier, and one multispectral (SPOT 5) image (dry season) and two C-band, VV-polarisation synthetic aperture radar (SAR: ERS-2) images (dry and wet season) were used separately and in combination.

Classifications were performed within two subset areas. Final classes identified were *Permanent waterbody*, *Other wetland* and *Non-wetland*. Statistical accuracy assessment was performed. Validation data was derived from a combination of high-resolution aerial photographs, the SPOT 5 image, high-resolution imagery on Google Earth and observations during a field visit. Wetland extent was defined as the total extent of wetland-specific vegetation, unvegetated seasonal pans and waterbodies. More detailed classes were originally envisaged, but available validation data was not considered adequate for assessing their accuracy with any confidence.

The supervised classifier was found to be more accurate overall than the developed expert system. The difference between the two was however not always significant. The two SAR images alone did not contain sufficient information for the accurate classification of Agulhas wetlands' extent, with recorded overall accuracies not exceeding 65% regardless of the classifier used. The SPOT image alone achieved accuracies higher than 80%; this was considered a good result. In comparison, combining the SAR and SPOT data did not improve the classification accuracy.

The potential of the expert system to be applied with little modification to images acquired over other areas or over the same area in other years should be further investigated. However, several reservations are noted in this regard. Future research could potentially improve the results obtained from supervised classification by augmenting it with expert system rules to identify more complicated classes.

KEYWORDS

ERS-2, SPOT 5, SAR, wetlands, expert system classifier, nearest-neighbour supervised classifier

OPSOMMING

Hierdie navorsing het die geoutomatiseerde afstandswaarneminggebaseerde klassifikasie van vleilandomvang binne die Nuwejaars- en Heuningnesrivier stelsels op die Agulhasvlakte ondersoek. Die klassifikasieproses was gebaseer op betekenisvolle beeldobjekte geskep deur middel van beeldsegmentasie eerder as op enkele beeldelemente. ‘n Deskundige stelsel klassifiseerder is vergelyk met ‘n naaste-naburige gerigte klassifiseerder. Een multispektrale (SPOT 5) beeld vir die droë seisoen, sowel as twee C-band, VV-polarisasie sintetiese diafragma radar (SAR, ERS2) beelde (vir die droë en nat seisoene) is afsonderlik en in kombinasie gebruik.

Klassifikasies is uitgevoer binne twee sub-areas in die beelde. Finale klasse wat geïdentifiseer is was *Permanente waterliggaam, Ander vleiland* en *Nie-vleiland.* Statistiese akkuraatheidsassessering is uitgevoer. Verwysingsdata is geskep vanuit ‘n kombinasie van hoë-resolusie lugfoto’s, die SPOT 5 beeld, hoë-resolusie beelde op Google Earth en waarnemings tydens ‘n besoek aan die studiegebied. Vleiland omvang is gedefinieer as die totale omvang van vleiland-spesifieke plantegroei, onbegroeide seisoenale panne en waterliggame.

Die gerigte klassifiseerder blyk om oor die algemeen meer akkuraat as die ontwikkelde deskundige stelsel te wees. Die verskil was egter nie altyd beduidend nie. Die twee SAR beelde alleen het nie genoegsame inligting bevat vir die akkurate klassifikasie van Agulhas-vleilande se omvang nie, met behaalde algehele akkuraatheidsvlakke wat nie 65% oorskry het nie, ongeag van die klassifiseerder. Die SPOT-beeld alleenlik het algehele akkuraathede van meer as 80% behaal; wat as ‘n goeie resultaat beskou kan word. In vergelyking hiermee kon die kombinering van SAR- en SPOT-data nie ‘n verbetering teweeg bring nie.

Die potensiaal van die deskundige stelsel om met min aanpassing op beelde van ander gebiede of van dieselfde gebied in ander jare toegepas te word, verg verdere ondersoek. Verskeie voorbehoude word egter in hierdie verband gemeld. Toekomstige navorsing kan potensieel die resultate van gerigte klassifikasie verbeter deur dit aan te vul met deskundige stelsel reëls vir die klassifikasie van meer komplekse klasse.

TREFWOORDE

ERS-2, SPOT 5, SAR, vleilande, deskundige stelsel klassifiseerder, naaste-naburige gerigte klassifiseerder.

ACKNOWLEDGEMENTS

I sincerely thank:

- My supervisor, Dr Adriaan van Niekerk, for his guidance and support;
- My parents, for their love and emotional support, and for giving me the opportunity to study;
- The South African National Research Foundation, for providing funding for this research;
- The European Space Agency, for providing SAR data;
- South African National Parks, for allowing access to Agulhas National Park, and particularly Samantha Schröder of Sanparks and Arnold Viegeland of Working for Water for their assistance;
- The Nuwejaars Wetland Special Management Area, for allowing access to wetland sites, and particularly Tom Ambrose and Rory Allardice for their assistance;
- Jeanine Engelbrecht and Jaco Kemp, for assistance with processing of SAR data; and
- My fellow students, particularly Byron Diergaardt and Schalk van Heerden, for all the hours spent in the lab and more cups of coffee than I can remember.

CONTENTS

TABLES

FIGURES

ACRONYMS AND ABBREVIATIONS

ADC	analogue to digital converter
ALOS-PALSAR	advanced land observation satellite – phased array type L-band synthetic aperture radar
ASAR	advanced synthetic aperture radar
ANN	artificial neural network
CFR	Cape Floristic Region
DEM	digital elevation model
DBF	dBase file
DN	digital number
DVW	difference between vegetation and water
ERS	European remote sensing
ES	expert system
ESA	European space agency
ETM+	enhanced thematic mapper plus
EVI	enhanced vegetation index
EVI_2	enhanced vegetation index 2
GCP	ground control point
GIS	geographic information systems
GLCM	grey level co-occurrence matrix
GLDV	grey level distance vector
GME	geospatial modelling environment
GPS	global positioning systems
HH	horizontal-horizontal
HV	horizontal-vertical
IHS	intensity-hue-saturation

IOF	image object fusion
IRS	Indian remote sensing
LIDAR	light detection and ranging
MED	mean Euclidean distance
SWIR	mid-infrared
ML	maximum likelihood
MNDWI	modified normalised difference water index
MODIS	moderate-resolution imaging spectroradiometer
MPED	mean pairwise Euclidean distance
MS	multispectral
$MSAVI_2$	modified soil-adjusted vegetation index
NDPI	normalised difference pond index
NDTI	normalised difference turbidity index
NDVI	normalised difference vegetation index
NDWI	normalised difference water index
NDWIF	normalised difference water index of McFeeters
NDWIT	normalised difference water index of Takeuchi
NGI	(chief directorate of) national geo-spatial information
NIR	near infrared
NN	nearest-neighbour
OBIA	object-based image analysis
PCA	principal components analysis
RADAR	radio detection and ranging
RADARSAT	radar satellite
RMS	root mean squared
RS	remote sensing

SANSA	South African national space agency
SAR	synthetic aperture radar
SAVI	soil-adjusted vegetation index
SLC	single look complex
SLAR	side-looking airborne radar
SMA	special management area
SPOT	satellite pour l'observation de la terre
SVM	support vector machine
SWIR	short-wave infrared
TerraSAR	terra synthetic aperture radar
TM	thematic mapper
USGS	United States geological survey
VI	vegetation index
VIR	visible and infrared
VNIR	visible and near-infrared
VH	vertical-horizontal
VV	vertical-vertical

CHAPTER 1: INTRODUCTION

Various anthropological developments have negatively impacted South Africa's wetland ecosystems. Water resources are intensively exploited, and pollution commonly occurs (Noble & Hemens 1978). Many rivers have been reduced from perennial streams to seasonal torrents, and almost every one of them has been impounded by one or more dams (Davies & Day 1998), while the size and effectiveness of palustrine wetlands have been reduced (Cowan 1995). Coastal lakes in the southern and south-western Cape have also been facing major adverse anthropogenic effects (Hart 1995).

To face these threats successfully, research is needed on scientifically based management and utilisation of inland waters (Noble & Hemens 1978). One important aspect of this is the regular inventorying of the spatial extent of these wetland areas to identify areas where losses are occurring. However, because of the large areas that need to be monitored, as well as the small size of many wetlands, this is an expensive and lengthy task (Kotze, Breen & Quinn 1995). This is especially true when field monitoring is used (Lang et al. 2008).

Remote sensing (RS) has long been used as an alternative method for monitoring wetland areas. Traditionally this involved manual interpretation of aerial photographs which, although accurate, is time-consuming, expensive and subjective (Lunetta & Balogh 1999; Lang et al. 2008). However, computer-assisted classification methods have been used in wetland mapping for a number of years, mostly in conjunction with data from satellite-borne sensors (Raitala, Rantunen & Hellsten 1984; Raitala & Lampinen 1986; Johnston & Barson 1993). The increase in the spectral, spatial and temporal resolution of these sensors in recent years has allowed for more efficient, reliable and affordable environmental monitoring (Jones et al. 2009).

1.1 Remote sensors and wetlands classification

Visible and infrared (VIR) sensors such as Landsat and SPOT are commonly used for wetlands classification (Raitala, Rantunen & Hellsten 1984; Raitala & Lampinen 1986; Johnston & Barson 1993; Lunetta & Balogh 1999; MacAlister & Mahaxay 2008). These sensors can accurately classify open water surfaces, but their inability to penetrate vegetation cover makes them less suitable for the classification of vegetated wetlands (Töyrä, Pietroniro & Martz 2001). Also, the wavelengths detected by VIR sensors are short enough to be scattered by clouds and thick smoke. VIR data availability is consequently subject to atmospheric conditions (Töyrä & Pietroniro 2005).

Synthetic aperture radar (SAR) sensors have also been used in various wetland classification studies (Pope et al. 1997; Töyrä, Pietroniro & Martz 2001; Hess & Melack 2003; Hess et al. 2003; Töyrä & Pietroniro 2005; Hamilton et al. 2007; Lang et al. 2008; Jones et al. 2009). Compared to VIR sensors, SAR sensors have several advantages for wetland classification. For instance, SAR sensors are active sensors, meaning that they generate their own electromagnetic (microwave) energy, transmit it to the earth's surface, and measure the returns which are scattered back to them. Most VIR sensors, on the other hand, are passive sensors, meaning that the energy that is reflected back to them by the earth's surface is generated by an external source (the sun). Consequently, the main advantage of SAR sensors is that they can be used to record data at any time of day or night (Mather 2004). Furthermore, compared to VIR energy microwave energy has several benefits for the remote sensing of wetlands. The latter's longer wavelength enables it to penetrate cloud cover and vegetation canopies. Also, its reflection is strongly affected by the dielectric constant of the surface reflecting it, and water has a much higher dielectric constant than dry or wet soil. Therefore, the presence or absence of water on the earth's surface has a significant influence on the signal returned to a SAR sensor (Kasischke & Bourgeau-Chavez 1997).

1.2 The case for object-based classification

Traditionally, the pixel has been the basic building block of automated RS-based classifications. However, this has been changing in recent years, with increasing emphasis being placed on object-based image analysis (OBIA). This methodology groups pixels in an image based on spectral and contextual information, forming readily usable objects. The classification is then performed on these objects rather than on individual pixels (Blaschke 2010).

This approach is advantageous as it facilitates better integration between geographic information systems (GIS) and RS data than is possible with pixel-based techniques, which arguably do not make use of spatial concepts (Blaschke 2010). OBIA also lessens or eliminates the salt-and-pepper effect commonly found in pixel-based classification, whereby lone spectrally-distinct pixels in larger spectrally-homogenous areas are wrongly assigned to different classes than the pixels surrounding them. This is especially important when modern high-resolution satellite imagery is used, as it is more susceptible to this problem (Blaschke et al. 2000; Blaschke 2010).

1.3 Classifiers in remote sensing

Traditionally, classifiers in RS were divided into two groups: supervised and unsupervised classifiers. More recently, several methodologies have been developed that fall outside these

clear-cut groups, such as artificial neural networks (ANNs), decision trees, expert systems (ESs), genetic algorithms and support vector machines (SVMs) (Mather 2004; Blaschke 2010). This study focuses on the two classifiers implemented in version 8 of the commercial OBIA software package eCognition, namely the rule-based expert system classifier and the nearest-neighbour (NN) supervised classifier (Trimble 2011b). An overview of the applications of other classifiers in RS literature will however be given.

An expert system applies artificial intelligence methods to classification (Mather 2004). It is guided by a set of decision rules which can use both RS and GIS data. These rules describe the relationship between the attributes and types of this data (Bolstad & Lillesand 1992; Sader, Ahl & Liou 1995). This approach has several advantages. First, it is intuitive and logical for the end-user. Second, classification rules for certain classes can be refined without affecting the rules for others, or compromising the classification. Such refinements, and the addition of more rules and datasets, can be done iteratively. Third, once an object (or a pixel) has been assigned to a certain class, it can be disregarded by further processing if necessary (Lucas et al. 2007).

The nearest-neighbour classifier implemented in eCognition is a relatively simple supervised classification algorithm. It can be termed nonparametric, as it requires no prior assumption as to the statistical distribution of the input data (Schowengerdt 1997). It projects a set of classified sample objects into a feature space defined by a specified set of spectral, textural or contextual features, along with the objects still to be classified. Each unclassified object is then assigned a membership value for the class represented by the sample object closest to it in feature space, based on its Euclidean distance to that object. If an unclassified object is further than a specified distance from the closest sample object in feature space, it is not classified (Trimble 2011b). In comparison to parametric supervised classifiers such as maximum likelihood (ML), nearest-neighbour classifiers should perform better if sample class proportions match those in the population, and should perform similarly if sample class proportions do not match those in the population (Hardin 1994).

1.4 Research problem, aim and objectives

Wetlands are globally, and specifically in Southern Africa, under threat from a range of anthropogenic activities. More effective methodologies are needed for their monitoring at national and local scales. To evaluate the effectiveness of automated remote sensing-based classification for monitoring of wetlands in the south-western Cape region in South Africa, a classification of various wetlands in the catchments of the Nuwejaars and Heuningnes Rivers in the Cape Agulhas area will be undertaken. This area supports a diverse range of wetland areas

experiencing different levels of anthropogenic interference. Different combinations of remote sensors and image classifiers will be used to provide an objective assessment of available methodologies.

1.4.1 Research aim and objectives

The aim of this research is to develop a methodology for the remotely sensed classification of wetlands using SPOT 5 and ERS-2 OBIA. Different classification algorithms available in commercial OBIA software will be compared. Images from the two sensors will be classified separately to assess the information available from each sensor, and then classified in combination in an attempt to obtain a significant improvement in accuracy over the separate classifications. The use of SPOT 5 and ERS-2 data is motivated by the need for a methodology that is cost-effective, accurate, simple to replicate at another time, and transferrable between different areas with little effort. The research will regard the diverse wetland systems of the Agulhas Plain, a low coastal peneplain at the southern tip of Africa.

Eight objectives will be pursued, namely:

1. Review the available literature to identify appropriate data types and preprocessing and classification methodologies;
2. Identify a suitable study area;
3. Obtain and preprocess RS data, and create required ancillary data;
4. Perform field observations for the identification of aquatic classes on images and the evaluation of classification accuracy;
5. Map wetlands using SPOT 5 data only;
6. Map wetlands using ERS-2 data only;
7. Map wetlands using a combination of SPOT 5 and ERS-2 data; and
8. Evaluate the use of SPOT 5 and ERS-2 data for wetland mapping.

1.5 Research methodology

Research methodology consists not only of the specific research methods used, but also the logic behind the use of these methods in the context of the specific study (Kothari 2004). Following Mouton (2001), this research can be contextualised as a methodological study; different methodologies for the classification of wetlands from remotely sensed data are developed and evaluated. Furthermore, this evaluation places the research within the quantitative paradigm: statistical accuracy measures are used to characterise the performance of the different

methodologies. The research design is depicted in Figure 1.1. More details are provided in the following chapters, to enable replication of the study.

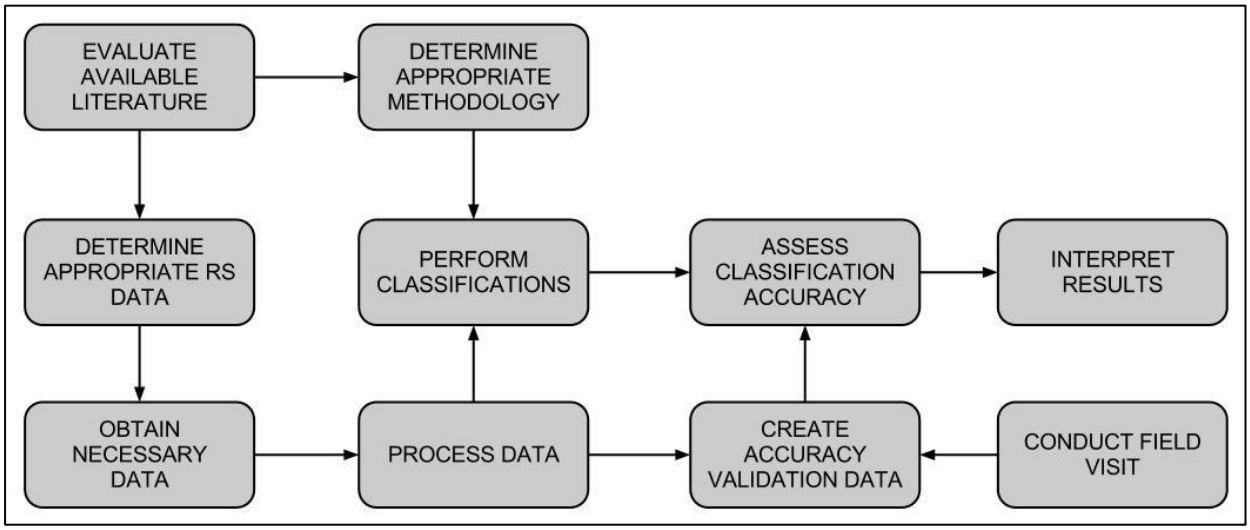

Figure 1.1: Simplified research design for automated classification of wetlands

1.6 Defining wetlands

Wetlands are ecosystems characterised by the interplay between land and water (Cowan & Van Riet 1998). They are easy to recognise; any area that is periodically saturated with water can usually be termed a wetland. However, formulating an exact definition of wetlands is more problematic (Davies & Day 1998). Also, there is some confusion in literature on whether the term wetlands includes all aquatic ecosystems (perhaps excluding the oceans), or only the interfaces between aquatic and terrestrial ecosystems (Breen, Heeg & Seaman 1993; Cowan & Van Riet 1998; Davies & Day 1998).

The Ramsar Convention, to which South Africa is a signatory, is an intergovernmental treaty facilitating international cooperation in conservation of wetlands. It states that wetlands are "areas of marsh, fen, peatland or water, whether natural or artificial, permanent or temporary, with water that is static or flowing, fresh, brackish or salt, including areas of marine water the depth of which at low tide does not exceed six metres" (Cowan 1995:5 quoting Article 1.1 of the Convention of Wetlands of International Importance especially as Waterfowl Habitat, known as the Ramsar Convention). Article 2.1 of this convention states that such areas may also include adjacent riparian and coastal zones (Cowan 1995).

Accordingly, this study will regard wetlands not only as palustrine wetlands (see section 1.6.1), but also as all inland aquatic ecosystems, including lakes, ponds and pans, and rivers and streams, as well as all coastal aquatic ecosystems with a depth at low tide not exceeding 6 m. Six

components of wetlands, namely palustrine wetlands, rivers, lacustrine wetlands and endorheic pans, and estuaries and estuarine lagoons are outlined in the following subsections.

1.6.1 Palustrine wetlands

Ecosystems which occur between terrestrial and aquatic systems and are predominantly influenced by an excess of water are known as palustrine wetlands (Cowan & Van Riet 1998). The main types occurring in the Western Cape are swamp and marsh areas and river-source sponges; floodplains are also found in some parts of South Africa (Noble & Hemens 1978).

River source sponges are seepage areas, usually on mountain slopes, where streams originate. They are seasonally or perennially waterlogged, and play an important role in regulating runoff from catchments (Breen, Heeg & Seaman 1993). In the south-western Cape, sponges with acidic, humic-stained water are found on slopes at almost any altitude. Dominant vegetation types are Restionaceae and Bruniaceae, and some immature peat soils are found (Noble & Hemens 1978).

Swamp and marsh areas, sometimes known as vleis in South Africa, are flat stretches in river systems which are inundated and become waterlogged in the wet season. They are covered in reeds and other marshy vegetation. Marshes are defined as having a water level not much above soil level in the wet season, and are characterised by emergent vegetation not exceeding 2 m in height. On the other hand, swamps have a water level well above soil level in the wet season, they are more perennial than marshes and swamp vegetation can exceed 3 m in height (Noble & Hemens 1978).

Most palustrine wetlands are not located in protected areas and various factors contribute to the loss of these wetlands. Direct factors include agricultural activities, erosion and the building of dams, while indirect factors include the disruption of the hydrological regime, either by afforestation or by water-resource development in catchment areas, and excess sedimentation. Also, the introduction of alien plants and animals can have profound negative impacts (Cowan & Van Riet 1998).

1.6.2 Rivers

Any study of an aquatic ecosystem requires an understanding of the rivers incorporated in it, as these rivers greatly influence the ecosystems around them through the state of their water and other material carried in their water (Noble & Hemens 1978). Modern limnological science views rivers as continuous longitudinal ecosystems. According to this view, rivers possess continuous gradients of physical and chemical conditions which are progressively and

continuously modified along the course of the river. This can be contrasted with more traditional views which saw rivers as a string of independent ecosystems (Davies & Day 1998).

1.6.3 Lacustrine wetlands and endorheic pans

Lacustrine wetlands are areas of permanent water with little flow (Barbier, Acreman & Knowler 1997) and include freshwater lakes and ponds (Dugan 1990). However, there is some disagreement in literature over whether this term also includes endorheic pans which are shallow basins characterised by a closed drainage system and are typically circular or oval in shape (Allan, Seaman & Kaletja 1995; Cowan & Van Riet 1998).

In South Africa, endorheic pans are commonly found in some of the drier areas in the interior, as well as certain wetter areas in Mpumalanga. The only natural freshwater lake in the interior is Lake Fundudzi in Limpopo province. However, several natural lakes occur along the coastline of the country (Hart 1995). Noble and Hemens (1978) classify these lakes as either coastal or estuarine, with the former category having no more than occasional seawater input, and the latter having a permanent or semi-permanent tidal connection to the sea. Salinity levels in coastal lakes range from low (fresh water) to brackish, while estuarine lakes can have salinity levels ranging from low to hyper-saline. However, estuarine lakes inevitably grade into estuaries with increasing salinity (Hart 1995).

1.6.4 Estuaries and estuarine lagoons

Estuaries are semi-enclosed coastal waterbodies characterised by an inflow of fresh water from land drainage and a connection to the open sea. Mixture occurs between fresh and sea water, and tidal influence is experienced at times (Noble & Hemens 1978; Cowan & Van Riet 1998). Estuaries are highly dynamic ecosystems. In times of flood, they can be entirely flushed by fresh water and the zone of salinity mixing can be pushed well out to sea. However, in times of abnormally low fresh-water inflow, evaporation can cause larger estuaries to reach salinity levels well above that of sea water (Noble & Hemens 1978). When the mouths of estuaries are closed for extended periods, lagoons form. Lagoons are shallow bodies of standing water which have an intermittent connection to the sea, and they are characterised by brackish water (Noble & Hemens 1978). The specific wetlands considered in this study will be examined in the next section.

1.7 The wetlands of the Nuwejaars and Heuningnes River systems on the Agulhas Plain

This research investigates the wetlands of the Nuwejaars and Heuningnes River systems, which are situated in the south-eastern part of the Agulhas Plain, at the southern tip of the African

continent. This section will regard these wetlands, along with their geographical context. The location of the study area is given in Figure 1.2.

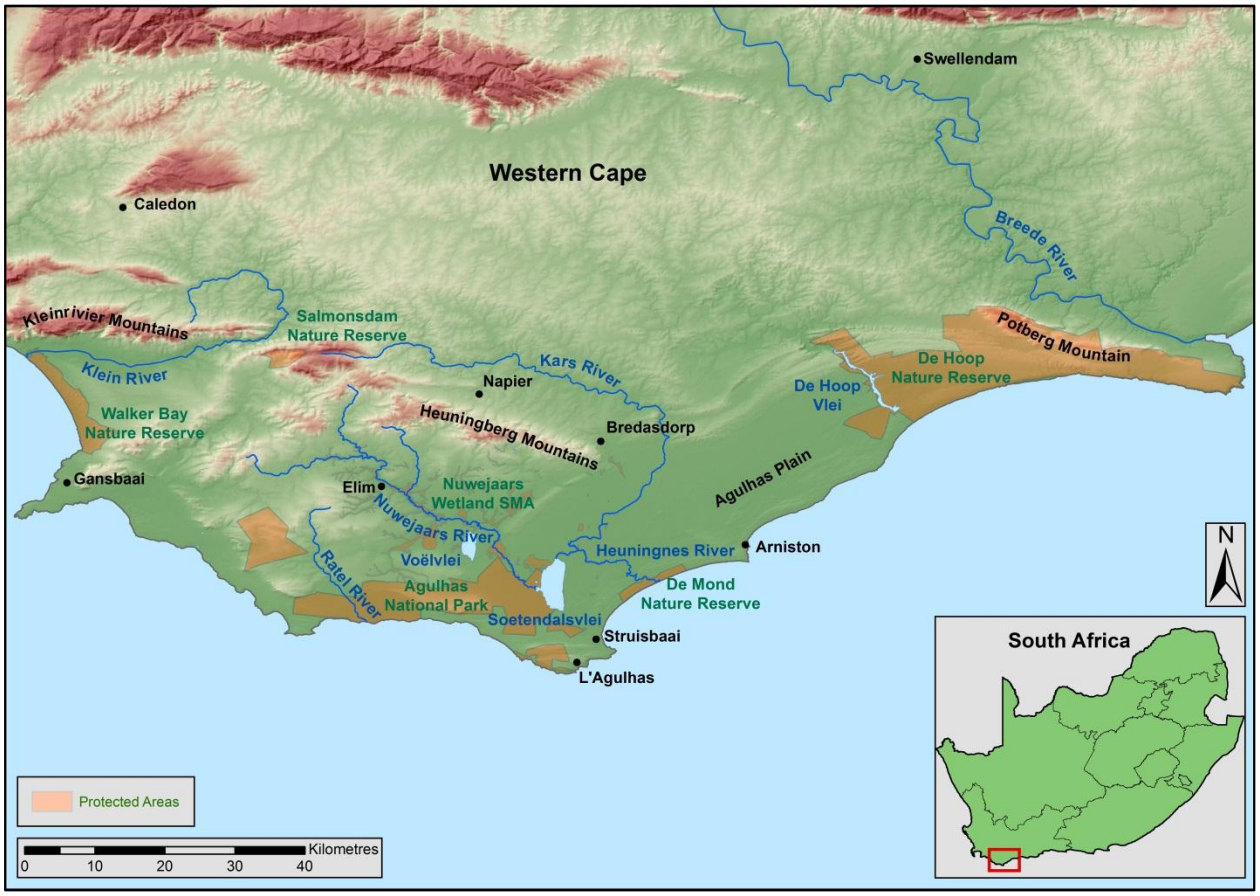

Figure 1.2: The location of the study area within the Agulhas Plain

1.7.1 The Agulhas Plain

The Agulhas Plain is a low coastal peneplain covering 270 000 ha. It stretches from the Klein River mouth in the west to the Breede River mouth in the east, and is separated from the interior of the country by the Kleinrivier-Heuningberg Mountains in the west and Tertiary hardened dunes and the Potberg Mountain in the east (United Nations 2003). Geologically, it is a remnant of an ancient wave-cut platform, mostly covered by calcareous sands of the Tertiary age. The mountains along the coastline mainly consist of Cape Fold Belt sandstone, which is sometimes capped by limestone. Inland, the plains are predominantly Bokkeveld shale with Malmesbury shale and Bredasdorp limestone also occurring (Russel & Impson 2006; SANParks 2008).

The region has a Mediterranean climate, with most (65-75%) of the rainfall occurring in the winter months (May to October). Mean annual rainfall ranges between 450 mm (in the east) and 540 mm (in the west) along the coast to 650 mm along the northern boundary of the plain (Lombard et al. 1997; United Nations 2003). Prevailing winds in the area are westerly in winter

and easterly in summer. The Cape Agulhas area is the windiest stretch of the whole South African coastline, and has the lowest percentage of calms (SANParks 2008).

The Agulhas Plain is globally recognized as being vulnerable and irreplaceable in terms of biodiversity. It forms part of the Cape Floristic Region (CFR), one of the world's 19 threatened biodiversity hotspots and the only floral kingdom found entirely within a single country. The plain is one of the largest remaining strongholds of lowland fynbos and renosterveld in the country and the world. The level of plant diversity is remarkable, harbouring almost 2500 known species, including an endemic vegetation type, Elim Asteraceous Fynbos (Rouget 2003; United Nations 2003). Additionally, it contains, or partly contains, three internationally recognised Important Bird Areas, namely De Hoop, Heuningnes River and Estuary and Overberg Wheatbelt (Barnes 1998; United Nations 2003). It also supports significant populations of two endangered amphibian species and a threatened snake species, and it provides one of the few extant habitats for endangered animal species such as the bontebok, the Cape mountain zebra and the honey badger (United Nations 2003).

The main agricultural crops of the region are wheat, barley, oats, triticale and canola, while lucerne, medics and clover are grown as grazing or feed for the region's approximately 30 000 sheep and 4000 cattle (Mangnall & Crowe 2002). These activities, along with alien infestation and urban development, cause extensive fragmentation of the area's natural vegetation. Rouget (2003) and Pence, Botha and Turpie (2003) record that some 40% of the plain has been transformed, although United Nations (2003) claims that approximately 74% is still covered by natural vegetation. Other threats to biodiversity include the unsustainable harvesting of wild flowers and inappropriate fire regimes (Lombard et al. 1997).

The need to conserve this crucial area against the aforementioned threats has led to the establishment of several protected areas of which one is a national park; the Agulhas National Park proclaimed in 1999. Wetlands management forms a major part of the conservation agenda in this park; several wetlands within the park boundaries were degraded by past agricultural activities and resource use (Russel & Impson 2006; SANParks 2008). The Working for Wetlands programme is tasked with addressing this degradation and it is currently engaged in rehabilitating several wetlands within the park. The programme focuses on clearing alien infestations, and on constructing and maintaining structural interventions which reduce or remove the hydrological impact of artificial drainage channels, a remnant of historical cultivation (SANBI 2010). Provincial government (CapeNature) also manages several reserves on the plain, including, in the east, De Mond and De Hoop, and, in the west, Salmonsdam and Walker Bay (Barnes 1998; United Nations 2003). Furthermore, the state-run conservation areas are

complemented by several privately managed conservation areas. A notable and relatively unique initiative is the Nuwejaars Wetland Special Management Area (SMA) established by the owners of the properties forming the core of the Nuwejaars wetland system (Germishuys 2007). The SMA is a formally recognised area where 25 private landowners work together to manage their land in such a way that development is sustainable and biodiversity is conserved. Conservation areas throughout the SMA have been consolidated and separated from farmlands, and natural corridors formerly broken by fences and agricultural land have been re-established. Furthermore, wetland management is one of the SMA's main priorities. Large tracts of alien vegetation are being cleared, and riparian alien trees are being replaced with indigenous trees. Structural interventions (ecologs created from chipped alien plant matter) are constructed in degraded river systems to restore their natural hydrology, particularly through achieving the re-establishment and rehydration of peat (Nuwejaars Wetland SMA 2011). The majority of the wetlands considered by this research are managed by this unit.

1.7.2 The Nuwejaars and Heuningnes River systems

The wetlands considered in this research either form part of the Heuningnes River system or part of the river system of one of its two major tributaries, the Nuwejaars River (the other tributary being the Kars River). Bickerton (1984) observed some disagreement in the literature over the area of the Heuningnes catchment, although most sources give it as about 1400 km^2 (including Noble & Hemens 1978). The Nuwejaars River rises through its various tributaries in the southern slopes of the Bredasdorp Mountains, the Koueberge, the hills to the south of Elim and the northern slopes of Soetanysberg. Its length from its westernmost source to its confluence with the Kars River is 55 km. The Kars River joins the Nuwejaars River (or technically the outflow of Soetendalsvlei, which is a coastal lake fed by the Nuwejaars) from the north to form the Heuningnes, and its length from its westernmost source to the confluence is 75 km. The length of the Heuningnes from this confluence to its estuary at De Mond is 15 km (Bickerton 1984; Barnes 1998).

Two palustrine wetland areas on the banks of the Nuwejaars River are considered in this study. Both are managed by the Nuwejaars Wetland SMA. The first one, at Moddervlei, is largely infested by alien trees but is being cleared (Ambrose 2010, pers com; Barnes 1998). Although dense stands of palmiet occur in the river channel itself, little or no fringing sedges occur where the aliens are dense. However, the river broadens out in parts with some sedgebeds and reedbeds occurring, as well as scrubs, restios and grass on higher land (Barnes 1998). The second wetland occurs between Wiesdrif and Heuningrug. It shows large variation in species composition and

water levels. Vegetation includes different clumps of sedges, stands of typha and phragmites, grass areas, isoplesis mats, short emergent vegetation, tall sedges and reeds around deeper pools and sparse emergent vegetation in some pans (Barnes 1998).

Another significant wetland forming part of the Nuwejaars River system is Waagschaalvlei (also known as Waskraalsvlei) where the confluence of the Uintjieskuil and Paalskloof Rivers flows into a depression and empties into the Nuwejaars (South Africa 2002; Gordon, Adams & Garcia-Rodriguez 2011; Nuwejaars Wetland SMA 2011). It has a surface area of approximately 1 km^2 and is characterised by clear water and extensive beds of reeds (phragmites and schoenoplechtus) and submerged macrophytes (Gordon, Adams & Garcia-Rodriguez 2011). Waagschaalvlei is also managed by the Nuwejaars Wetland SMA which has released a small group of hippo into it. In addition to being tourist attractions, these hippo assist in the management of wetland hydrology; by walking through the wetland they spread water into the peat and open up blocked channels (Nuwejaars Wetland SMA 2011).

Voëlvlei is a coastal lake to the west of Waagschaalvlei also managed by the Nuwejaars Wetland SMA (Germishuys 2007). It is approximately 2 km wide and 2 km long with a mean water depth of 2.25 m. Extensive reedbeds (phragmites and schoenoplechtus) occur on its northern and southern shores. It has an output channel that flows into the Nuwejaars River, but its hydrology is unique in that it receives reverse flow from this outlet during flood events. If it fills up during such an event, excess water flows eastwards toward a larger coastal lake, Soetendalsvlei (Gordon, Adams & Garcia-Rodriguez 2011).

Soetendalsvlei, the largest wetland on the Agulhas Plain, has a surface area of approximately 20 km^2, a maximum length of about 8 km and maximum width of about 3 km. It has a mean water depth of around 2 m, but this can increase during times of flooding. It is fed mainly by the Nuwejaars River and overflows during times of higher flow into the channel that joins the Kars River to form the Heuningnes. Reed growth (phragmites and schoenoplechtus) occurs mainly on the western and southern shores, but a large bed in the middle of the lake stretches across its width, splitting it in two (Noble & Hemens 1978; Gordon, Adams & Garcia-Rodriguez 2011). The western and south-western edges of the lake are managed by Agulhas National Park along with the associated palustrine wetlands, while the rest, including most of the lake itself, is managed by the Nuwejaars Wetland SMA. This also includes substantial palustrine wetlands north-west of the lake (Germishuys 2007; SANParks 2008).

Other wetlands in the Nuwejaars River system are some small endorheic pans and a larger seasonal pan on the farm Brakpan (South Africa 2002). The system's most important wetland

areas are illustrated in Figure 1.3. The boundary of the analysis subset used in the Nuwejaars River system is also shown; as discussed in later chapters, this subset was chosen to include a diverse range of wetland areas, but to exclude the fire scars visible in the southern part of the map (dark brown areas).

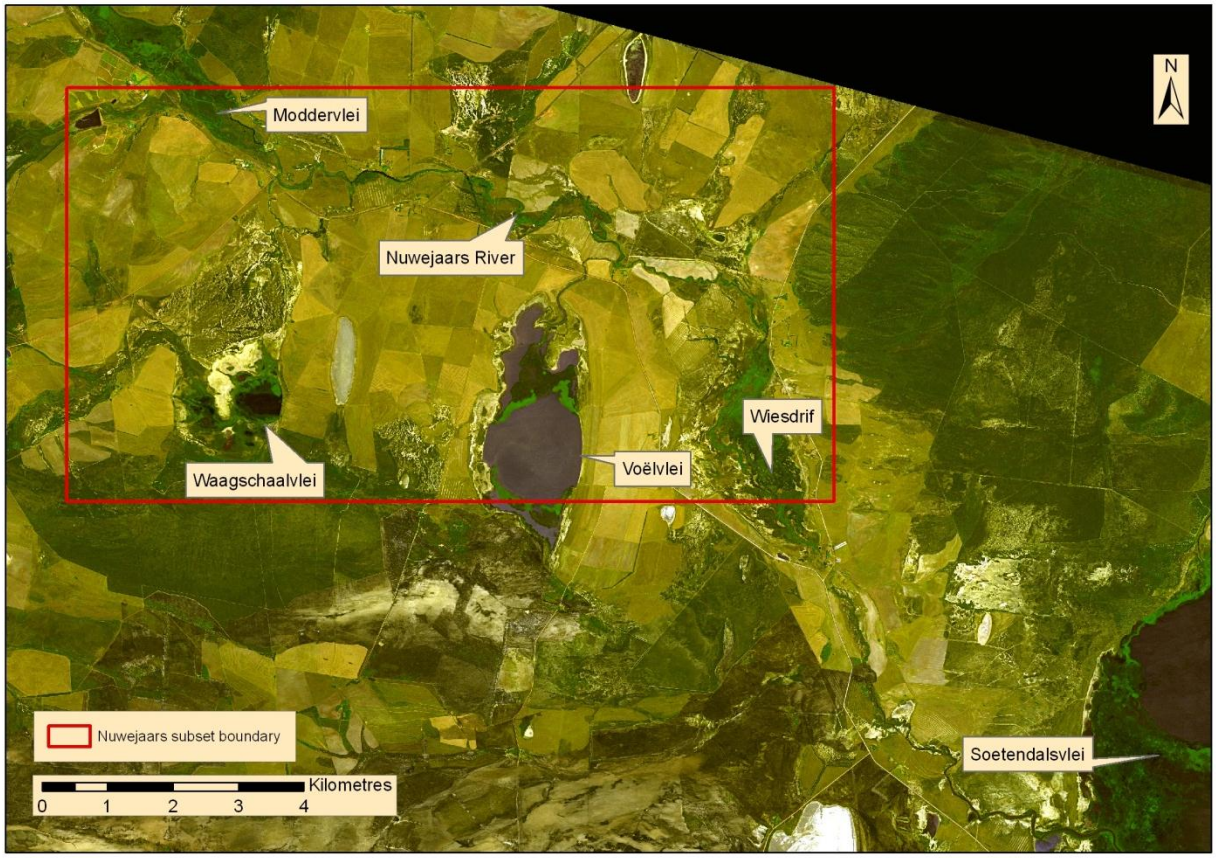

Figure 1.3: Wetlands in the Nuwejaars River System

Eastwards from Soetendalsvlei, some small wetlands occur on agricultural land south of the Heuningnes River. Also, palustrine wetlands occur along the course of the Droë River, a seasonal river entering the Heuningnes north-east of De Mond (South Africa 1986).

The Heuningnes estuary forms where the river reaches the sea through a double ridge of sand dunes (Barnes 1998). The area around the mouth itself is part of the De Mond Nature Reserve, while the riparian zone further upstream is managed by the Heuningnes Riparian Owners Association (United Nations 2003). Marginal tidal influence stretches for around 12 km upstream, however, a causeway across the river 1.3 km from the mouth obstructs tidal flow considerably, so that only the last 2 km of the river show the characteristics of a true estuary (Bickerton 1984; Barnes 1998).

The mouth of the estuary comprises a bay with sand, mudflats and tidal saltmarsh. Historically, the periodic closing of the mouth of the estuary caused extensive flooding of agricultural land

upstream. Consequently the mouth has been artificially managed since the beginning of the previous century. One feature that resulted from the mouth being kept permanently open is an inner delta where the river channel meanders irregularly in the sandy plain between the dunes (Bickerton 1984; Barnes 1998). Figure 1.4 shows various wetlands visited during field data collection and De Mond is shown in Figure 1.4(h).

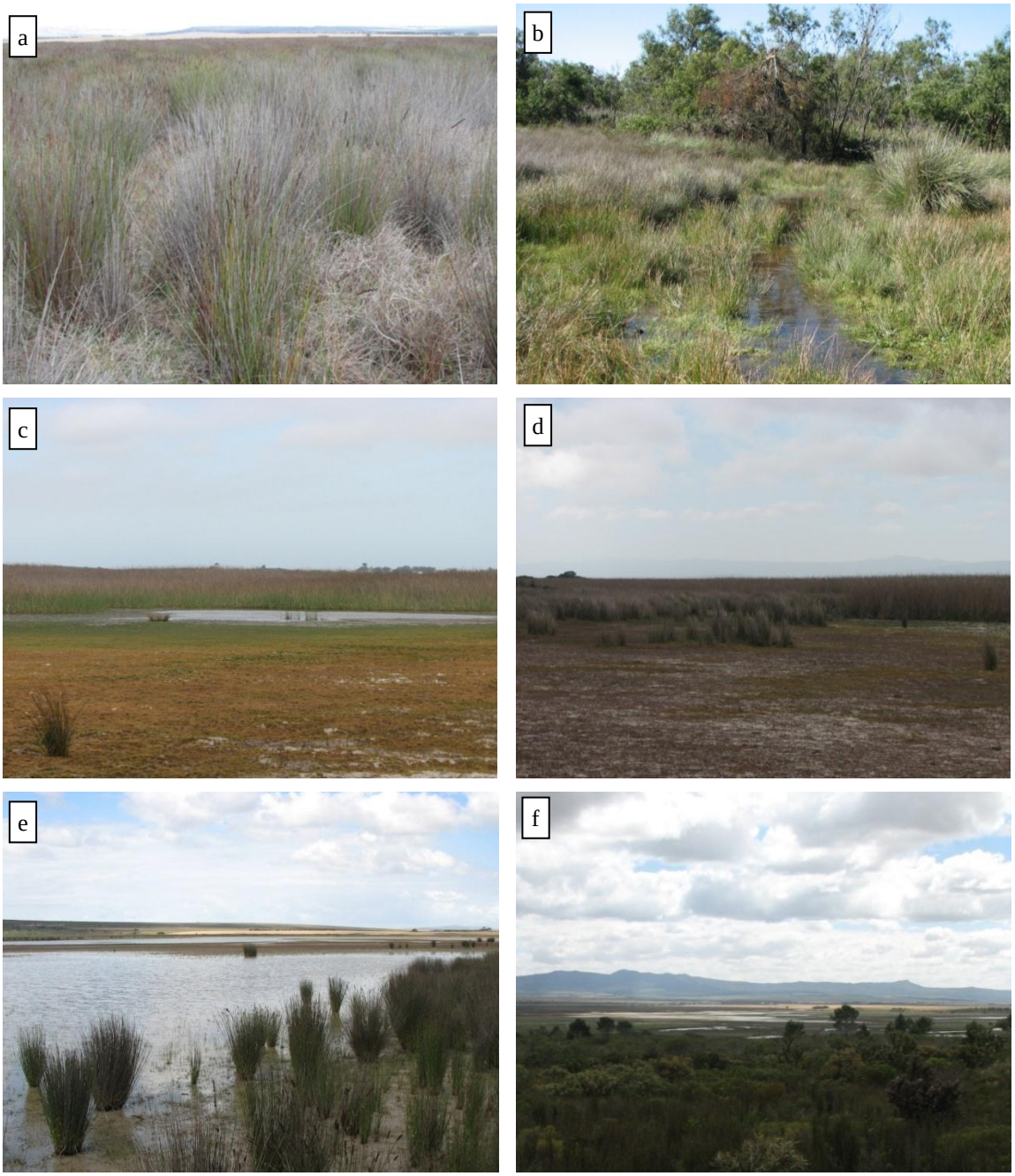

Figure 1.4: Wetlands visited during field data collection: (a) Wiesdrif; (b) Moddervlei; (c) and (d) Soetendalsvlei; (e) and (f) Waagschaalvlei (continued overleaf).

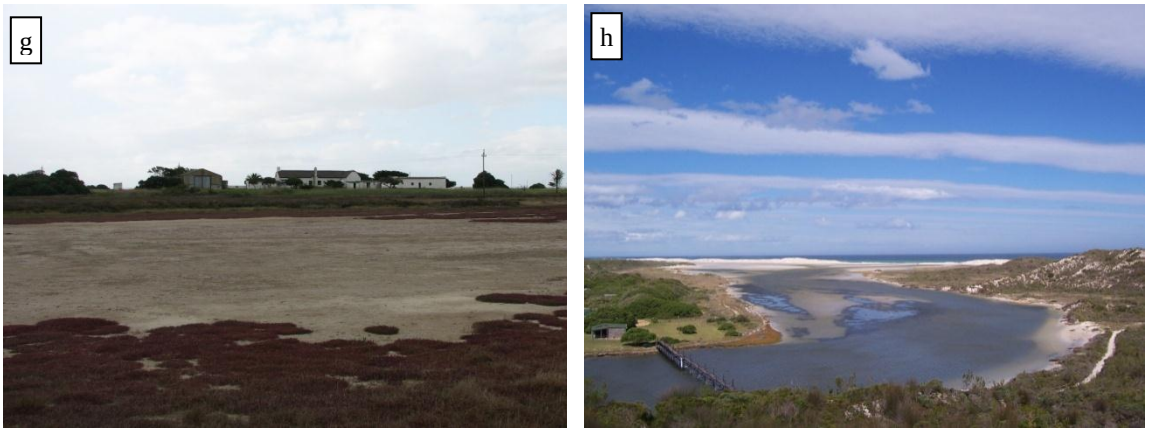

Figure 1.4 (continued): Wetlands visited during field data collection: (g) Droë River; (h) De Mond.

The major wetlands in the Heuningnes River system are illustrated in Figure 1.5. As discussed in later chapters, the analysis subset shown here was chosen to include a diverse range of wetland areas.

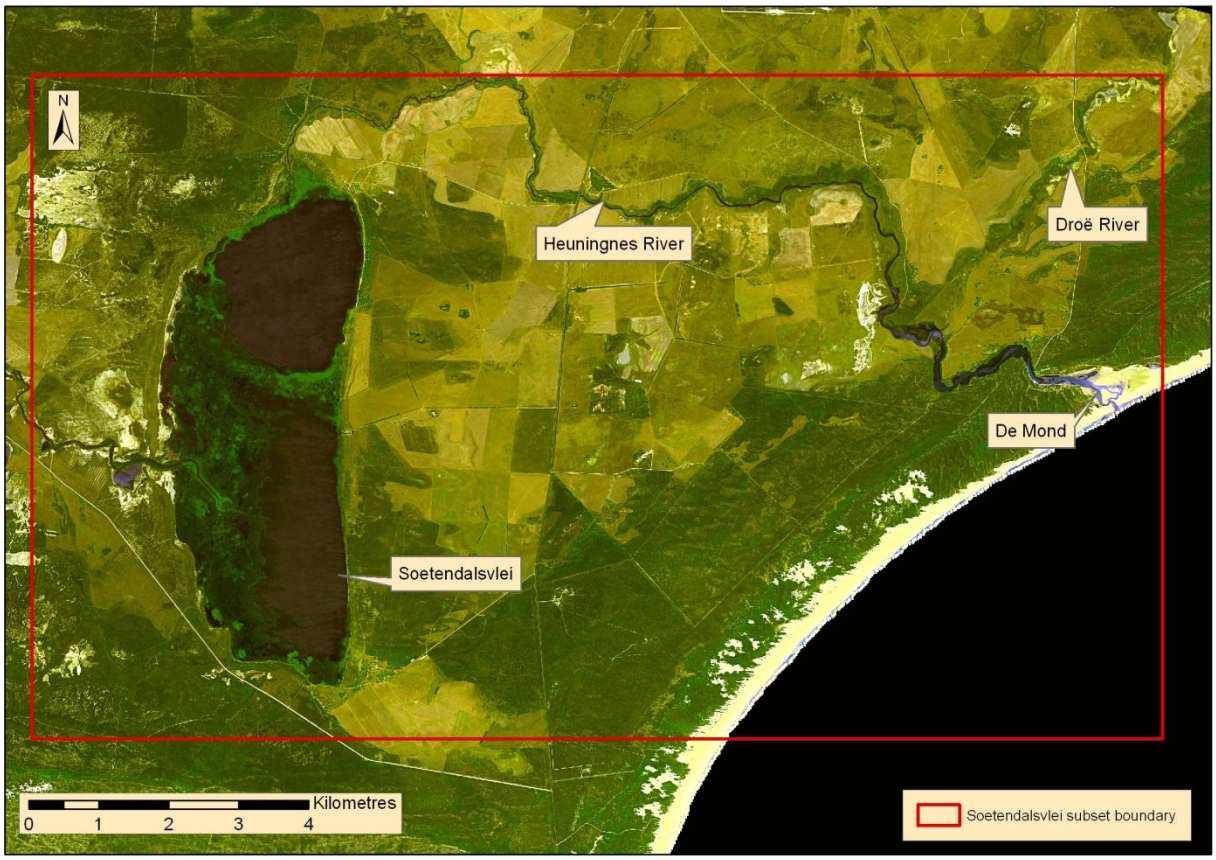

Figure 1.5: Wetlands in the Heuningnes River system

This chapter has provided an introduction to this research. The context of the study has been established, and the specific objectives have been given. In the next chapter, literature on the remotely sensed classification of wetlands will be considered in more detail.

CHAPTER 2: REMOTE SENSING FOR WETLANDS CLASSIFICATION

This chapter evaluates the existing literature on wetlands classification using remotely sensed data. First, the use of VIR and SAR data in wetlands classification is compared. Second, the various classifiers used in RS expounded. Third, the natures and implications of the OBIA paradigm are discussed.

2.1 Remotely sensed data for wetlands classification: VIR vs. SAR

Visible and infrared (VIR) and synthetic aperture radar (SAR) sensors feature prominently in the existing literature on wetlands classification. This section considers the applications and limitations of both in turn.

2.1.1 VIR sensors in wetlands classification

These sensors, as the name implies, operate in the visible and the infrared regions of the electromagnetic spectrum. The visible spectrum contains those wavelengths of radiation that can be perceived by human vision, i.e. blue, green and red light. Wavelengths longer than those of the visible spectrum (but shorter than those of microwave radiation) are termed infrared, and this spectrum can be subdivided into near-, mid- and far-infrared. The primary source of near- and mid-infrared radiation is the sun and they are reflected by the earth's surface like visible light. Hence, the near- and mid-infrared wavebands, together with the visible bands, are sometimes collectively known as the optical bands. Far-infrared radiation, however, is emitted by the earth's surface in the form of heat, or thermal energy, and is sometimes known as thermal infrared radiation. Thermal infrared bands are generally less common in VIR sensors than visible and near- and mid-infrared bands (Campbell 2002; Mather 2004).

Concerning wetlands, water is characterised by strong absorption of near-infrared radiation, particularly when it is calm, clear and deep (Dogan, Akyurek & Beklioglu 2008). This has the effect that VIR sensors can be used in the automated classification of open water with high levels of accuracy. Töyrä, Pietroniro and Martz (2001) reported very high accuracies for SPOT-based classifications of open water (user's and producer's accuracies ranged between 88 and 100%), while Sawaya et al. (2003), using relatively unsophisticated methods, were able to accurately discriminate between water and non-water using Landsat, but reported some errors when using Quickbird (however no statistical accuracy measures were given). Lewinsky and Bochenek (2008) did a SPOT-based land-cover classification for 13 classes, and reported the water class having the highest accuracy (user's accuracy was 94% and producer's accuracy 97%), while

Fuller, Morgan and Aichele (2006) reported that water could be accurately identified from Ikonos data, although they did not provide statistical motivation for this claim.

VIR sensors have also been extensively used in classifications of vegetated wetlands. Submerged vegetation is best identified in the green and red regions of the visible spectrum. Because of strong absorption of electromagnetic radiation in the optical region by water, the reflectance values for this class are generally very low. Notably, energy in the green region is more effective at penetrating water with high concentrations of suspended or dissolved materials (Malthus & George 1997; Silva et al. 2008). Emergent vegetation species usually return higher reflectance values than submerged vegetation if water attenuation is absent. However, this class is characterised by substantial variation in reflectance values when flooding is present, due to the combination of returns from plant and water surfaces. The spectral signature of this class often overlaps those of terrestrial vegetation, water and occasionally soil (Ozesmi & Bauer 2002; Silva et al. 2008).

In practice, automated classification of vegetated wetland classes from VIR images is more problematic than for open water. Töyrä, Pietroniro and Martz (2001) have reported some confusion between various flooded and non-flooded vegetation classes when using SPOT. Fuller, Morgan and Aichele (2006) comment on having difficulty using Ikonos to distinguish between vegetated wetland and upland classes so that automated classification was eventually abandoned in favour of manual digitising. Specific sources of error mentioned in their article include shadows of trees and clouds, as well as open areas having similar features to emergent wetland areas. Shanmugam, Ahn and Sanjeevi (2006) obtained relatively high overall levels of accuracy in a wetland classification based on a combination of IRS LISS-III and Landsat TM data, but point out some confusion between spectrally-similar vegetated wetland classes. They also noted a decrease in overall classification accuracy with an increase in the number of classes. Wright and Gallant (2007), in using Landsat TM to discriminate between wetland and upland areas, reported large errors of commission for the wetland class (i.e. wetland false positives), although other measures indicated the accuracy of their study to be reasonably high. Similarly, Davranche, Lefebvre and Poulin (2010), using SPOT to identify two classes of wetlands, recorded large errors of commission for the class of submerged macrophytes, although the overall accuracy achieved in their study was very high. Lunetta and Balogh (1999) had difficulty identifying wetland shrub and wetland agriculture in a broader classification based on Landsat TM data, but the former problem was overcome by merging wetland shrub and wetland forest into a woody wetland class.

A number of other studies tell of fewer problems. MacAlister and Mahaxay (2008) obtained good results in identifying a wide range of wetland classes from Landsat 7 data. Ordoyne and Friedl (2008) predicted flooding with high levels of accuracy from MODIS data, and the errors that occurred were mostly attributed to DEM errors. Yuan and Zhang (2008) used Quickbird images successfully to identify areas of submerged aquatic vegetation.

2.1.2 SAR sensors in wetlands classification

The longest wavelengths commonly used in remote sensing fall in the microwave spectrum. In this spectrum, solar irradiance is negligible although the earth itself emits some microwave energy. However, this emitted energy is rarely measured in remote sensing as most microwave sensors are active sensors. Active sensors use their own energy to illuminate the ground and then measure the portion of energy reflected back to them, whereas passive sensors measure energy generated by an external source (usually the sun) (Campbell 2002; Mather 2004). Active microwave sensors are radar (radio detection and ranging) sensors. An imaging radar system consists of the following basic components: a transmitter, a receiver, an antenna array and a recorder. The transmitter transmits repetitive microwave pulses at a specific frequency through the antenna array, which controls the propagation of the electromagnetic wave through devices known as waveguides. Usually, the same antenna then receives the echo of the signal. This is then accepted by the receiver, which filters and amplifies it as required, and passes it on to the recorder (Campbell 2002).

The first airborne imaging radar sensors were known as side-looking airborne radars or SLARs. These systems had the significant drawback that their spatial resolution was proportional to the length of their antennas. This meant that satellite-borne sensors would have needed antennas several kilometres in length to obtain meaningful levels of detail (Mather 2004). However, the limitations of SLAR systems can be addressed by moving a shorter antenna along the orbital path of the sensor, and, for a given target, recording its level of backscatter from a range of positions, thereby simulating an antenna of the necessary length. This is the basic principle behind SAR sensors (Mather 2004; Chuvieco & Huete 2010). For the SAR sensor to model this simulated antenna, its exact position relative to the target has to be known for each recording of backscatter. The ranging capability of the sensor enables it to accurately determine the distance between the antenna and the target, while the recorded phase and amplitude of the return signal are used to calculate the position of the sensor relative to the target according to the Doppler principle (Campbell 2002; Mather 2004).

Four aspects important to consider when regarding data from imaging radar systems, particularly in the context of wetlands classification, are wavelength, incidence angle, polarisation, and scattering mechanisms and surface interactions. They are treated in the following subsections.

2.1.2.1 Wavelength

Only a small part of the microwave spectrum is used in imaging radars. These bands are summarised in Table 2.1. Of these bands, L, C and X are the most commonly found in satellite-borne SAR sensors.

Table 2.1: Microwave wavelengths and frequencies used in imaging SAR systems

Band	Frequency (GHz)	Wavelength (cm)
X	8 – 12.5	2.4 – 3.8
C	4 – 8	3.8 – 7.5
S	2 – 4	7.5 – 15
L	1 – 2	15 – 30
P	0.3 – 1	30 - 100

Source: Schowengerdt (1997)

Generally, the L-band is more suitable for studies of forested wetlands, while the C-band is more suitable for studies of herbaceous wetlands (Kasischke, Melack & Dobson 1997; Bourgeau-Chavez et al. 2001; Henderson & Lewis 2008). The longer wavelength of L-band radiation allows it to penetrate denser canopies, as it is primarily scattered and attenuated by larger branches and tree trunks, but renders it less sensitive to lower vegetation and smoother surfaces (Kasischke, Melack & Dobson 1997; Frappart et al. 2005). Conversely, the shorter wavelength C-band radiation primarily interacts with smaller branches and leaves, which makes it less suitable for the mapping of dense forested wetlands, but gives it a unique capability to monitor wetlands with lower levels of biomass (Kasischke, Melack & Dobson 1997; Kasischke et al. 2003). The short wavelength X-band SAR has been less commonly applied in wetland studies, but it is also able to identify wetlands with lower levels of biomass (Ormsby, Blanchard & Blanchard 1985), as well as open water (Hahmann et al. 2008). It is particularly suitable for the detection of water hyacinths (Shouten, Leeuwen & Twongo 2000).

2.1.2.2 Incidence angle

The incidence angle for a given target is the angle between the direction of observation (the straight line between the sensor and the target) and the surface normal (the line perpendicular to

slope of the earth's surface at the target). Generally, the degree of backscatter increases with decreasing incidence angle (Mather 2004). Smaller incidence angles are preferred for wetlands studies as they allow for better penetration of vegetation layers (Töyrä, Pietroniro & Martz 2001; Töyrä & Pietroniro 2005). However, if different incidence angles are available, higher incidence angles could assist in wetland vegetation mapping (Kasischke, Melack & Dobson 1997).

2.1.2.3 Polarisation

The polarisation of microwave signals refers to the vibrational planes in which they are transmitted and received (Chuvieco & Huete 2010). Different SAR sensors can transmit and receive different combinations of horizontally and vertically polarised signals. Like-polarised modes are designated HH and VV, where sensors in HH mode transmit and receive horizontally polarised energy and those in VV mode transmit and receive vertically polarised energy. Conversely, cross-polarised modes are designated HV and VH, where HV transmits horizontally and receives vertically polarised signals, and VH transmits vertically and receives horizontally polarised signals (Mather 2004).

Concerning wetlands classification, like-polarised radiation has been shown to be more effective at identifying flooding underneath canopies (Kasischke, Melack & Dobson 1997), although cross-polarised radiation gives important information on vegetation structure in specific cases (Jones et al. 2009). The type of wetland considered determines which polarisation(s) will be most effective in its classification. Pope et al. (1997), in a study of emergent macrophyte marshes in Mexico, found that VV (in C-band) was more effective in classifying wetlands with low cover than HH or the mean of HV and VH. Conversely, various studies have found that HH is more effective than HV (Hess & Melack 2003) and VV (Lang et al. 2008) for the classification of forested wetlands. The latter difference is attributed to higher levels of interaction between VV-polarised radiation and large vertical structures, which lead to more radiation being lost through scattering or attenuation before reaching the ground (Lang et al. 2008).

More recently, the introduction of fully-polarimetric SAR sensors has led to the development of various methods of polarimetric decomposition which have been shown in some studies to be useful parameters for wetlands classification (Yajima et al. 2008; Hong, Wdowinski & Kim 2010). Polarimetric decomposition breaks down a matrix representation of the electromagnetic energy received by the SAR sensor to estimate the contribution of different scattering mechanisms to the total backscatter (Yamaguchi 2007; Boerner 2008; Yajima et al. 2008).

Two commonly used decomposition methods are the Freeman-Durden decomposition and the Cloude-Pottier decomposition. The Freeman-Durden decomposition decomposes the total

backscatter into three contributions: surface, volume and double-bounce scattering. The Cloude-Pottier decomposition models these three contributions, but represents them as a combination of the measures entropy, anisotropy and α-angle (Schmitt et al. 2010). Other polarimetric decompositions include the Pauli decomposition and the Touzi decomposition (Touzi et al. 2009; Hong, Wdowinski & Kim 2010).

2.1.2.4 Scattering mechanisms and surface interactions

The interaction between microwave energy and a target is governed by the roughness and geometry of the target surface, as well as its dielectric constant. The roughness of the surface is simply the variation in its height; however whether or not a specific surface is considered rough is strongly dependent on the wavelength and incidence angle of the microwave radiation interacting with it. Rough surfaces cause diffuse scattering of radiation (i.e. approximately equal levels of scattering in all directions) and backscatter generally increases with an increase in surface roughness. However, smooth surfaces cause specular reflection (i.e. radiation is reflected away from the sensor) which is associated with very low levels of backscatter (Campbell 2002; Mather 2004; Chuvieco & Huete 2010). The geometry of a surface should be taken into consideration in addition to its roughness. Objects characterised by adjacent smooth surfaces can act as corner reflectors and cause double-bounce scattering which is associated with very high levels of backscatter (Lillesand, Kiefer & Chipman 2004). The dielectric constant of a target measures its ability to conduct electrical energy. This value is strongly affected by moisture, consequently the presence of moisture in both soil and vegetation has a significant impact on radar backscatter (Campbell 2002).

Practically, these characteristics make SAR sensors very suitable for the classification of wetlands. Smooth water generally acts as a specular reflector and it is characterised by very low returns, although returns sometimes increase in the presence of waves caused by wind (Horritt, Mason & Luckman 2001; Lillesand, Kiefer & Chipman 2004; Töyrä & Pietroniro 2005). The presence of flooding in vegetated areas is characterised by two possible responses depending on the type of vegetation. In sparse vegetation, flooding causes a decrease in backscatter because of increased specular reflection of radiation away from the sensor (Pope et al. 1997; Kasischke et al. 2003). In tall, dense vegetation flooding causes an increase in backscatter because of double-bounce reflection between the water surface and the vegetation (Pope et al. 1997; Podest & Saatchi 2002; Töyrä & Pietroniro 2005). However, these two responses could cancel each other in certain cases, leading to no change being observed (Pope et al. 1997). Also, when comparing flooded and unflooded sites (or the same site before and after flooding) variations in soil

moisture in the absence of flooding should be kept in mind, as they might have a larger impact on observed backscatter differences than vegetation size or density (Kasischke et al. 2003). Soil moisture has been shown in various studies to be positively correlated with SAR backscatter, although this is dependent on vegetation cover (Wang et al. 1995; Kasischke et al. 2003; Kasischke et al. 2009). It should be noted that SAR signals are scattered or reflected by water surfaces, or absorbed in water columns, whereas VIR signals are able to penetrate water to some extent and detect certain subsurface features, such as submerged vegetation (Marcus & Fonstad 2007; Silva et al. 2008).

In addition to selecting the data to be used, the selection of an appropriate classifier is a crucial aspect of a remote sensing-based classification project. Classifiers commonly applied to remotely sensed data are considered in the following section.

2.2 Classifiers in remote sensing

Traditionally, two main classification approaches were followed. Supervised classification uses user-classified samples to classify areas of unknown identity, while unsupervised classification identifies natural groups in input imagery, which the user then aggregates into classes (Campbell 2002). However, some modern methods combine elements from both groups (Chuvieco & Huete 2010).

2.2.1 Unsupervised classifiers

An unsupervised classifier divides the input image into natural classes sharing similar characteristics without the use of training data. Each of the natural classes is assigned to its corresponding output class by the interpreter. The initial classification requires no input information from the interpreter, except for the selection of the number of classes to be created, making this method suitable for situations where little a priori information is available. Yet, aggregating the initial classes into output classes does require some knowledge of the study area (Campbell 2002; Canty 2007; Chuvieco & Huete 2010).

The basic assumption of this method is that unique pixel clusters with similar spectral characteristics exist in the input data and that these correspond to real-world classes with similar characteristics. But this assumption does not always hold; spectral homogeneity often does not correspond to homogeneity in cover so that the identified classes do not necessarily correspond to the informational categories desired by the user (Campbell 2002; Chuvieco & Huete 2010).

Traditional unsupervised classifiers include the k-means, modified k-means and ISODATA algorithms (Mather 2004). However, some sources regard ISODATA as a supervised algorithm

(Campbell 2002). Little attention is paid in literature to unsupervised classification for wetland studies. Lang et al. (2008) used ISODATA for the creation of wetland hydroperiod maps. Sawaya et al. (2003) used unsupervised classification to distinguish water from non-water, and then to classify water into different groups with the purpose of using certain distinct groups as signatures for a supervised classification of water into subclasses.

2.2.2 Traditional supervised classifiers

Supervised classification starts with the manual identification of a number of areas that are representative of the different classes desired; these are known as training areas. Their selection is complicated as unusual areas should be avoided and areas representing boundaries between classes should not be included. Once suitable training areas have been selected, they are used to train the classifier in recognising the different classes. The classifier then applies this knowledge in order to obtain a classification (Campbell 2002; Chuvieco & Huete 2010).

An important distinction within the family of supervised classifiers is between parametric and non-parametric classifiers. Parametric classifiers assume a particular statistical distribution within the input data, usually the normal distribution, and they require estimates of the distribution parameters. The parametric classifier most commonly used in remote sensing is the maximum likelihood classifier. The minimum distance (centroid) algorithm is another example, as are most versions of the parallelepiped classifier. Conversely, nonparametric classifiers require no assumptions regarding the statistical distribution of input data. A common nonparametric classifier is the nearest-neighbour classifier. The classifiers discussed in Section 2.2.3 belong to this category (Schowengerdt 1997; Mather 2004).

The maximum likelihood algorithm calculates the probability of a given pixel belonging to a given class by using estimates of mean vectors and covariance matrices and then assigning the pixel to the class that it most probably belongs to. The probability calculation is based on the assumption that the data is normally distributed. When this is true, and the parameters are estimated accurately, this classifier has a minimum overall probability of error. However, the distribution assumption often does not hold, particularly when considering data from multiple sources. Furthermore, this assumption is not appropriate for SAR data (Schowengerdt 1997; Michelson, Liljeberg & Pilesjö 2000; Liu, Skidmore & Van Oosten 2002).

The minimum distance algorithm is frequently used as it is quick and simple. It measures the distance in feature space between each pixel (or object) and the centre of each training category, the distance calculation usually being based on Euclidean distance. It is capable of providing

accurate results, but it is more suitable to classes that show little overlap (Chuvieco & Huete 2010).

The parallelepiped algorithm is a parametric classifier that is quickly and easily implemented, but it is not particularly accurate, so that it is most often used for initial, exploratory classifications or combined with more complicated algorithms. It works through defining a domain area around the centre of each training class in feature space. This definition usually involves a multiple of the standard deviation. The domain takes the form of a multidimensional polygon with parallel sides, hence the name. Any pixel falling within a domain is assigned to the class represented by it and pixels falling outside these domains are left unclassified or classified through a different algorithm (Chuvieco & Huete 2010). A nonparametric modification of this classifier provided in certain software defines the parallelepiped through an interactive process involving spectral scattergrams and it does not require any statistical assumptions (Schowengerdt 1997).

Nearest-neighbour classifiers are nonparametric classifiers that assign labels to unclassified pixels or objects based on the labels of the training vectors closest to them in feature space. In the simplest case, the unclassified object is assigned the label of the single training pixel or object closest to it in feature space (Schowengerdt 1997). A modification of this version of the classifier is implemented in the commercial OBIA software package eCognition. Here the unclassified object is assigned a membership value for the class represented by the training object closest to it in feature space, based on the Euclidean distance between the two. If this value is less than a specified threshold, the object is not classified (Trimble 2011b). A more complicated variant of the classifier is the k nearest-neighbours classifier where the unclassified object is assigned the label represented by the majority of the k training objects closest to it in feature space. This model is extended in the distance-weighted k nearest-neighbours classifier, where the labels of the k closest training objects are assigned weights based on their Euclidean distance to the unknown object, and the object is assigned the label with the highest aggregate weight (Schowengerdt 1997). Other variations of the nearest-neighbour classifier are listed in Hardin (1994).

2.2.3 Alternative classifiers

In recent years the focus in research has shifted from traditional unsupervised and supervised classifications to various alternative classifiers. This is largely due to the acknowledgement of the limits of both unsupervised and parametric supervised classifiers, with various studies showing significant improvements in classification accuracy when alternative methods are used

(Sader, Ahl & Liou 1995; Liu, Skidmore & Van Oosten 2002). Four alternative classifiers prevalent in current research are neural networks, support vector machines, decision trees and expert systems. They will be considered in the following subsections.

2.2.3.1 Neural networks

Artificial neural networks (ANNs) attempt to predict a complex behaviour from a set of input variables through the simulation of human learning processes. They consist of multiple interconnections between activation units, termed neurons, which are organised in various layers. This includes an input layer, an output layer, and various hidden intermediate layers. In an ANN classifier for remote sensing, the input layer consists of the input dataset, and the output layer consists of the required set of classes. The neurons in each layer are connected to those in the next layer through a specific function, termed an activation function. The value of each output neuron is dependent on the values of all the different input neurons, although the importance of these values varies according to weights calculated for each activation function (Campbell 2002; Chuvieco & Huete 2010).

The operation of an ANN classifier can be divided into two stages: learning and classification. During the learning stage the network structure is defined and the weights of the activation functions are determined. Many learning algorithms are available; one of the most popular is termed backpropagation. In this algorithm the desired and actual outputs of the ANN for a set of training samples are compared for different sets of activation function weights and the set of weights providing the least errors is selected. During the classification stage the system developed through the learning algorithm is applied to obtain a classification (Liu, Skidmore & Van Oosten 2002; Chuvieco & Huete 2010).

ANN classifiers have several advantages. Compared to parametric supervised classifiers, similar or higher levels of accuracy can be obtained with the use of fewer training samples (Tseng et al. 2008). Subtle, non-linear patterns in input data can be identified. No assumption about the distribution of input data is required and different types of data with different structures and different distributions can be integrated. Also, noisy data is handled well (Michelson, Liljeberg & Pilesjö 2000; Liu, Skidmore & Van Oosten 2002).

However, the complexity of ANN systems restricts their application. ANNs are very difficult to train as there are no fixed rules for their configuration and often it is based on trial and error. Also, there is a risk of overtraining the system, so that it becomes too specific to the training set and cannot predict the classification for the rest of the input dataset accurately. Another issue, termed the “black box factor”, implies that the interpreter cannot readily grasp how the specific

problem is learnt, making interpretation of the results difficult (Michelson, Liljeberg & Pilesjö 2000; Tseng et al. 2008).

Liu, Skidmore and Van Oosten (2002) found that an ANN classifier significantly outperformed a maximum likelihood classifier and an expert system classifier in a general land-cover classification in the Netherlands, although accuracy could further be improved by adding the result of the expert system as an additional input layer in the ANN. Wilkinson et al. (1992) recorded that an ANN provided slightly more accurate results than an expert system in a classification of general land-cover classes in central France, and noted that both approaches fared better than parametric supervised classifiers. Michelson, Liljeberg and Pilesjö (2000) obtained slightly (1%) less accurate results from an ANN than from a maximum likelihood classifier when combining a Landsat TM image with a multitemporal ERS1 SAR dataset, however the overall accuracy of the study was low. Masocha and Skidmore (2011) report that an ANN outperformed a support vector machine (SVM) classifier in classifying alien vegetation.

2.2.3.2 Support vector machines

A support vector machine (SVM) is a supervised, non-parametric statistical learning algorithm. During an iterative learning process, a set of training samples is used to develop an optimal separation hyperplane defined as a decision boundary between different classes in classification feature space that minimises misclassifications. Only those data points that fall on the margin of the class in feature space are used to develop the hyperplane; they are known as support vectors. Those points forming the class kernel in feature space are considered redundant (Masocha & Skidmore 2011; Mountrakis, Im & Ogole 2011). In its simplest form, an SVM is a binary classifier, however it can be adapted to recognize multiple classes through methods such as one-against-all, one-against-others, and directed acyclic graph (Mountrakis, Im & Ogole 2011).

SVMs have the advantage of being able to generalise well from limited training data. Compared to ANNs, SVMs can obtain similar accuracies from smaller training samples. Also, as they are nonparametric, SVMs require no assumption about the distribution of the input data. However, they are sensitive to the choice of the function defining the class kernel with some existing kernel functions being sub-optimal for remote sensing applications. Furthermore, they are not optimised to handle noisy data, and the theory behind them can be intimidating to less experienced users (Mountrakis, Im & Ogole 2011).

As mentioned in Section 2.2.3.1, Masocha and Skidmore (2011) found that an SVM provided less accurate results than an ANN in the classification of alien vegetation. Boyd, Sanchez-Hernandez and Foody (2006) reported an SVM to be more accurate than both a decision tree and

a maximum likelihood classifier in a binary classification discriminating between fenland and other areas. Watanachaturaporn, Arora and Varshney (2008) reported an SVM performing better than a decision tree, a maximum likelihood classifier and a radial basis function network classifier in a Himalayan land-cover classification, however it did not perform significantly better than a back-propagation neural network.

2.2.3.3 Decision trees

A decision tree classifier recursively applies a set of decision rules to an input dataset, categorising the dataset into a set of target classes. A decision tree classifier is composed of a root node (the input dataset), internal nodes (splits) and terminal nodes (the target classes, known as leaves). Each node in the tree can only have one parent node, but can have two or more descendant nodes. Decision rules are applied at each non-terminal node, splitting the data into smaller subsets until the leaf nodes are reached and the data is classified (Friedl & Brodley 1997; Chuvieco & Huete 2010).

Various approaches have been proposed for the construction of decision trees. Rules are sometimes created manually based on analyst experience. According to Chuvieco and Huete (2010), such approaches can also be regarded as expert systems (see Section 2.2.3.4). Accordingly, they will be treated as such throughout this research to avoid any confusion. However, supervised approaches where statistical procedures are used to infer the rules from training data are also commonly used. The statistical procedures used are known as learning algorithms (Friedl & Brodley 1997; Chuvieco & Huete 2010). Learning algorithms can be differentiated according to whether the set of algorithms used to estimate the splits at non-terminal nodes are uniform or heterogeneous and further, in the former case, whether a single variable is used for each split (univariate decision tree), or multiple variables (multivariate decision tree). If a heterogeneous set of algorithms is used, the tree is known as a hybrid decision tree. Such a tree can use various algorithms in different subtrees, potentially combining for example uni- or multivariate decision trees with parametric supervised classifiers (Friedl & Brodley 1997).

Decision trees have various advantages compared to other classifiers. A wide variety of input data can be accepted, including both continuous and categorical data. Thus, ancillary data can easily be included. The simplicity of the structure of the classifier has the effect that it can be easily interpreted, and easily tested and refined if needed (Brown de Colstoun et al. 2003). Rogan, Franklin and Rogers (2002) found a decision tree to be significantly more accurate than a maximum likelihood supervised classifier in monitoring changes in forest vegetation in

California. Similarly, Friedl and Brodley (1997) reported decision trees to provide significantly higher accuracies than maximum likelihood, with hybrid decision trees performing better than uni- or multivariate decision trees. Brown de Colstoun et al. (2003) noted that the accuracy of a decision tree classifier was significantly higher than that of traditional classifiers and comparable to that of a neural network. However, the decision tree in their study was significantly less computationally intensive than the neural network.

2.2.3.4 Expert systems

Expert systems (ESs) use symbolic knowledge to mimic the reasoning of human experts in solving a problem, with the expectation of coming to similar conclusions (Skidmore 1989; Skidmore et al. 1996; Masocha & Skidmore 2011). In remote sensing, ESs have been used for user assistance, low-level processing, data fusion, GIS applications and classification (Tsatsoulis 1993). This research will only consider their role in the latter.

Structures of expert systems vary wildly, but two basic components can be identified: a knowledge base and an inference engine. The knowledge base stores the input data (remotely sensed and ancillary data), as well as the knowledge rules linking the data to the hypotheses (target classes). These knowledge rules are created during a learning phase, where distinguishable relationships between the data and the hypotheses are identified and formalized. The inference engine uses the knowledge base to infer logically-valid conclusions through controlling the order in which the rules and data are considered (Skidmore 1989; Skidmore et al. 1996; Cohen & Shosheny 2002; Masocha & Skidmore 2011). Two approaches to the implementation of inference engines exist: a sequence oriented approach and a state-oriented approach (Cohen & Shosheny 2002).

A sequence-oriented inference approach is followed when a set of definitive (binary) knowledge rules are to be applied in a specific order. Conversely, a state-oriented approach accounts for uncertainty and partial knowledge by associating expert-derived confidence values with each knowledge rule and it bases recognition decisions on convergence of evidence. In the former approach the inference engine consists of a simple tool applying the rules in order, and in the latter, a complex inferential mechanism is needed, such as that provided by the Dempster-Shafer or Gordon-Shortlife algorithms (Cohen & Shosheny 2002).

The flexibility of expert systems regarding input data is advantageous as ancillary data from diverse sources can be integrated with remotely sensed data. Also, prior knowledge of distributions of target classes can be captured in knowledge rules (Masocha & Skidmore 2011). Furthermore, additional data layers can easily be added at later stages of the classification

process without affecting existing rules (Skidmore 1989). However, a major disadvantage of expert systems is the time needed to develop an effective rule-base (Tseng et al. 2008). Also, expert systems are negatively influenced by increasing dimensionality of data (Li et al. 2010). As the number of input layers increase, their relation to the desired product classes becomes more difficult for the interpreter to comprehend.

Generally, existing research reports accuracy of expert system classifiers to be relatively high. Lewinsky and Bochenek (2008) achieved high (89%) overall accuracy in a SPOT-based general land-cover classification in Poland. Chen et al. (2009) found a significant improvement when comparing an object-based expert system classifier to an unnamed pixel-based traditional classifier (89% vs 69%). However, the expert system used LIDAR-derived surface data in addition to the Quickbird imagery used in the traditional classification. Sader, Ahl and Liou (1995) found an expert system to be significantly (8%) more accurate than an unsupervised classification, but found no significant difference between the expert system and a supervised/unsupervised hybrid classification. Several studies have combined expert systems with traditional or other alternative classifiers to achieve marked improvements in accuracy (Wilkinson et al. 1992; Lunetta & Balogh 1999; Liu, Skidmore & Van Oosten 2002; Nangendo, Skidmore & van Oosten 2007; Masocha & Skidmore 2011). Contrarily, Liu, Skidmore and Van Oosten (2002) found an expert system to be less accurate than both a maximum likelihood and a neural network classifier in classifying general landcover in the Netherlands.

In this section, the application of various classifiers in the context of remote sensing was considered. In recent research, these classifiers have increasingly been applied to meaningful image objects rather than to single image pixels. This is considered in the following section.

2.3 Object-based image analysis

Object-based image analysis (OBIA) aims to delineate and classify meaningful spatial units in an integrated way (Lang 2008). This can be contrasted with the more traditional pixel-based classification approaches which regard each pixel separately. It can be argued that a major limitation of pixel-based approaches is their disregarding of spatial concepts (Blaschke et al. 2000). Lang (2008) states that in such approaches geographical features are characterised only by their spectral attributes or related statistical attributes such as texture. (This statement arguably disregards alternative pixel-based classifiers which have the capacity to integrate ancillary data – see Section 2.2.3). Conversely, each image object in OBIA is aware of its context, neighbourhood and sub-objects. This means that geographical features can be characterised by their spatial, structural and hierarchical properties in addition to their spectral properties (Bock et

al. 2005; Lang 2008). Furthermore, objects offer additional spectral information that single pixels lack, including mean, median, minimum, maximum and variance values (Blaschke 2010). Using objects as classification units rather than pixels reduces spectral variation within classes and removes the so-called "salt-and-pepper" effect (Liu & Xia 2011). Also, the increased availability of fine spatial resolution satellite imagery has exposed further limitations of pixel-based techniques. For many applications the pixels of these images are significantly smaller than most objects of interest. In such cases it becomes more likely that most pixels will belong to the same classes as their neighbours (Blaschke et al. 2000; Lang 2008).

The building blocks of OBIA are termed segments (Blaschke 2010). They are created through the process of segmentation which divides an image into non-overlapping objects (Chen et al. 2009). Before the advent of OBIA this process was seen as being separate from classification; images were first segmented and then classified. However, this workflow disregards the role of scale. Segmentation attempts to delineate objects which are both homogenous and semantically significant, however the scale at which an object obtains semantical significance is dependent on the class represented in that object. Often, objects created at different scales need to be considered within the same image in order to perform an effective classification. Therefore, OBIA is an iterative process rather than a linear one and it is inextricably linked to concepts of multi-scale analysis (Lang 2008; Blaschke 2010).

This section will first regard the various segmentation algorithms available, and then the application of the previously investigated classifiers to OBIA.

2.3.1 Segmentation algorithms

Segmenting an image into a given number of objects is a problem with a very large set of possible solutions (Blaschke et al. 2000) and various algorithms exist that attempt to arrive at effective ones. The following groups are distinguished: point-based, edge-based and region-based algorithms, as well as combined algorithms (Blaschke 2010).

Point-based approaches use global threshold values to identify groups of homogenous elements (pixels) throughout a scene. Segmentation is performed in two steps. In the first, the category in which each element falls relative to the given thresholds is identified. In the second, all spatially connected elements falling in the same categories are grouped into regions. Threshold values can be static or dynamic (histogram-based). However, this approach is less suitable for remote sensing applications as spectral values for a given object will vary for different locations within a scene (Schiewe 2002).

In edge-based approaches, edges are regarded as object boundaries. They are identified through an edge-detection filter (e.g. a Sobel filter), and then transformed to object outlines through a contour-generating algorithm. The main drawback of such approaches is their sensitivity to noise (Blaschke et al. 2000; Schiewe 2002).

Region-based approaches compare available elements (pixels or existing regions) with other elements in an image to determine whether they are similar. Two approaches are distinguished: region growing (bottom-up) starts with seed pixels and grows into neighbouring elements, whereas region splitting (top down) starts with the entire scene and recursively splits it into smaller objects. Splitting algorithms can sometimes lead to oversegmentation, as non-homogenous regions are split into a predetermined number of subregions, however some algorithms can remerge newly formed subregions if they are similar (Schiewe 2002). One region-based approach that has been widely applied is the multiresolution segmentation algorithm implemented in eCognition (Trimble 2011b).

Multiresolution segmentation is a pair-wise region-merging algorithm which can take pixels or existing objects as input. Input elements are merged into a set of objects in such a way that the average heterogeneity for the set is minimised, while the respective homogeneities of the objects are maximised. A mutual-best-fitting approach is used for merging. In this approach the neighbourhood of a given seed object is evaluated and its best-fitting neighbour is identified. The neighbourhood of that neighbour object is then evaluated and if the seed object is also the best-fitting neighbour of that object they are merged, if not that object becomes the new seed. A merge is only performed if its cost is less than a specified degree of fitting (this threshold is termed the scale factor in eCognition). The algorithm continues looping until no more merges are allowed. The degree of fitting is defined according to a spectral homogeneity measure and a shape homogeneity measure (Baatz & Schäpe 2000; Trimble 2011a). eCognition allows one to specify homogeneity in terms of two parameters: shape and compactness. The shape criterion determines the degree of influence that object shape has compared to colour, while the compactness criterion determines the degree of influence that compactness has in comparison to smoothness. These values are specified as fractions of 1 (Trimble 2011b).

2.3.2 Classifiers in OBIA

Several classifiers have been successfully applied to object-based classifications. Rule-based expert systems feature prominently in the literature on OBIA. Lang (2008) lists them as one of the two methodological pillars of OBIA, implying that no other classifier is true to the principles of the paradigm. Expert systems attempt to model the complex network of knowledge and

experience that humans use to understand the information in an image, a network largely based on our perception of that image as a series of objects (Blaschke et al. 2000). Many of the wealth of additional features available in OBIA correspond to the features that enable us to understand such objects, making expert systems inherently suitable for OBIA. Several studies report good results when using expert systems in object-based classification. Whiteside and Ahmad (2005) found an object-based expert system to significantly outperform a pixel-based supervised classification in land-cover classification, and Chen et al. (2009) found the same for an urban study using a combination of LIDAR and Quickbird data. Drăguţ and Blaschke (2006) showed that an object-based expert system can be successfully applied to landform classification. Van der Sande, de Jong and de Roo (2003) described an object-based expert system that performed well in a complex land-cover classification for flood-risk assessment, although some difficulties were encountered.

Other researchers have noted some limitations of rule-based expert systems. As mentioned in Section 2.2.3.4, creating an effective rule-base is complicated and takes a lot of time, and expert systems are adversely influenced by increasing dimensionality of data. For these reasons, various studies have applied either other alternative classification algorithms or traditional supervised algorithms to OBIA. Li et al. (2010) compared a SVM classifier to a nearest-neighbour supervised classifier for object-based classification and the SVM was found to be more accurate. Mallinis et al. (2008) compared a decision tree to a nearest-neighbour supervised classification and revealed the decision tree to produce a significant increase in accuracy. Straatsma and Baptist (2008) successfully used a linear discriminant analysis supervised classifier in an object-based classification for the purpose of floodplain roughness parameterisation. Platt and Rapoza (2008), in a study evaluating different aspects of object-based classification, found a maximum likelihood classifier to achieve a significantly higher user's accuracy than a nearest-neighbour classifier, but a slightly lower producer's accuracy. Yet, the nearest-neighbour classification could be significantly improved by integrating it with an expert system. Several studies have applied the principle where a nearest-neighbour (or other statistical) classification based on spectral values is combined with an expert system formalising known spatial or structural relationships (Bock et al. 2005; Conchedda, Durieux & Mayaux 2008).

In this chapter, three important aspects of remote sensing-based classification of wetlands have been considered, namely the type of remote sensor and the classifier used, and the application of these in the OBIA paradigm. The following chapter will consider the selection of specific sensors as data sources, and the pre-processing of the data obtained from these sensors.

CHAPTER 3: SOURCING AND PREPROCESSING REMOTELY SENSED DATA

In the previous chapter relevant literature was assessed to determine the current state of knowledge on wetlands mapping. It was found that both SAR and VIR sensors feature prominently in existing research. Different aspects of the use of these datasets in this context were considered in order to determine the specific data needs of this study. In this chapter, available data sources are examined to determine which specific sensors' data best meets these needs. After the data is obtained, it is transformed into an appropriate projection and various undesirable effects of the terrain, atmosphere and sensor properties are compensated for to ready the data for analysis. Furthermore, various transformations are applied to the imagery to secure products that can ensure effective classification. Finally the assessment of the accuracy of remote sensing-based classification is considered.

3.1 RS data sourcing

Existing research has shown that SAR data, VIR data or a combination of the two can be successfully used for wetlands mapping (Lunetta & Balogh 1999; Töyrä & Pietroniro 2005; MacAlister & Mahaxay 2008; Jones et al. 2009). In this section, an inventory of available VIR and SAR data is created. Suitable data is then selected from this inventory based on cost and potential for wetlands mapping.

3.1.1 VIR sensors

Various factors have to be considered when selecting a specific source of VIR data for a classification project. The spatial, spectral and temporal resolutions are important factors, as is cost. Table 3.1 summarises the prominent VIR sensors. Modern sensors such as Ikonos, Quickbird, Worldview and GeoEye offer sub-metre spatial resolution (in panchromatic bands at least). But compared to sensors with lower spatial resolutions such as SPOT 5 and IRS P6, the aforementioned sensors have smaller image footprints on the ground and significantly higher costs per scene. Consequently, they were deemed unsuitable for this study as cost-effectiveness was an important requirement. Another option was the Landsat 5 (TM) and 7 (ETM+) sensors which have lower spatial resolutions than most of the other sensors considered here (15 m panchromatic) but higher spectral resolutions. Data from these Landsat sensors is available gratis over the Internet. Unfortunately the scan-line corrector of ETM+ has been inoperative since

2003, rendering large areas of any image unusable. Algorithms are available to correct this problem, but separate images taken shortly before or after the image in question are needed. Landsat TM was considered as an option, but no images for suitable dates were available. ASTER was also an interesting alternative, particularly due to its high spectral resolution. However its spatial resolution is relatively low at 15 m for visible and near-infrared (VNIR) bands and 30 m for short-wave infrared (SWIR) bands. Furthermore, no recent cloud-free imagery was available for the study area. This left SPOT and IRS as the most suitable options. Archival SPOT 5 data is available free of charge for South African academic use from the South African National Space Agency (SANSA) and its higher spatial (in panchromatic and pansharpened form) and spectral resolution make it the most appropriate choice.

Table 3.1: VIR sensor characteristics

Sensor	Bands	Spatial Resolution	Scene Footprint	Estimated cost per km^2 (Eurimage, archive, non-orthorectified, US$, 17-06-2012)
Quickbird	Panchromatic: 450-900 nm Multispectral: Blue: 450-520 nm Green: 520-600 nm Red: 630-690 nm NIR: 760-900 nm	Panchromatic: 0.61-0.72 m Multispectral: 2.44-2.88 m	272 km^2	$14 (pan or MS) $17 (pan/MS bundle)
Ikonos	Panchromatic: 450-900 nm Multispectral: Blue: 450-530 nm Green: 520-610 nm Red: 640-720 nm NIR: 770-880 nm	Panchromatic: 1 m Multispectral: 4 m	11 km (swath width)	$20 (pan or MS or pan/MS bundle)
GeoEye-1	Panchromatic: 450-800 nm Multispectral: Blue: 450-510 nm Green: 510-580 nm Red: 655-690 nm NIR: 780-920 nm	Panchromatic: 0.41 m Multispectral: 1.65 m	225 km^2	$25 (pan or MS or pan/MS bundle)

Table 3.1 continued

Sensor	Bands	Spatial Resolution	Scene Footprint	Estimated cost per km^2 (Eurimage, archive, non-orthorectified, US$, 17-06-2012)
Worldview-2	Panchromatic: 450-800 nm Multispectral: Coastal: 400-450 nm Blue: 450-510 nm Green: 510-580 nm Yellow: 585-625 nm Red: 630-690 nm Red edge: 705-745 nm NIR1: 770-895 nm NIR2: 860-1040 nm	Panchromatic: 0.46-0.52 m Multispectral: 1.85-2.07 m	224 km^2	$14 (pan) $35 (MS) $39 (pan/MS bundle)
SPOT 5	Panchromatic: 450-690 nm Multispectral: Green: 500-590 nm Red: 610-680 nm NIR: 790-890 nm SWIR: 1580-1750 nm	Panchromatic: 2.5 m Multispectral: 10 m SWIR: 20 m	3600 km^2	$0.95 (10 m MS) $1.89 (2.5 m pan)
IRS-P6 (LISS-IV)	Panchromatic: Any MS band Multispectral: Green: 520-590 nm Red: 620-680 nm NIR: 770-860 nm	5.8 m	490 km^2	$1.16 (MS)
Landsat TM and ETM+	Panchromatic (ETM+): 520-900 nm Multispectral: Blue: 450-520 nm Green: 520-600 nm Red: 630-700 nm NIR: 750-900 nm SWIR5: 1550-1750 nm SWIR7: 2080-2350 nm Thermal: 10400-12500 nm	Panchromatic: 15 m (ETM+) Multispectral: 30 m Thermal: 120 m (TM) 60 m (ETM+)	185 km (swath width)	Free (USGS)

Table 3.1 continued

Sensor	Bands	Spatial Resolution	Scene Footprint	Estimated cost per km^2 (Eurimage, archive, non-orthorectified, US$, 17-06-2012)
ASTER	VNIR: B1: 520-600 nm B2: 630-690 nm B3N/3B: 780-860 nm SWIR: B4: 1600-1700 nm B5: 2145-2185 nm B6: 2185-2225 nm B7: 2235-2285 nm B8: 2295-2365 nm B9: 2360-2430 nm TIR: B11: 8475-8825 nm B12: 8925-9275 nm B13: 10250-10950 nm B14: 10950-11650 nm	VNIR: 15 m SWIR: 30 m TIR: 90 m	3600 km^2	$0.03

It should be noted that SANSA resamples the mid-infrared band of SPOT 5 from 20 m to 10 m upon retrieving the data from the sensor, so that it matches the other bands. Cubic convolution resampling is used (Padayachee 2011, pers com).

3.1.2 SAR imagery

Compared to VIR data, more factors are at play when a source of SAR data is to be selected for use in a specific classification. As mentioned in Section 2.1.2, polarisation, wavelength, incidence angle and spatial resolution are important factors, as is cost. Table 3.2 lists the characteristics of commonly used SAR sensors. Ideally quad-polarised data with high spatial resolution and a combination of bands should be used for wetlands mapping, but this is a costly option, particularly if large areas are to be classified. Quad-polarised data is available for C-band (RADARSAT-2) and X-band (TerraSAR-X), and it was available until recently for L-band (ALOS-PALSAR was decommissioned in May 2011; ALOS 2 is planned for launch in 2013). Dual-polarised datasets offer a slightly less expensive option and they are available for the aforementioned sensors, as well as for Envisat-ASAR. Single-polarisation data would be the cheapest to acquire and it is available for all the aforementioned sensors, as well as for ERS-2 and RADARSAT-1. Regrettably, a major limiting factor in this study was data unavailability as

few sensors had archival data available covering the study area. Tasking a sensor to obtain new data would have been prohibitively expensive even for a feasibility study.

Table 3.2: SAR sensor characteristics

Sensor	Bands	Polarisations	Spatial Resolution	Estimated cost per km^2 (Eurimage, archive, non-orthorectified, US$, 17-06-2012)
ERS-2 SAR (decommissioned)	C	VV	30 m	$0.05
Envisat ASAR (decommissioned)	C	VV HH VV+HH HV+HH VH+VV	30 m	$0.05
RADARSAT-1	C	HH	Fine: 8 m Std: 30 m Wide swath: 30 m	$1.41 (Fine) $0.35 (Std) $0.15 (Wide)
RADARSAT-2	C	HH VV HV VH HH+HV VV+VH HH+VV+HV+VH	Single pol: 3 m, 10 m Dual pol: 10 m, ~28 m (depending on incidence angle) Quad pol: 10 m, ~28 m	$13.19 (3 m single-pol) $1.40 (10 m single-pol) $1.49 (10 m dual-pol) $0.35 (25 m single-pol) $0.37 (25 m dual-pol) $8.44 (any quad-pol)
TerraSAR-X	X	HH VV HH+VV HH+HV VV+VH HH+HV+VH+VV (designated missions only)	1 m, 3 m or 16 m, depending on mode	$85.30 (1 m single- or dual-pol) $42.65 (2 m single- or dual-pol) $1.57 (3 m single- or dual-pol) $0.12 (16 m single- or dual-pol) **(Prices from Astrium)**

Table 3.2 continued

Sensor	Bands	Polarisations	Spatial Resolution	Estimated cost per km^2 (Eurimage, archive, non-orthorectified, US$, 17-06-2012)
ALOS PALSAR (decommissioned)	L	HH VV HH+HV VV+VH HH+HV+VH+VV	Single pol: 7-44 m Dual pol: 14-88 m Quad pol: 24-89 m	$0.13 (Fine resolution) $0.32 (Polarimetric) **(Prices from ALOS-Pasco)**

An examination of the inventory of available imagery revealed that several ERS-2 SAR images of the study area were available. Single band, single polarisation SAR data has some limitations, but it has been found that C-band, single polarisation SAR can be effectively combined with SPOT for wetlands classification (Töyrä & Pietroniro 2005). Furthermore, the C-band and VV polarisation combination employed by ERS2 had proved to be the most effective single combination at identifying herbaceous wetlands in research by Pope et al. (1997). These findings, along with the importance of cost-effectiveness as a criterion, prompted the selection of ERS-2 as the source of SAR data for this study. An application was submitted to ESA for registration as a category-1 (academic) user and two ERS-2 SAR images were requested. The application was successful.

3.2 Preprocessing

This section covers the preprocessing steps needed to prepare the VIR and SAR imagery used in this study for analysis.

3.2.1 VIR imagery

Various preprocessing procedures must be applied to raw VIR satellite imagery to prepare it for further analysis. Orthorectification corrects geometric errors caused by sensor geometry and terrain, radiometric correction corrects radiometric errors caused by earth's atmosphere and topographic shadows and, optionally, pan-sharpening fuses high spectral resolution multispectral imagery with high spatial resolution panchromatic imagery. Preprocessing of the VIR imagery was performed in PCI Geomatica software (versions 10.2 and 10.3). The SPOT image used in this study was obtained in RAW format, and the first correction applied to it was orthorectification.

3.2.1.1 Orthorectification

Geometric correction aims to transform a remotely sensed image in such a way that it obtains the scale and projection properties of a specific map projection. Two basic approaches are followed. The first uses orbital models that model known geometric errors mathematically to inversely transform the image so that it fits the required projection. This method requires precise information about the orbit of the platform and the characteristics of the sensor. The second method uses a set of points with known coordinates (known as ground control points or GCPs) to model geometric distortion present in the image and then uses this model to compute an empirical transformation to relate the image to its true coordinates (Mather 2004; Chuvieco & Huete 2010). When geometric correction also applies terrain data to correct for topographical displacement, the process is known as orthorectification (ERDAS 2010).

In this study, orthorectification was performed in PCI OrthoEngine. An orbital model (Toutin's model) was used to model geometric errors. Toutin's model requires a limited number of GCPs. These were collected from a set of orthorectified colour aerial images with a spatial resolution of 0.5 m for the rectification of the panchromatic image and subsequently from the orthorectified panchromatic image for the rectification of the multispectral image. The aerial photographs had been acquired in 2005 by South Africa's Chief Directorate for National Geo-spatial Information (NGI). The output projection for orthorectification was set to Gauss Conform projection, a polysuperficial version of the Transverse Mercator projection. The LO19 coordinate system was used throughout the study. The elevation source was a contour-derived DEM with a spatial resolution of 20 m. The resampling method used was bilinear interpolation, which avoids the noticeable positional errors associated with nearest-neighbour resampling, but does not alter pixel values as much as cubic convolution resampling (Campbell 2002). The resulting orthorectified images were compared with the aerial photographs. No significant offsets were present, indicating that the quality of the orthorectification was good. This was affirmed by low root mean squared (RMS) error values, which evaluate the goodness of fit of the orthorectification model (Mather 2004). For the panchromatic image the X RMS error was 0.38 pixels and the Y RMS error was 0.39 pixels. For the multispectral image the X and Y RMS errors were both 0.32 pixels.

3.2.1.2 Radiometric calibration and correction

During radiometric preprocessing the brightness values of an image are adjusted to compensate for sensor malfunctions and atmospheric influences (Campbell 2002). VIR imagery obtained from data suppliers usually represents radiation as relative radiation, denoted as digital numbers

(DNs). However, if values from different images are to be compared, this relative radiation has to be converted to physical parameters such as radiance or reflectance. Radiance is the total amount of energy emitted per unit area as viewed through a unit solid angle. Radiance can be used to compare images taken at the same time from different sensors or to generate ratios such as NDVI (see Section 3.3.1). However, if images taken at different times are to be compared, reflectance should be calculated. Reflectance is the ratio between the amount of energy incident upon a surface and the amount of energy reflected by that surface. It compensates for differences in solar irradiation. Calibration parameters for the specific sensor at the time of the image acquisition are required by these calculations and these are usually stored in the header accompanying the image file. However, to obtain true reflectance or radiance values for the surface of the earth, atmospheric correction should be applied in addition to these calculations (Mather 2004; Chuvieco & Huete 2010; Lück et al. 2010).

Atmospheric correction aims to eliminate the contribution of the atmosphere to brightness values in remotely sensed imagery, leaving only the contribution of earth-surface reflectance. Four main approaches to this problem exist. The first involves the use of in situ measurements of atmospheric conditions. Although this method is accurate, it is limited by its requirement of such measurements having been taken at the time and location of image acquisition. The second technique is relatively new and involves the simultaneous use of two or more sensors (usually on the same platform), where one is designed to measure the returns from the earth surface and the other(s) to measure atmospheric properties. This method is promising, but it is limited to platforms designed for this purpose (e.g. Terra). The third approach involves the use of physically-based radiative transfer models. Their accuracy is dependent on the availability of external data required for model calibration, as well as the validity of the assumptions made by the model. Popular algorithms in this category include 6S, FLAASH and ATCOR 2 and 3. The fourth approach is based only on the image itself and involves the use of objects with known optical properties, as well as known interrelationships between spectral bands. The most popular methods in this category are probably the dark-object-based methods (Campbell 2002; Chuvieco & Huete 2010).

Another aspect of radiometric correction is the removal of the effects of topography. In rough terrain, incident energy is affected significantly by slope and aspect. As the amount of reflected energy varies with variations in incident energy, these effects need to be accounted for. Various algorithms addressing this problem are available. Notably, the ATCOR3 algorithm combines an atmospheric correction based on a physical radiative transfer model with topographic correction.

PCI's implementation of ATCOR 3 was used for radiometric correction in this study, although ATCOR 2 could also have been used as the effects of topography are limited in the study area.

3.2.1.3 Pan-sharpening

Image fusion, or pan-sharpening, refers to the fusion of high spatial resolution panchromatic data with lower spatial resolution, higher spectral resolution multispectral data to obtain a combined dataset with both high spectral and spatial resolution. Most modern remote sensing platforms carry both a higher spatial resolution panchromatic sensor and a lower spatial resolution multispectral sensor (e.g. SPOT, IRS, Landsat7, Ikonos and Quickbird). Effective fusion techniques can significantly extend the applications of the data they provide (Zhang 2004).

A wide range of image fusion techniques are available; the most popular ones include those based on intensity-hue-saturation (IHS) transforms, principal components analysis (PCA) transforms, arithmetic combinations and wavelet base fusion. However, the longer spectral range detected by panchromatic sensors of some newer platforms has proved problematic for some traditional fusion techniques. One approach that overcomes this issue is the statistical fusion approach followed by the PANSHARP module in PCI Geomatica. It uses the least-squares technique and a set of statistical calculations, and it is less prone to colour distortion and operator dependency than other approaches (Zhang 2004). This module was used in this study.

3.2.2 SAR sensors

SAR preprocessing is significantly more complicated than VIR preprocessing, largely due to the complicated nature of the SAR system. An overview of the most important steps is given here. All preprocessing steps were performed with the use of the open-source software package NEST. Versions 3B and 3C were originally used, but all processing of images used in the final classification analysis was done in version 4A. As with VIR sensors, data is available from providers at various levels of preprocessing. The following six steps will be considered here: focusing, antenna pattern correction, multi-looking, geocoding, radiometric calibration and correction and speckle filtering. The two SAR images used in this study were obtained in SLC format, meaning that focusing had already been performed. However it will be briefly considered for the sake of completeness.

3.2.2.1 Focusing

Raw data from SAR images is difficult to work with and needs to be processed with specialised software to be usable (Woodhouse 2006). In raw SAR images the energy returned from any point target is spread through range and azimuth. Range refers here to slant range which is the

actual range measured by the sensor as derived from the time delay of an echo. This can be translated to ground range if it is assumed that the earth's surface corresponds to a chosen reference surface (Woodhouse 2006). The spreading in (slant) range is determined by the duration of the transmitted pulse, and the spreading in azimuth is determined by the duration of the illumination of the target. SAR focusing combines the dispersed energy from a point target into a single output image pixel through range and azimuth compression. The result of this process is a single-look complex (SLC) image which relates amplitude to radar reflectivity and phase to acquisition geometry and earth topography (Sarmap 2009; ESA s.a.).

3.2.2.2 Antenna pattern correction

The first SAR preprocessing step performed in this study was antenna pattern correction. This operator removes antenna pattern and range spreading loss corrections originally applied to the data. Its application is dependent on the software and data used. When a slant-range product (such as SLC) is corrected in NEST, a replica pulse power correction is performed and an analogue to digital converter (ADC) power-loss correction is applied (Laur et al. 2004; NEST 2010).

3.2.2.3 Multi-looking

In a single-look complex image, the entire synthetic aperture and signal history is used to provide an image that has the highest possible resolution, but also high levels of speckle (Sarmap 2009; ESA s.a.). Speckle is the grainy, so-called "salt-and-pepper" noise found in all coherent imaging systems. It is a result of interference between the coherent echoes of different scatterers within a resolution cell. Multi-looking addresses the speckle problem by dividing the synthetic aperture into several synthesised "sub-apertures," known as looks. Separate images are created for the different looks, representing different perspectives on the same targets and having azimuthal resolutions poorer than the azimuthal resolution of the original image by a factor of the number of looks. These images are then incoherently averaged, i.e. only the amplitudes are averaged, not the phase angles, and a multi-looked image is obtained (Woodhouse 2006). Multi-looking was performed in this case with one range look and five azimuth looks, which produced a multi-looked image with approximately square pixels with a spatial resolution of approximately 20 metres.

3.2.2.4 Geocoding

A geocoded image is a SAR image that has been projected onto the topography of the earth so that topographic distortions are removed and each pixel lies at its correct location. Such an image is equivalent to an orthorectified VIR image (Woodhouse 2006).

The most commonly used method for SAR image geocoding is the range-Doppler approach, which calculates the relationship between the sensor, each backscatter element, and their respective velocities. Thus, the imaging and processing geometries are completely reconstructed, topographic effects are accounted for, and the influence of the earth's surface topography and rotation on Doppler frequency shift and azimuth geometry is taken into consideration. This approach is usually implemented using a backwards solution, with the DEM as starting point (Woodhouse 2006).

Another possible method is the SAR-simulation terrain correction. In this approach the DEM, the orbit state vectors and geocoding information from the original SAR image, as well as a mathematical model of the SAR imaging geometry, are combined to generate a simulated SAR image. This image is then co-registered to the original image and a warp function relating each pixel in the simulated image to its corresponding pixel in the original image is produced. During terrain correction each pixel in the DEM is related to its corresponding pixel position in the simulated SAR image through the SAR model, which is then related to its corresponding pixel position in the original SAR image through the warp function. The pixel value for the geocoded image is then obtained by interpolation of the original image (NEST 2010).

The GCP and empirical transformation-based method described in Section 3.2.1.1 is also sometimes used for the correction of SAR imagery. However, this method will only produce reasonable results when topographical variation is minimal, as geometric distortions in SAR imagery is too variable and sometimes too localized in small areas. Images produced in this way are said to be geocorrected, but they are not truly free of geometric distortions (Woodhouse 2006).

Terrain correction cannot remove radar layover or shadow effects caused by the side-looking architecture of SAR systems. Radar shadow occurs in areas that are obscured from the sensor by topographical or other features; these areas contain no data and are merely projected to their correct location. Foreshortening occurs when upward (from nadir) slopes are projected as narrower than equivalent downward slopes. Layover is an extreme case of foreshortening, where the top of an object (e.g. a mountain) is closer to the sensor than the base of the object and is wrongly mapped as being closer to nadir than the base (i.e. the object/mountain appears to topple

over). Layover areas have to be recreated from a small number of slant range pixels representing a larger area on the ground (Woodhouse 2006).

Range-Doppler terrain correction was applied in this study. The same DEM used for VIR preprocessing was used for terrain correction. The range-Doppler terrain correction operator in NEST also performs radiometric calibration and normalisation. This is explained in the following sub-sections.

3.2.2.5 Radiometric calibration and normalisation

Radar backscatter is the ratio between the energy transmitted and received by a radar sensor. If backscatter from different images is to be compared, calibration is necessary. This is especially true for images from different sensors or differently processed images from the same sensor (ESA s.a.). Three calibrated measures of backscatter are of note. Sigma nought (σ^0) is the backscattering coefficient, also known as the normalised radar cross-section. The radar cross-section quantifies the effectiveness of a scatterer and this value is normalised in σ^0 so that it relates to a unit area. σ^0 is the measure most commonly used in radar remote sensing. Beta nought (β^0) is the radar brightness and it is most often used when the topographical information required to compute the area values for the calculation of σ^0 is missing. Gamma (γ) normalises the backscattering coefficient by the cosine of the local incidence angle. It is useful when an extended volume scattering target (e.g. a forest) is considered, as in that case it stays approximately constant with variation in incidence angle and σ^0 does not. The following equations relate these three measures:

$$\sigma^0 = \frac{\beta^0}{\sin \theta_i}$$

$$\gamma = \frac{\sigma^0}{\cos \theta_i}$$

(Woodhouse 2006, θi represents the local incidence angle).

However, after calibration is applied variations in backscattering coefficient values are still clearly evident in the range direction. This is caused by the dependence of backscatter on the radar look angle, and is usually normalised by use of a modified cosine correction (ESA s.a.). As mentioned earlier, NEST integrates radiometric calibration and normalisation into their terrain correction operator. In this case, the terrain-corrected image was also calibrated to σ^0 and normalised. The resulting image was then converted to decibel (dB) units for further analysis.

3.2.2.6 Speckle filtering

Significant amounts of speckle remain in SAR imagery even after multi-looking. During postprocessing various filters can be applied which further reduce its occurrence. In the simplest case a mean or median filter can be applied. However, these are not optimal and several filtering algorithms have been especially developed for SAR imagery. Some of the more popular ones are summarised here. For these algorithms, as with the simpler mean and median algorithms, it is important to select an appropriate moving window size. Too large a window will result in a loss of spatial resolution, but too small a window will be ineffective at removing speckle (ESA s.a.).

The Lee, Lee-Sigma and refined Lee filters are based on the assumption of a Gaussian distribution in image noise. The Lee filter assumes that the mean and variance of the pixel being considered is equal to the local mean and variance of all pixels within the selected neighbourhood (Mansourpour, Rajabi & Blais 2006). The refined Lee filter works in a similar way, but it computes the mean and variance from a reduced set of neighbourhood pixels: those pixels separated from the focal pixel by an edge are left out (Lee 1981). In NEST, this filter is combined with an edge threshold: if local variance is less than this threshold, a local statistics filter is performed, if not the refined Lee filter is performed (NEST 2010). The Lee-Sigma filter assumes that 95.5% of random pixels fall within a range of two standard deviations. The pixel of interest is replaced with the average of all pixels in the selected window falling within that range (Mansourpour, Rajabi & Blais 2006).

Conversely, the Gamma-MAP filter assumes a Gamma distribution in image noise. It is based on a multiplicative noise model, with mean and variance parameters which are non-stationary, and it combines geometrical and statistical properties of the local area (Mansourpour, Rajabi & Blais 2006).

The local region filter divides the moving window kernel into eight geographical regions (N, S, W, E, SW, SE, NW, NE) and replaces the central pixel value with the mean for the region with the lowest variance (Mansourpour, Rajabi & Blais 2006).

The Frost filter replaces the value of the pixel being considered with a weighted sum of the values of the other pixels in the selected window. The weighting factors decrease with distance from the kernel, but increase for central pixels with an increase in kernel variance (Mansourpour, Rajabi & Blais 2006).

Speckle filtering was performed in this study on the calibrated images. After experimenting with different methods, first a Refined Lee filter was applied with edge threshold of 10, and then a Gamma MAP filter with a 3x3 window was applied to the result. The reasoning was that the

Refined Lee filter seemed to preserve edges well, but created an image that still contained higher levels of speckle than desired. However, extreme cases of speckle had been removed which meant that using this image as an input for Gamma MAP filtering provided more satisfactory results than simply using the unfiltered image. The 3x3 window was selected in order to minimise the loss of effective spatial resolution; larger windows would have removed more speckle. However, maintaining spatial resolution was deemed more important than removing all possible speckle effects, especially since the spatial resolution of the SPOT image was substantially higher than that of the SAR images.

3.2.3 Preprocessing problems

Originally, this research intended to study the wet and dry seasons of 2008. A SPOT image of the study area for March 2008 was obtained from SANSA in July 2009 and had been preprocessed successfully. Furthermore, De Hoop, a large and significant wetland system toward the east of the study area, was being considered for inclusion in the research. SPOT images of this area for January and December 2008 had also been obtained and preprocessed.

ERS-2 images covering the entire area had also been obtained for September and December 2008. However, the preprocessing of these images proved to be problematic. Radiometric correction of the September image resulted in a σ^0 image with an artefact in the form of a bright strip along the eastern edge. The original suspicion was that this was caused by software error. This was tested by running the radiometric calibration of the image on SARSCAPE software. This appeared to confirm the suspicion, as no bright strip was visible in the resultant image. However, further correspondence with the developers of NEST and ESA revealed that the artefact was caused by sensor error. From February to 24 November 2008 there was an error in the pointing of the ERS-2 SAR sensor at certain latitudes, resulting in a shift of the mean incidence angle, and therefore the antenna pattern, by one degree or more. This meant that no data for this period could be correctly calibrated (Lu 2010, pers com). The problem was not visible in SARSCAPE as the software extrapolated the antenna pattern for the invalid range.

The implication of this problem was that, for this area, all ERS-2 imagery acquired during the 2008 wet season was rendered unusable. Alternatives considered at this point included sourcing 2008 SAR imagery from a different sensor, or continuing the study with only VIR imagery. Further investigation led to a better option, namely to continue using ERS-2 but to obtain images for the 2009 wet season (September 2009) and for the 2009/2010 dry season (February 2010). This meant that the SPOT imagery obtained earlier was no longer applicable; consequently a new SPOT image from January 2010 was acquired from SANSA. Unfortunately, again there

were no cloudless wet season SPOT images available. This time round all SAR and VIR images were preprocessed successfully. However, it was decided not to include the De Hoop area in the study, due to time constraints and the fact that it did not fall within the boundary of the new SAR images.

3.2.4 Subset selection

Shifting the study period to a later date presented further problems regarding the selection of the specific study area subsets. Subsetting is common practice in remote sensing based classification studies as it speeds up processing and limits the study to areas that are relevant to its specific objectives. The study was initially intended to focus on the wetlands in the Agulhas National Park. A preliminary field visit was undertaken in November 2009, and some field verification data was collected. Unfortunately, much of the park was ravaged by a veld fire during December 2009, including most of the sites where preliminary field data had been collected. The occurrence of the fire between the dates of the two SAR images complicated matters. The effects of the removal of the vegetation cover on the backscatter observed from the SAR images are difficult to gauge, and might be confused with the effects of the changes in soil moisture or inundation levels expected in wetland areas between the two dates. Consequently, no burnt areas were included in the final classification subsets. Two subsets were selected, both of which include a diverse range of wetlands. These subsets were described in Section 1.7.2. The western subset includes various wetlands in the Nuwejaars River system and it is referred to henceforth as the Nuwejaars subset. The eastern subset includes Soetendalsvlei and its surrounding wetlands, as well as the Heuningnes River and its estuary. It is referred to as the Soetendalsvlei subset. The two subset areas are illustrated in Figure 1.3 and Figure 1.5.

Subsetting of images was performed in PCI Focus, but before this task could be completed the SAR images had to be projected. NEST only supports a limited number of projections, and does not allow editing of the parameters of those projections that it does support, so the LO19 projection used throughout this research was not supported. Thus, products generated in NEST were kept in geographic projection and reprojected to LO19 in PCI Focus, with a 20-metre spatial resolution being specified. Furthermore, eCognition requires all input imagery to have the same spatial resolution and extent. This meant that the SAR imagery had to be resampled and registered to the SPOT imagery. This task was also performed in Focus. The SAR images were first clipped to an extent slightly larger than that of the SPOT subsets, then resampled to 2.5-metre spatial resolution using nearest-neighbour resampling, then clipped to the actual extent of the SPOT images. At that point, the dimensions and pixel sizes of the images matched, but the

actual extents were still not exactly registered as the clipping tool does not shift the pixels of the input image. This was rectified by manually changing the bounding coordinates of the SAR image to those of the SPOT image. The effect of these procedures was that the maximum amount of displacement occurring between pixels in the original (projected) SAR images and the equivalent 8x8-pixel blocks in the resampled SAR images was less than 2.5 metres.

3.3 Image transforms

Various methods are available to extract more information from remotely sensed imagery than simply the spectral values in the bands. Vegetation indices and other indices combining different spectral bands will be considered here, along with texture and object-based shape metrics. All indices used in this study were calculated through EASI scripts implemented in PCI, and the texture measures were calculated through built-in modules in PCI, or EASI scripts where applicable. Object-based shape metrics were calculated in eCognition.

3.3.1 Vegetation indices

Vegetation indices (VIs) attempt to measure biomass or vegetative vigour. Combinations of different VIR spectral values are used to derive a VI value for each pixel (Campbell 2002). Various VIs make use of the properties of vegetation in the red and near-infrared bands: vigorous vegetation reflects strongly in the near infrared band, but absorbs radiation in the red band (Campbell 2002; Mather 2004).

The normalised difference vegetation index (NDVI) is one of the best-known VIs. This index uses the spectral values from the red and near-infrared bands. The difference between these two bands is computed and normalised so that the resulting index has a range that varies between limits that provide desirable statistical properties. It ranges from -1 to 1, and increases with increasing vegetation vigour (Mather 2004). The index is expressed as:

$$NDVI = \frac{\rho_{NIR} - \rho_{RED}}{\rho_{NIR} + \rho_{RED}}$$ (Campbell 2002)

where ρ_{NIR} is the reflectance in the near-infrared band; and

ρ_{RED} is the reflectance in the red band.

NDVI has some limitations. It saturates in high vegetation cover and canopy background variation in arid and semi-arid areas causes it to vary appreciably; both situations can lead to inaccurate assessment of vegetative cover. Other vegetation indices are available which extend the range of VIs into densely and sparsely vegetated areas, for example the enhanced vegetation index (EVI, formerly known as $SARVI_2$) and the soil-adjusted vegetation index (SAVI) (Huete

et al. 1997). However, in cases where soil type is relatively constant and atmospheric interference minimal, NDVI has been shown to be a better predictor of percentage vegetative cover than EVI and SAVI (Nagler, Glenn & Huete 2001).

EVI is sensitive to higher levels of biomass, but is only minimally affected by the influences of soil and atmospheric particles. However, EVI's applications are limited by its requirement for a blue band, which is lacking in several satellite-borne VIR sensors. EVI_2, a modified version of EVI which does not use the blue band, has been introduced recently. The difference between this modified index and EVI is insignificant when applied to areas free of snow and ice where atmospheric interference is minimal (Jiang et al. 2008). EVI and EVI_2 are symbolised as:

$$EVI = 2.5\,\frac{\rho_{NIR}-\rho_{RED}}{\rho_{NIR}+6\rho_{RED}-7.5\rho_{BLUE}+1}\ \text{(Jiang et al. 2008; constants defined for MODIS); and}$$

$$EVI_2 = 2.5\frac{\rho_{NIR}-\rho_{RED}}{\rho_{NIR}+2.4\rho_{RED}+1}\ \text{(Jiang et al. 2008)}$$

where ρ_{NIR} is the reflectance in the near-infrared band;

ρ_{RED} is the reflectance in the red band; and

ρ_{BLUE} is the reflectance in the blue band.

SAVI aims to minimise soil brightness influences (Huete 1988). The modified soil-adjusted vegetation index ($MSAVI_2$) is a modification of SAVI. The formula for SAVI includes a constant soil-adjustment factor, L, which attempts to minimise soil influences on canopy spectra. This is replaced with a variable L function in $MSAVI_2$, which varies with the amount of vegetation present. Compared to SAVI, $MSAVI_2$ has a greater dynamic range and further minimises soil background influences (Qi et al. 1994). SAVI and $MSAVI_2$ are expressed as:

$$SAVI = \frac{\rho_{NIR}-\rho_{RED}}{\rho_{NIR}+\rho_{RED}+L}\times(1+L)\ \text{(Huete 1988; L specified as 0.5); and}$$

$$MSAVI_2 = \frac{2\rho_{NIR}+1-\sqrt{(2\rho_{NIR}+1)^2-8(\rho_{NIR}-\rho_{RED})}}{2}\ \text{(Qi et al. 1994)}$$

where ρ_{NIR} is the reflectance in the near-infrared band;

ρ_{RED} is the reflectance in the red band; and

L is the soil adjustment factor.

NDVI, $MSAVI_2$ and EVI_2 were implemented in this study.

3.3.2 Other indices

Lacaux et al. (2007), in a classification of ponds in the African rift valley, introduce two indices potentially useful for a study on wetlands. The first, termed the normalised difference pond index (NDPI), combines mid-infrared (SWIR) and green radiation, and it has been shown to effectively discriminate small and medium ponds from other land-cover types. This index corresponds to, but switches the terms of, an earlier index introduced by Xu (2006), called the modified normalised difference water index (MNDWI). These indices are:

$$NDPI = \frac{\rho_{MIR} - \rho_{GREEN}}{\rho_{MIR} + \rho_{GREEN}} \text{(Lacaux et al. 2007); and}$$

$$MNDWI = \frac{\rho_{GREEN} - \rho_{MIR}}{\rho_{GREEN} + \rho_{MIR}} \text{(Xu 2006)}$$

where ρ_{MIR} is the reflectance in the mid-infrared band; and

ρ_{GREEN} is the reflectance in the green band.

The second index useful for studying wetlands is termed the normalised difference turbidity index (NDTI). It combines red and green radiation and is able to differentiate turbid water from clear water. Clear water is characterised by low reflectance in the green band and even lower (almost none) reflectance in the red band. However, highly turbid water behaves in a manner analogous to bare soils, which reverses the relationship between red and green radiation (Lacaux et al. 2007). NDTI is derived as:

$$NDTI = \frac{\rho_{RED} - \rho_{GREEN}}{\rho_{RED} + \rho_{GREEN}} \text{(Lacaux et al. 2007)}$$

where ρ_{RED} is the reflectance in the red band; and

ρ_{GREEN} is the reflectance in the green band.

The normalised difference water index (NDWI) was introduced by Gao (1996). It combines near- and mid-infrared radiation to measure vegetation liquid water content. The index was defined in terms of MODIS wavelengths, with a 1.24 μm SWIR band specified, but Davranche, Lefebvre and Poulin (2010) successfully applied it to the 1.58-1.75 μm SWIR band of SPOT. NDWI is calculated as:

$$NDWI = \frac{\rho_{NIR} - \rho_{MIR}}{\rho_{NIR} + \rho_{MIR}} \text{(Gao 1996)}$$

where ρ_{MIR} is the reflectance in the mid-infrared band; and

ρ_{NIR} is the reflectance in the near-infrared band.

McFeeters (1996) proposed an index which is also called the normalised difference water index. The name is perhaps more appropriate for this index than for the Gao (1996) index as this index attempts to identify open water. This is achieved by quantifying the relationship between the green and near-infrared bands. To avoid confusion with Gao's index, this research refers to it as NDWIF (normalised difference water index of McFeeters) throughout, following Davranche, Lefebvre and Poulin (2010). NDWIF is expressed as:

$$NDWIF = \frac{\rho_{GREEN} - \rho_{NIR}}{\rho_{GREEN} + \rho_{NIR}} \text{(McFeeters 1996; Davranche, Lefebvre \& Poulin 2010)}$$

where ρ_{NIR} is the reflectance in the near-infrared band; and

ρ_{GREEN} is the reflectance in the green band.

Another index also labelled normalised difference water index is proposed byTakeuchi and Yasuoka (2004). Like NDWIF, it attempts to identify open water (Kouchi & Yamazaki 2007), but it quantifies the relationship between red and mid-infrared radiation. This index has been successfully applied to mapping Tsunami-affected areas (Kouchi & Yamazaki 2007), inundated rice paddies (Yamaguchi et al. 2010) and land surface water coverage (Mori, Takeuchi & Sawada 2009). To avoid confusion, this research will refer to it as NDWIT (normalised difference water index of Takeuchi). It is calculated as:

$$NDWIT = \frac{\rho_{RED} - \rho_{MIR}}{\rho_{RED} + \rho_{MIR}} \text{(Takeuchi \& Yasuoka 2004)}$$

where ρ_{MIR} is the reflectance in the mid-infrared band; and

ρ_{RED} is the reflectance in the red band.

The difference between vegetation and water (DVW) is another index that could be applicable to wetland studies and is simply the difference between NDVI and NDWI (Gond et al. in Davranche, Lefebvre & Poulin 2010). DVW represents the difference between vegetation vigour and vegetation water content and is expressed as:

$DVW = NDVI - NDWI$ (Gond et al. in Davranche, Lefebvre & Poulin 2010).

3.3.3 Texture

Texture is the tonal variability within a specific neighbourhood of pixels. Its application to remote sensing is highly scale-dependent: the scale of the feature under investigation has to be considered, as well as the scale of the data used (Mather 2004). The grey level co-occurrence matrix (GLCM) was the first published approach to the quantification of texture in remote sensing, and it remains one of the most popular (Arzandeh & Wang 2002; Mather 2004). The

matrix represents the distant and angular spatial relationships over a specified region within an image. It was originally proposed by Haralick, Shanmugam and Dinstein (1973) who defined 14 different textural measures that could be computed from it, although not all of them are commonly used (Mather 2004). Baraldi and Parmiggiani (1995), in a study investigating the statistical meaning of specific GLCM parameters, name energy (angular second moment), contrast, variance, correlation, entropy and inverse difference moment (homogeneity) as the most relevant. Arzandeh and Wang (2002), in a study of the use of GLCM texture in wetlands classification from SAR data, use the same measures listed above, except that standard deviation is substituted for variance, and mean is added. These GLCM measures can be summarised as follows:

- Energy, or angular second moment, is a measure of textural uniformity; high energy values are associated with either a constant or periodic grey-level distribution over a window (Baraldi & Parmiggiani 1995).
- Contrast measures the amount of local variation in an image (Haralick, Shanmugam & Dinstein 1973).
- Variance is a measure of heterogeneity. It increases when grey-level values in a window differ from their mean (Baraldi & Parmiggiani 1995).
- Standard deviation is the square root of the GLCM variance (Arzandeh & Wang 2002).
- Correlation measures the linear dependencies of grey tones in an image; high values imply a linear relationship between pixel pair grey levels (Baraldi & Parmiggiani 1995; Arzandeh & Wang 2002).
- Entropy measures image disorder; high entropy is associated with very small values in GLCM elements caused by an image that is not texturally uniform (Baraldi & Parmiggiani 1995; Arzandeh & Wang 2002).
- Inverse distance moment is also known as homogeneity; high levels of homogeneity are associated with low differences between grey-level pairs (Baraldi & Parmiggiani 1995; Arzandeh & Wang 2002).
- Mean measures both tone and texture information. It incorporates the grey level of each GLCM line in the calculation of texture (Arzandeh & Wang 2002).

GLCM texture measures were calculated only for the SAR images in this project. PCI's TEX module was used for the calculation and parameters were chosen based on the strength of conclusions drawn in a comprehensive study by Arzandeh and Wang (2002) on the use of GLCM texture in wetlands classification with SAR imagery. Following their recommendations,

directional invariant orientation was used, and windows of 11x11 and 25x25 were selected. A 17x17 window size had been recommended, but the TEX module only offers certain fixed window sizes. Also, their study was based on RADARSAT-1 images which have a higher spatial resolution at 6.25 m, suggesting that a smaller window size might be appropriate here. Measures computed were homogeneity, contrast, dissimilarity, mean, standard deviation, entropy, angular second moment, correlation, inverse difference, grey level distance vector (GLDV) angular second moment and GLDV entropy. The GLDV measures are computed from the GLDV, a derivation of the GLCM which lists all possible values for the difference between a reference pixel and a neighbouring pixel, and counts the number of times each value occurs (Geomatica 2009). To obtain texture values for the edges of the classification subsets, slightly larger subsets were used in texture calculation, and the results were clipped to the extent of the smaller subsets. The procedure described in Section 3.2.4 was then used to resample the texture images to a resolution of 2.5 m for use in eCognition.

A different approach to statistical quantification of texture incorporated in this research is the mean pairwise Euclidean distance (MPED) algorithm. This measure was introduced by Rocchini, Chiarucci and Loiselle (2004) who used it to estimate levels of wetland biodiversity. Each pixel in a given window is represented by a point in multidimensional feature space, with each dimension in feature space corresponding to an image band that was input to the algorithm. For the given window, the Euclidean distances between all pairs of points present in feature space are computed and summed, and the sum is divided by the number of pairs present. This measure was implemented in an EASI script in PCI and calculated on all four SPOT bands for 3x3, 5x5 and 11x11 windows. Note that this differs from the mean Euclidean distance (MED) algorithm implemented in most commercial remote sensing software packages, as that algorithm only considers a single band at a time (ERDAS 2010). MED was also used in this research where it was computed through PCI's HISTEX module.

3.3.4 Object-based shape metrics

eCognition provides several indices characterising the shape of objects. Three used in this study are briefly considered next, namely the shape, border and asymmetry indices.

The shape index characterises the smoothness of an image object's border. It is calculated by dividing the length of an object's border by four times the square root of its area, meaning that it relates the border length of an object to that of a square with the same area (Trimble 2011a). The shape index is thus expressed as:

$$Shape\ index = \frac{object\ border\ length}{4\sqrt{object\ area}}$$ (Trimble 2011a).

The border index characterises the jaggedness of an object. It is similar to the shape index, but uses a rectangle to approximate the object rather than a square. It divides the length of an object's border by that of the smallest rectangle able to completely enclose it, that is:

$$Border\ index = \frac{object\ border\ length}{smallest\ enclosing\ rectangle\ border\ length}$$ (Trimble 2011a).

The asymmetry index describes the relative length of an image object in comparison to a regular polygon. An ellipse is approximated around the image object, and the ratio between its minor and major axes is calculated (Trimble 2011a), viz:

$$Asymmetry\ index = 1 - \frac{minor\ axis\ of\ approximating\ ellipse}{major\ axis\ of\ approximating\ ellipse}$$ (Chen et al. 2009).

After all necessary indices and texture measures had been computed, the classification process could commence. However, the reference data for accuracy assessment still needed to be created. The accuracy assessment process is described in the following section, and the classification process in the next chapter.

3.4 Assessing the accuracy of remotely sensed classifications

Meaningful and consistent measures of accuracy are needed when a classified map is produced. Map users need such measures to assess the suitability of the map for their particular purposes and map producers need them to assess their particular classification strategies, or to compare two or more strategies (Liu, Frazier & Kumar 2007).

Congalton and Green (2009) divide the history of digital accuracy assessment into four stages. The first stage was when remote sensing technology first emerged. At that time no real accuracy assessment was performed in classification studies with only superficial qualitative visual assessment being attempted. In the second stage, non-site-specific accuracy assessment prevailed. Total area per class was compared between the map and reference estimates, but locational accuracy was ignored. The third stage introduced site-specific accuracy assessment. Actual locations on the ground were compared to their corresponding locations in the map and the overall accuracy was reported as percentage correct. The fourth and current age is characterised by the use of the error matrix, which compares reference information to map information for a set of sample areas. This section will start off by defining the error matrix and the accuracy measures computed from it, after which the sampling process will be regarded,

followed by the specific steps taken in this study to prepare for accuracy assessment. Finally, the level of accuracy regarded as acceptable in this study will be established.

3.4.1 The error matrix and measures of thematic accuracy

An error matrix is a square matrix with rows representing a range of classes from one classification, and columns representing the same range of classes from another classification. Each cell counts the number of samples having in the first classification the label indicated by the row, and in the second classification the label indicated by the column. One of the classifications is assumed to be correct; this is referred to as the reference data, and is usually presented in the columns. The other classification represents the classes from the remotely sensed classification and is usually presented in the rows (Congalton & Green 2009).

Error matrices are effective at displaying accuracy, as the individual accuracies of different classes are clearly presented, as are errors of omission and commission. When regarding a particular category, an omission error is an area that is wrongly excluded from that category and a commission error is an area that is wrongly included in that category. Various accuracy measures can easily be computed from an error matrix. In addition to overall accuracy, producer's and user's accuracies are usually computed to evaluate the accuracies of individual categories. For a given category, producer's accuracy indicates the probability of a reference area assigned to that category being assigned the correct label in the classification, and user's accuracy indicates the probability of an area assigned to that category in the classification representing it in reality. Another commonly reported measure is the Kappa statistic which compares the actual agreement between the reference data and the classification reported in the error matrix to the chance agreement between the two as indicated by the row and column totals (Story & Congalton 1986; Liu, Frazier & Kumar 2007; Congalton & Green 2009).

3.4.2 Sampling and reference data

To populate an error matrix it is necessary to perform sampling, as it is seldom economically feasible to visit every place during collection of reference data. Congalton and Green (2009) note four critical considerations in designing an accuracy assessment sample, namely the characteristics and spatial distribution of the thematic classes involved, the appropriate sample unit, the number of samples required, and the method of sample selection. Once the sample has been designed, the reference data has to be collected for which three steps are suggested by Congalton and Green (2009). First, the locations of the sample sites must be accurately determined in both the reference source and the classified map. Then, these sites must be

delineated in such a way that they represent exactly the same area in both cases and finally the reference and the map label for each site must be assigned.

3.4.3 Preparation for accuracy assessment

Accuracy assessment in this study was problematic. Initially, the intention was to concentrate on wetland hydrology, and to differentiate areas according to inundation and soil water-saturation levels. The classification would be verified by data collected during a field visit. This strategy was complicated by the use of archival images as no field verification data was available for the dates of image acquisition, which constitutes a significant limitation in a study of systems as dynamic as wetlands. However, it was assumed that field data collected at a similar stage in the 2010 wet season would be comparable to the conditions in the 2009 wet season represented in the SAR image.

Historical rainfall data had been obtained from Agulhas National Park prior to the selection of the specific images used. The wet season SAR image used was selected because it had been acquired towards the end of the wet season (in late September) and one week after a major rainfall event. It was reasoned that the conditions represented in the image approximated the maximum volume of water present in wetland systems during that year, but that water stored in non-wetland areas for a short period directly after the rainfall event would have dried out. The accumulation of rainfall during the 2010 wet season was monitored to identify a time when conditions would be approximately equivalent to those represented in the image. However, it became apparent that 2010 was a much drier year than 2009. By the end of the 2010 wet season, the accumulated rainfall had not reached the levels recorded for the previous wet season. A field visit was undertaken in early November 2010 when the chances of further significant rainfall events were considered to be slim. Conditions in wetland areas were recorded in the form of transects, with GPS points taken at transitions between wetland and non-wetland areas and at points where conditions within the wetland changed significantly regarding vegetation, inundation or soil saturation. During the field visit it became clear that the area was much drier than it would have been at the time of image acquisition. Consequently, visible indications of wetland conditions such as changes in vegetation types or signs of water influence on soil (i.e. dried mud) were considered as surrogate for actual water. Although this recorded field data was very valuable to train the image classification it was deemed unsuitable for accuracy assessment as it did not represent the conditions present at the time of image acquisition and consequently could not be used to draw conclusions on those conditions at the level of confidence required for statistical accuracy assessment.

Following the field visit, examination of available information led to the conclusion that the only property of wetlands assessable with any level of confidence was their total extent as indicated by wetland-specific vegetation types, unvegetated seasonal pans, and waterbodies. Thus, the different wetland classes would have to be grouped, and the only distinction within wetland areas would be between permanent waterbodies and other wetlands. Because the number of field points was insufficient for statistical accuracy assessment (most points had been recorded within wetlands and few represented wetland boundaries or extent), the field survey was supplemented with points obtained from visual inspection of high-resolution colour aerial photographs. An expert-created polygon shapefile representing the extents of certain wetlands within the Nuwejaars Wetland SMA was also used as reference (Euston-Brown & Wessels 2009). By studying all the available data, it was concluded that wetland extent could be identified from the aerial images with high levels of confidence when compared with more recent high-resolution satellite images from Google Earth and SANSA to compensate for changes that may have occurred since 2005 when the aerial photographs were acquired. All wetland areas within the two classification subsets were digitised from these images with non-wetlands being distinguished from permanent waterbodies and other wetlands.

Following digitisation of wetland areas, the two subsets were separately sampled to obtain data to populate the error matrices for the different classifications. The stratified random sampling tool in Geospatial Modelling Environment (GME, a free toolset for ArcMap formerly known as HawthsTools) was used to obtain a specified number of random points for each category. The number of sampling points needed for each category was calculated using the following formula provided by Congalton and Green (2009):

$$n = B\Pi_i(1 - \Pi_i)/b_i^2$$

where n is the total number of samples needed to adequately fill an error matrix for the specific classification;

B is the upper (α/k) x 100th percentile of the χ^2 distribution with 1 degree of freedom;

1 - α is the confidence level;

k is the number of categories;

Π_i is the proportion of the population which falls in the ith category; and

b_i is the absolute precision of the sample.

The formula was applied to each category in the classification and the largest result obtained (the worst case) was divided by *k* to obtain the number of samples to be collected for each class. In this case, 150 samples were required for each of the categories.

One set of sampling points was created with GME for each subset. All classification results were exported from eCognition into polygon shapefiles and these were loaded in ArcMap along with the sample points and the digitised reference dataset. The intersect tool in ArcMap was used to extract, for each sample point, the reference classification and the class assigned to it in each of the classifications performed in eCognition. The reference classification of each sample point was checked against the aerial photographs again to ensure that no misclassifications occurred. The attribute tables for the classified sample points for the separate subsets were exported from ArcMap into DBF format and loaded into Excel for the calculation of the error matrices.

3.4.4 Interpretation of accuracy measures

Before assessing classification results, it is necessary to establish the level of classification accuracy that is regarded as adequate for a particular application. Regarding overall accuracy, various sources consider a value of 85% to be the lower cut-off for an acceptable result (Congalton & Green 2009; Lück et al. 2010). However, this value was originally proposed for application to general land-use and land-cover categories which were less specialised than the classes involved here (Anderson et al. 1976). Some sources have questioned the validity of 85%, with Laba et al. (2002) noting that producer's and user's accuracy in regional land-cover mapping projects have generally stabilised in the 50 to 70% range.

A more appropriate way to assess the results of this study is to compare its results with those in similar existing studies. Töyrä, Pietroniro and Martz (2001) combined SPOT and RADARSAT-1 data for flood mapping in Canada. Classes distinguished were open water, flooded vegetation and non-flooded land. Although the authors provided error matrices, only Kappa index values were listed. The best Kappa values obtained were 0.76, 0.8 and 0.92 from SAR data only, SPOT data only and a combination of the two respectively. Overall accuracies as computed from the error matrices provided in the study were 84% from SAR data only, 87% from SPOT data only, and 95% from a combination of the two. These results were obtained from single images from both sensors. However, the Canadian study differs from this Western Cape study in that the former included forested wetlands and focused on the extent of flooding rather than total wetland extent. Other studies include Baghdadi et al. (2001) who achieved overall accuracies between 73% and 86% using data from an airborne polarimetric SAR sensor. Categories considered included forested and non-forested wetlands. Bourgeau-Chavez et al. (2001) used multipolarised,

multi-band SAR data from the SIR-C mission. Their single-band and polarisation combinations corresponding to existing satellite-borne sensors (including ERS) achieved overall accuracy levels of around 65%, which they regarded to be reasonably accurate. Hess et al. (2003) achieved an overall accuracy of 95% in distinguishing between wetland and non-wetland areas using L-band SAR; however, the spatial scale of the study was significantly lower than for the Agulhas study, and the focus was on flooding rather than on wetland characteristics. Concerning studies using VIR imagery only, Davranche, Lefebvre and Poulin (2010) recorded accuracies ranging from 86% (submerged macrophytes) to 99% (common reeds) from SPOT images, while Lunetta and Balogh (1999) obtained an overall accuracy of 69% in wetland extent mapping from single-date Landsat TM imagery, and 88% from imagery acquired at two different dates.

From the above it is clear that no conclusive appropriate accuracy level has been established. For the purposes of this study an accuracy level of 80% was considered sufficient, given the complexity of the target features. The next chapter describes the procedures followed to reach this level of accuracy.

CHAPTER 4: WETLAND CLASSIFICATION

This chapter describes the process of classifying wetlands using satellite imagery. A rule-based expert system classifier, as well as a nearest-neighbour supervised classifier was used on one SPOT image and two SAR images. The images from the different sensors were used separately and in combination in both classifiers, and classifications were performed for both subsets. The classification process is portrayed in Figure 4.1. The process starts with the classification of the SPOT image as described in Section 4.1 and is followed by the classification of the SAR imagery as described in Section 4.2. The next step is the classification of SPOT and SAR data in combination, which is described in Section 4.3. Examples of the results are provided in Section 4.4.

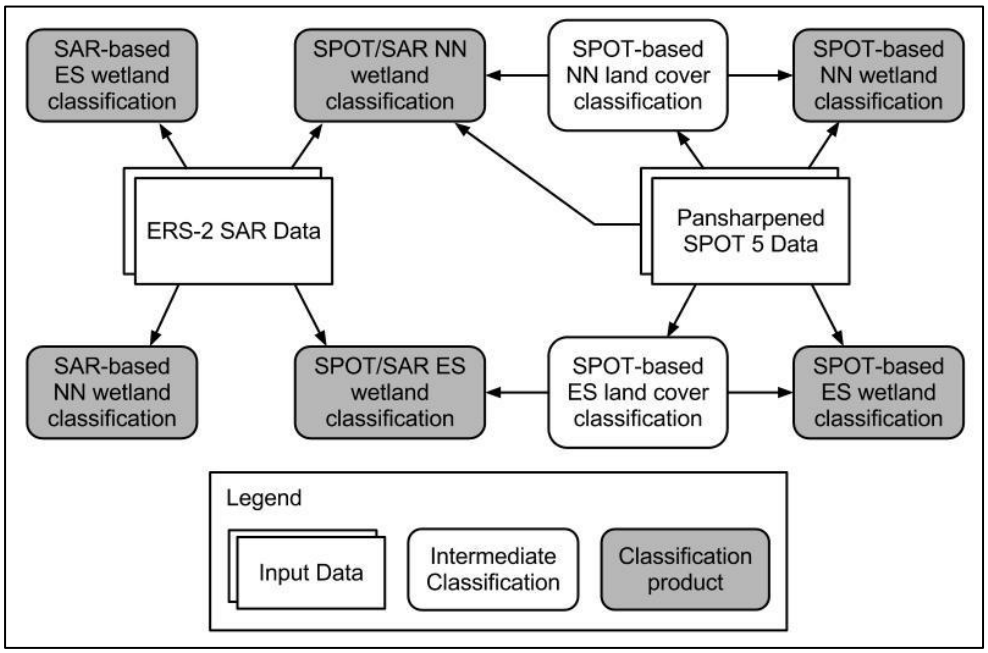

Figure 4.1: Schema of the process for classifying wetlands from satellite imagery

4.1 SPOT-based classifications

This section considers the classifications obtained from SPOT data. The first subsection describes the initial segmentation on which both classifications were based, the second describes the expert system classification and the third describes the supervised classification.

4.1.1 Initial segmentation

To effectively assess the suitability of the different classification algorithms, it was necessary to minimise the effects the different segmentation parameters have on the results. Consequently,

both SPOT-based classifications, along with both SPOT/SAR combined classifications described in Section 4.3, were based on the same segmentations derived from the SPOT image.

The basic segmentations for the two subsets were obtained using the multiresolution segmentation algorithm. A scale parameter of 5, a shape criterion of 0.1 and a compactness criterion of 0.5 were applied. All four SPOT bands were used, as were Canny edge-detection layers created in eCognition for the NIR and SWIR bands. All bands were assigned a weight of 1, except for the Canny layer of the NIR band which was assigned a weight of 3. The reasoning was that edges in the NIR band were considered to be important for wetland delineation because water is characterised by very low reflectivity at near-infrared wavelengths. Other band combinations were tested, but this combination gave the best results across the range of different classes that had to be identified in the preliminary and final classifications. The segmentation was modified for specific applications during the classification process.

4.1.2 Expert system classification

The classification process commenced following the development of a satisfactory segmentation. The first classification performed was the expert system classification of the SPOT data. This classification was performed in two phases. The first phase was a basic landcover classification that identified areas potentially representing wetlands, and the second phase was a wetlands classification based on the landcover classes. The landcover classification from the first phase was also used as input for the SPOT/SAR combined expert system classification described in Section 4.3.1.

4.1.2.1 Landcover classification

The first step in the SPOT-based and the SPOT and SAR combined expert system classifications was a SPOT-based landcover classification which differentiated the input image into five classes, namely *Permanent waterbody*, *Natural and semi-natural vegetation*, *Cultivated area*, *Bare ground* and *Roads*. The classification process started with the identification of *Permanent waterbody*.

According to the literature, water identification from optical imagery should be relatively simple as it is characterised by distinct, very low values in near- and mid-infrared bands. In practice this process was complicated by the complex aquatic environments of the study area, particularly in the Nuwejaars subset where various waterbodies had high or very high levels of turbidity or they were very shallow, allowing measured returns from lake- or riverbeds. The classification process is illustrated in Figure 4.2 and the specific rules are given in Appendix A (Figure A.1). The rule-

set starts with a set of rules identifying dark, deep waterbodies. The next set of rules identified highly turbid water, such as shallow endorheic pans. Water surfaces in shallower pools and river channels were identified last. The rules used a combination of spectral values, indices and texture measures.

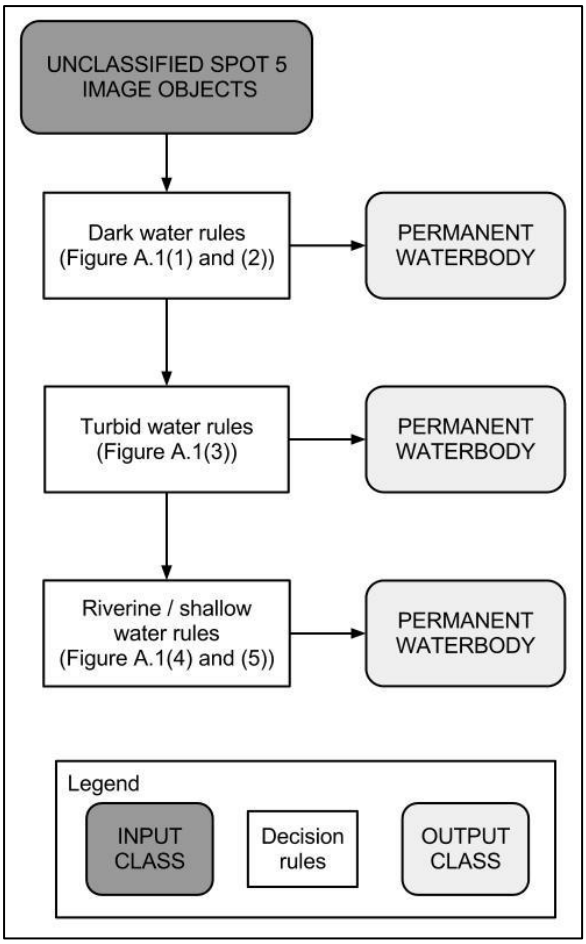

Figure 4.2: Classification process followed for *Permanent waterbody* (see Figure A.1)

After completion of the classification of *Permanent waterbody*, the *Cultivated area* class was considered. At the time of the acquisition of the SPOT image in January, wheat and barley crops had been harvested (harvesting usually takes place in October or November) but not yet replanted (planting usually takes place in May), so croplands were mainly covered in stubble, or perennial pasture crops (Mangnall & Crowe 2002). Vineyards only occurred in a small patch in the north-western corner of the Nuwejaars subset. Consequently, cultivated lands could be characterised by low values for vegetation indices and texture, with the addition of thresholds in other indices, shape measures and spectral bands to help recognition of problematic areas.

Objects in the initial segmentation were smaller than required for effective identification of the *Cultivated area* class as they were significantly smaller than most fields and pastures. Using small objects limits the effectiveness of texture measures and renders shape measures irrelevant.

Multiresolution segmentation was applied using existing objects to generate a new image object level with a larger scale. The existing image object level (and the *Permanent waterbody* classification) were copied to the new, higher level, and segmentation was then performed on unclassified objects in the new level. The scale parameter for the segmentation was set to 40, and the shape and compactness parameters to 0.1 and 0.5 respectively. The green and red bands were used as input, both with layer weights set to 1, as well as a Canny edge detection layer of the red band which was assigned a layer weight of 5. The latter was added after it was observed that field boundaries were more clearly visible in the red band than in any other band. This is a consequence of the spectral characteristics of vegetation in the red band: vigorous vegetation strongly absorbs red radiation.

After completion of the new segmentation, decision rules were applied to unclassified image objects to identify *Cultivated area* areas. The classification process is illustrated in Figure 4.3, and specific rules are given in Appendix A (Figure A.2). The first set of rules used a combination of spectral values, indices, texture and shape measures to identify large fields and pastures with low levels of vegetation cover. The second set of rules targeted the remaining agricultural areas, particularly smaller, irregularly shaped fields.

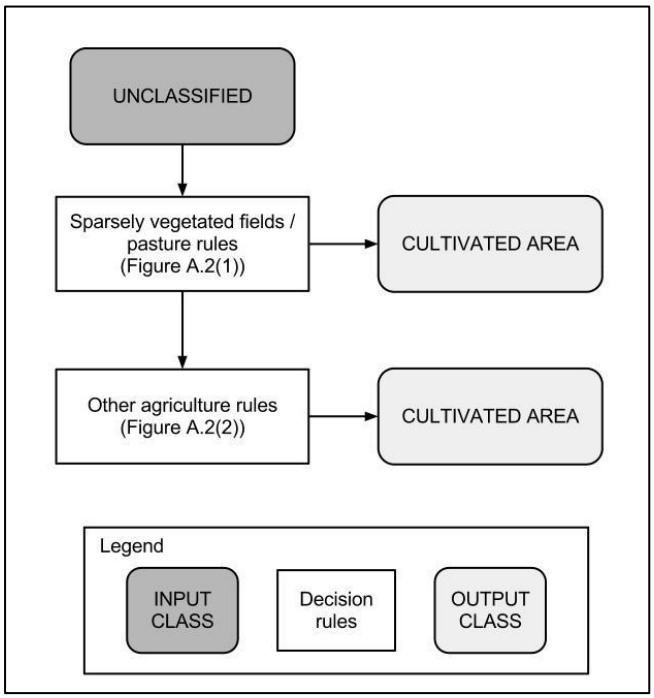

Figure 4.3: Schema for classification of *Cultivated area* (see Figure A.2)

Once the *Cultivated area* classification had been performed, specific contextual rules were added to refine it. The process is illustrated in Figure 4.4 and the specific rules are illustrated in Appendix A (Figure A.3). These rules identified *Cultivated area* commission errors occurring on the boundaries of waterbodies and they removed certain objects that had been assigned to

Cultivated area even though they were too small to belong to that class. Furthermore, certain small *Permanent waterbody* objects occurring in agricultural fields were assigned to *Cultivated area*.

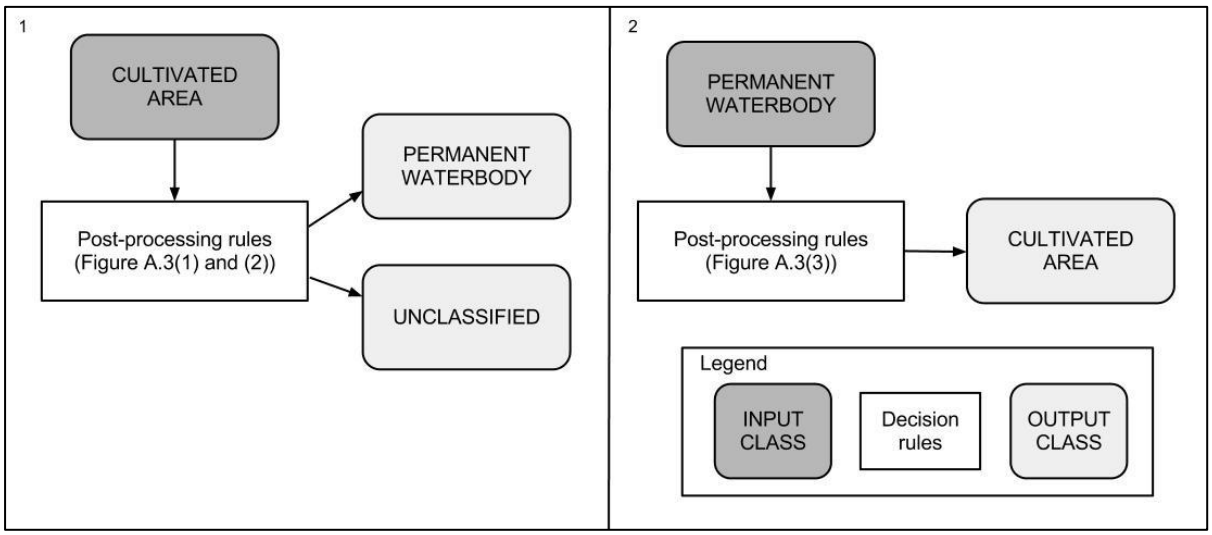

Figure 4.4: Schema for post-processing of *Cultivated area* and *Permanent waterbody* objects (see Figure A.3)

Following completion of the *Cultivated area* classification, the classification results were copied from the *Cultivated area* object level (with larger objects) to the original object level. Only *Bare ground* and vegetation classes remained unclassified. The classification process for *Bare ground* is illustrated in Figure 4.5 and the rules are given in Figures A.4 and A.5 (Appendix A). This class could be identified through a single threshold in the green band, but further post-processing rules were added to identify certain *Bare ground* areas wrongly identified as *Cultivated area.*

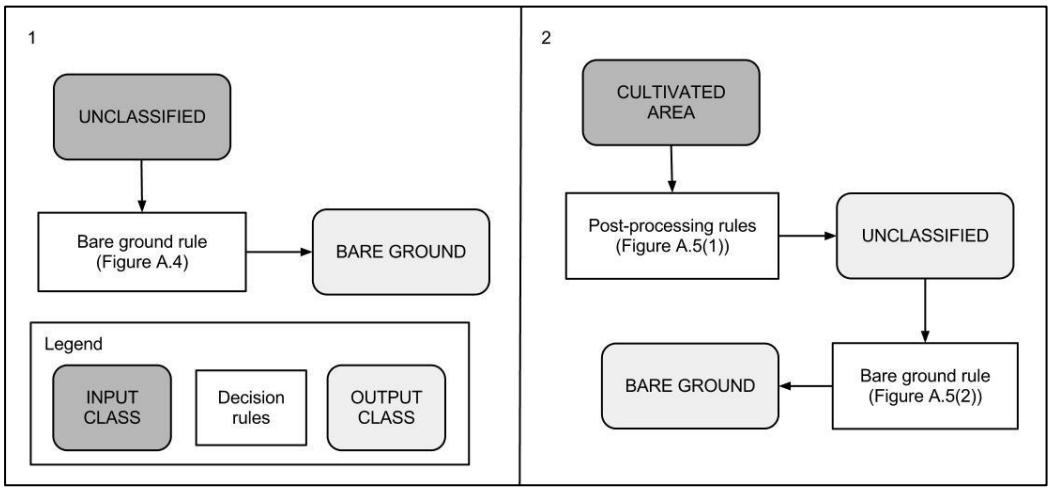

Figure 4.5: Schema for classification of *Bare ground* (see Figures A.4 and A.5)

All remaining unclassified areas belonged to the class *Natural and semi-natural vegetation*. Semi-natural vegetation refers to vegetation not planted by humans, but influenced by human actions (Lück et al. 2010). *Natural and semi-natural vegetation* consequently refers to all non-

agricultural vegetation. To simplify wetland discrimination, *Natural and semi-natural vegetation* was divided into three subclasses: *Dense vegetation*, *Medium vegetation* and *Sparse vegetation*. The process followed in their discrimination is portrayed in Figure 4.6 and the specific rules are given in Appendix A (Figure A.6). *Dense Vegetation* was identified first, followed by *Sparse Vegetation.* All remaining unclassified objects were assigned to *Medium vegetation.*

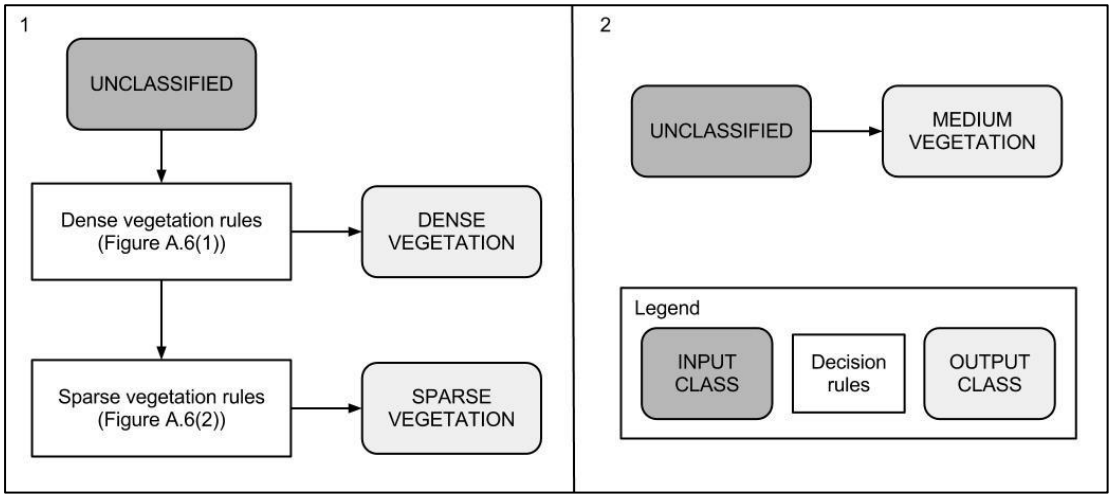

Figure 4.6: Schema for classification of *Natural and semi-natural vegetation* (see Figure A.6)

The classification of *Bare ground* was refined by identifying objects representing *Roads*. Gravel roads are spectrally very similar to unvegetated seasonal pans, so spectral rules could not be used to remove *Roads* from the initial *Bare ground* classification. The only alternative was to apply shape metrics. However, these were ineffective for application to the initial segmentation which featured relatively small objects not optimised for shape. The problem was addressed by merging all neighbouring *Bare ground* objects and applying a multiresolution segmentation to the merged objects. The parameters of this segmentation were set so that shape was the most important factor (0.9). The compactness parameter was set to 0.5 and the only layer used was the green band. The scale parameter was set to 40.

After completion of the segmentation, thresholds in shape metrics were used to identify objects representing *Roads*. Next, the roadside verges (narrow strips of vegetation directly next to the roads) were also assigned to the *Roads* class so that they could be disregarded during wetlands classification. Finally a post-processing rule identified *Roads* commission errors representing narrow lake or river shores. The classification process is illustrated in Figure 4.7 and the rules are given in Appendix A (Figures A.7, A.8 and A.9).

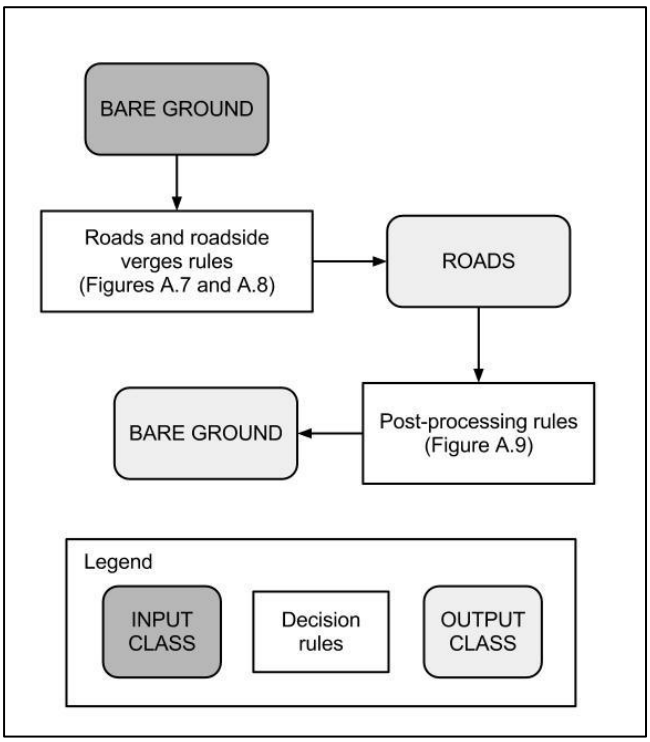

Figure 4.7: Schema for classification of *Roads* (see Figures A.7, A.8 and A.9)

The initial landcover classifications for both subsets were applied in the wetland identification rules presented in Section 4.1.2.2 (SPOT-based) and Section 4.3.1 (SAR-based).

4.1.2.2 Wetlands classification

The landcover classification performed by the steps set out in Section 4.1.2.1 was modified to create a dedicated classification of wetlands. The *Permanent waterbody* class was kept as is and the *Roads* and *Cultivated area* classes were assigned to *Non-wetland*. This section explains how the *Sparse vegetation*, *Medium vegetation* and *Dense vegetation* classes were refined to distinguish three wetland classes. The process followed in the classification is given in Figure 4.8 and the full ruleset in Appendix A (Figure A.10).

The first step in the classification of vegetated wetland areas was the application of a rule identifying *Inundated vegetation* from *Medium vegetation* objects (Figure 4.8(1) and see Figure A.10(1) for individual rules). This rule identified vegetated areas with low SWIR reflection which is an indication of water below the vegetation canopy. A number of rules were then applied to *Sparse vegetation* and *Medium vegetation* objects to identify objects representing wetland vegetation of low or intermediate density which were subsequently labelled *Sparse to medium wetland vegetation* (Figure 4.8(2), see Figure A.10(2) for individual rules). These rules made use of EVI_2 and water-related indices (see Section 3.3.2). The next step was to identify *Dense wetland vegetation*. This was accomplished with rules using a combination of SWIR

reflection, EVI_2, water-related indices and texture (Figure 4.8(3) and see Figure A.10(3) for individual rules). These rules also removed *Non-wetland* objects which were spectrally similar to the target class, from contention. Finally, all neighbouring wetlands objects of specific classes were merged and a set of refinement rules was applied to all vegetated wetland and *Bare ground* (seasonal pan) objects to refine the classification. Erroneously classified objects were assigned to *Non-wetland* and the remaining correctly classified objects to *Other wetland* (Figure 4.8(4-6) and see Figure A.11 for individual rules). The assignment of the *Bare ground* objects to *Other wetland* was done because *Roads* and *Agriculture* bare areas had been removed during the landcover classification (Section 4.1.2.1), meaning that most of the remaining *Bare ground* objects represented seasonal pans.

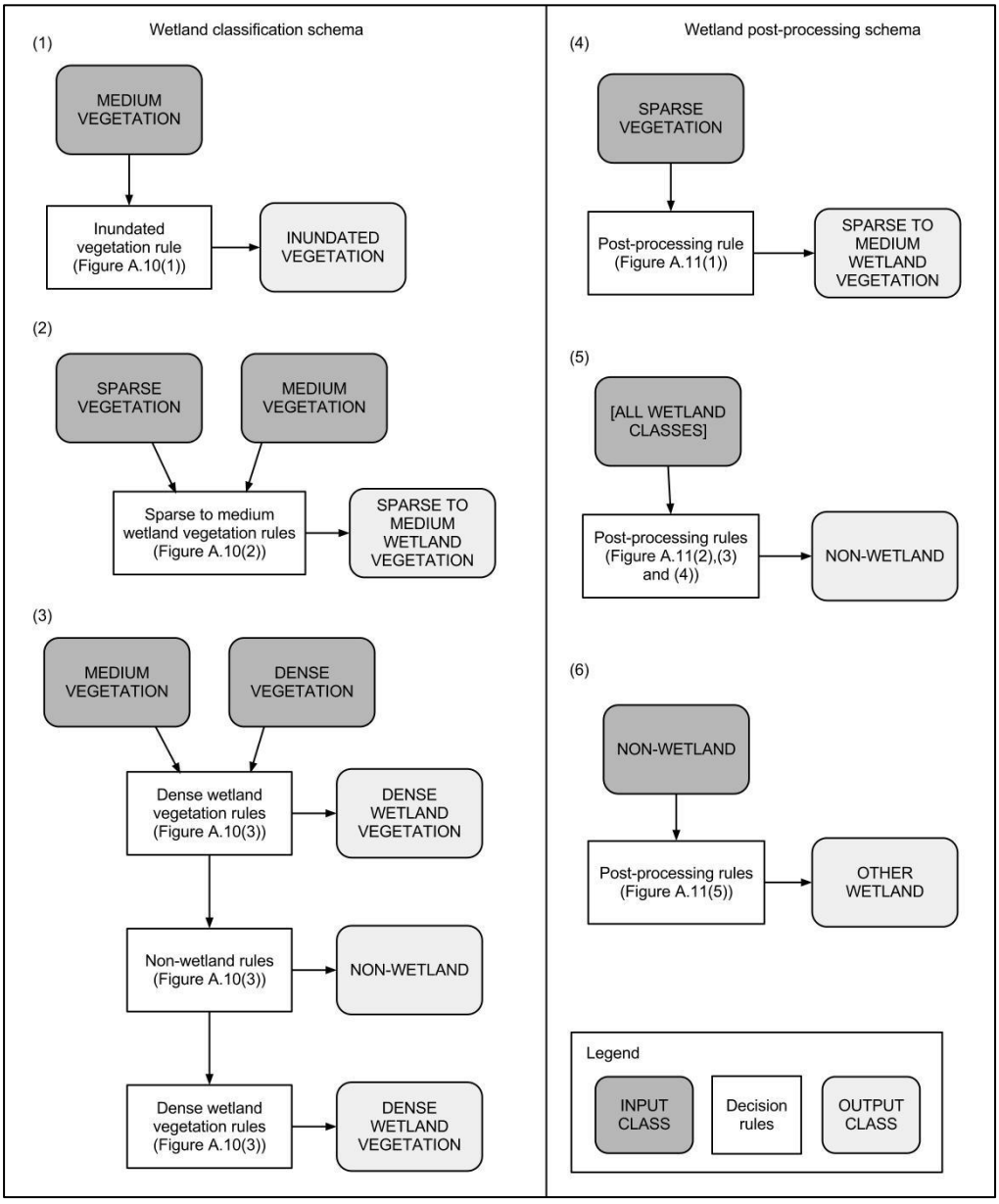

Figure 4.8: Schema for the classification and post-processing of wetlands from SPOT data only (see Figures A.10 and A.11)

4.1.3 Nearest-neighbour supervised classification

The nearest-neighbour classifier implemented in eCognition was used for the SPOT-based supervised classification. This classifier projects an unclassified image object into a feature space representing a specified set of input bands and compares its coordinates to those of the set of classified sample objects. The unclassified object is then assigned to the class of the sample closest to it in feature space, or left as unclassified if it is more than a specified distance away from the closest sample (Trimble 2011b).

The SPOT-based supervised classification process was split in two phases: the landcover classification phase and the wetlands classification phase. The landcover classification process identified the same classes as in the expert system landcover classification, namely *Permanent waterbody, Cultivated area, Bare ground* and *Natural and semi-natural vegetation.* However, the *Roads* class was not differentiated from other *Bare ground objects* and *Natural and semi-natural vegetation* was not divided into subclasses as was done in the expert system classification. As done in the expert system classifications, this landcover classification was used as input for the SPOT-based supervised wetlands classification, and for the SPOT/SAR combined supervised wetlands classification described in Section 4.3.2.

A number of post-processing rules were added to refine the SPOT-based supervised landcover classification before the wetlands classification was performed (Figure 4.9, full rules given in Figure A.12). In traditional pixel-based supervised classifications, such post-processing steps are commonly performed in a GIS environment. These included reassigning small *Natural and semi-natural vegetation* objects completely surrounded by *Cultivated area* objects to the *Cultivated area* class, reassigning small *Cultivated area* objects completely surrounded by *Natural and semi-natural vegetation* to the *Natural and semi-natural vegetation* class, and allocating the smallest *Permanent waterbody* objects to the *Natural and semi-natural vegetation* class to remove commission errors.

The supervised wetlands classification was performed after the supervised landcover classification had been refined. This classification inputted the *Natural and semi-natural vegetation* class created by the landcover classification and identified the upland classes *Alien upland vegetation* and *Natural upland vegetation* from it (combined in one class in the Soetendalsvlei subset), and the wetland classes *Dense wetland vegetation, Medium wetland vegetation, Sparse wetland vegetation* and *Inundated vegetation.* Note that the differences between wetland areas in the two subsets meant that the latter two classes were not needed in the Soetendalsvlei subset because an accurate result could be obtained without them.

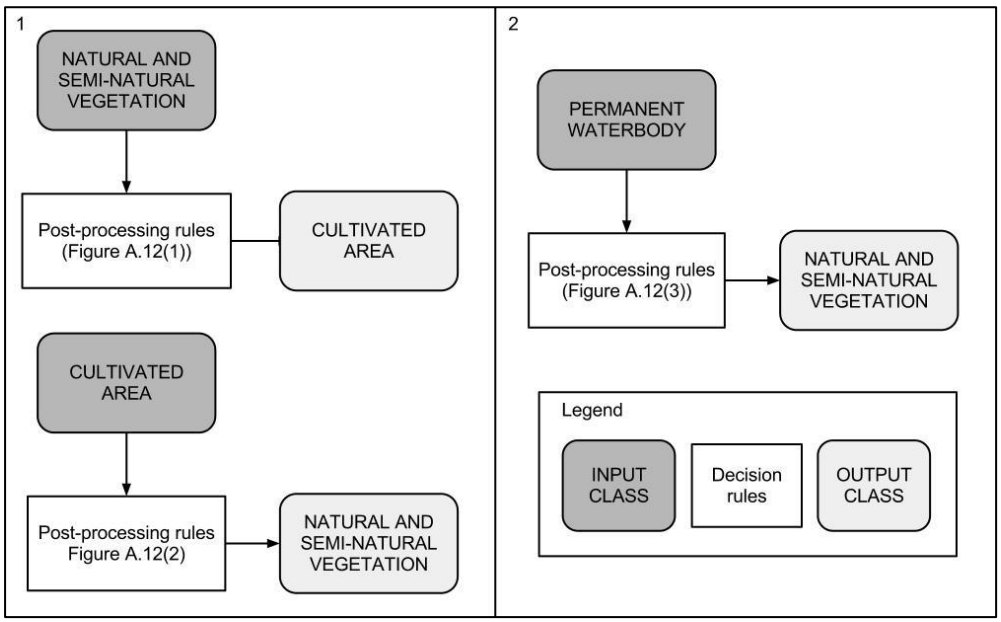

Figure 4.9: Schema for the post-processing of the supervised landcover classification from SPOT (see Figure A.12)

The methodology of both phases of the SPOT-based supervised classification was also followed in the SAR-based and SPOT/SAR combined supervised classifications described in Sections 4.2.3 and 4.3.2 respectively. In each case the classification process started with the manual classification of a set of representative sample objects. The strategy was to initially identify a maximum of 20 samples per class and to then run the classification. The result of this first classification was evaluated to determine whether more samples were required and if deemed so, samples were added and the process repeated. This iterative process was taken to be complete only when a sufficient level of accuracy was achieved or when the addition of more samples was unable to further increase accuracy levels. The number of samples used for each class in the SPOT-based supervised landcover and wetlands classifications is given in Tables 4.1 and 4.2 respectively.

Table 4.1: Number of samples used in the SPOT-based landcover classification

Class	Number of samples: Nuwejaars subset	Number of samples: Soetendalsvlei subset
Permanent waterbody	72	50
Cultivated area	71	60
Bare ground	69	50
Natural and semi-natural vegetation	73	66

Table 4.2: Number of samples used in the SPOT-based wetlands classification

Class		Number of samples: Nuwejaars subset	Number of samples: Soetendalsvlei subset
Upland vegetation	Alien	20	100
	Natural	51	
Dense wetland vegetation		61	30
Inundated vegetation		14	n/a
Medium wetland vegetation		40	73
Sparse wetland vegetation		21	n/a

The definition of the classification feature space in each of the supervised classifications was based on the feature space optimisation tool in eCognition. This tool uses the sample classification to find the combination of features that maximises the average minimum distance between samples of different classes. The tool was run before each classification and the feature space adapted to match the optimum set of features selected by the tool. The features used included object mean values of all image bands, indices and texture bands. The sets of features used in each classification are listed in Table 4.3.

Table 4.3: Features included in the classification feature space for supervised classification

Classification	Features used: Nuwejaars subset	Features used: Soetendalsvlei subset
SPOT only (landcover)	NIR SWIR NDWI EVI_2 NDTI MPED (11x11) NDWIF	NIR SWIR NDWI NDTI EVI_2
SPOT only (wetlands)	Red NIR SWIR NDWIF NDWI NDTI NDWIT MPED (11x11) EVI_2	NIR SWIR NDWI NDTI NDWIT MPED (5x5, 11x11) EVI_2

Upon completion of the classification the classes not representing wetlands were assigned the label *Non-wetland*, while the vegetated wetland classes were allocated to the *Other wetland* class. The *Bare ground* class from the landcover classification was also added to the *Other wetland* class, as these objects mostly represented seasonal pans. This had the effect that some gravel roads were classified as *Other wetland* because they could not be separated from other *Bare ground* objects without the contextual information applied in the expert system (Section 4.1.2.1). *Cultivated area* objects were assigned to the *Non-wetland* class, while the *Permanent waterbody* class was kept intact in the final classification.

4.1.4 Accuracy assessment of SPOT-based classifications

Statistical accuracy assessments were performed after the completion of the SPOT-based classifications. The results for the expert system are reported first, followed by the results for the supervised classification.

The error matrix and computed accuracy measures for the SPOT-based expert system classification are given in Table 4.4. This classification obtained the highest overall accuracy score of all the classifications done in this study (almost 84%). In addition, producer's and user's accuracy levels were high, particularly for *Permanent waterbody*. The only exception was the producer's accuracy for the *Other wetland* class, which at 65% was less than satisfactory, indicating substantial omission errors.

Table 4.4: Error matrix for the expert system classification of wetlands from SPOT data

		Reference image			
		Permanent waterbody	*Other wetland*	*Non-wetland*	**Totals**
Classification product	*Permanent waterbody*	140	6	0	**146**
	Other wetland	8	98	12	**118**
	Non-wetland	2	46	138	**186**
	Totals	**150**	**150**	**150**	**450**

	Producer's accuracy (%)	**User's accuracy (%)**	**Omission errors (%)**	**Commission errors (%)**
Permanent waterbody	93.33	95.89	6.85	4.11
Other wetland	65.33	83.05	44.07	16.95
Non-wetland	92.00	74.19	6.45	25.81

Kappa index	**0.75**
Overall accuracy (%)	**83.56**

The error matrix and computed accuracy measures for the supervised classification are summarised in Table 4.5. The results are comparable with those of the expert system classification. All the producer's and user's accuracy values exceeded 72%. The producer's accuracy for *Other wetland* was 79%, which is a significant improvement over the 65% recorded by the SPOT-based expert system. The overall accuracy for the classification was 83% and the kappa index value of 0.74 indicates a good result.

Table 4.5: Error matrix for the nearest-neigbour classification of wetlands from SPOT data

		Reference image			
		Permanent waterbody	*Other wetland*	*Non-wetland*	**Totals**
Classification product	*Permanent waterbody*	128	2	0	**130**
	Other wetland	22	119	24	**165**
	Non-wetland	0	29	126	**155**
	Totals	**150**	**150**	**150**	**450**

	Producer's accuracy (%)	**User's accuracy (%)**	**Omission errors (%)**	**Commission errors (%)**
Permanent waterbody	85.33	98.46	16.92	1.54
Other wetland	79.33	72.12	18.79	27.88
Non-wetland	84.00	81.29	15.48	18.71

Kappa index	**0.74**
Overall accuracy (%)	**82.98**

4.2 SAR-based classifications

This section first considers the segmentation used for the SAR-based classifications. The expert system and the supervised classifications are then described and it concludes with a statistical assessment of the results.

4.2.1 SAR-based segmentation

As with the SPOT-based classifications, one segmentation was created per subset as basis for both the SAR-based expert system and supervised classifications. This ensured that only the classifiers influenced the results and not the segmentations. Multiresolution segmentation was used for segmenting the SAR images. After experimenting with different parameter values and visually examining the results, the scale parameter was set to 10, the shape criterion to 0.1 and

the homogeneity criterion to 0.5. The σ^0 values of both SAR images were used as input for the segmentation with both layer weights set to 1. These parameters were deliberately chosen to produce a segmentation with objects that are homogenous, but too small for effective use in this classification. The image object fusion (IOF) tool in eCognition was then used to merge neighbouring similar objects. A custom object variable was created that added the per-object standard deviation in σ^0 pixel values for the wet season image to the per-object standard deviation in σ^0 pixel values for the dry season image. Low values in this variable would indicate that an object was homogenous in both layers, while higher values indicate that an object was heterogeneous in at least one of the two layers. After experimenting with different values, IOF was set to merge objects so that resulting objects had values less than 1 for this variable. Furthermore, IOF was set to merge each object with all fitting neighbour objects. The resulting segmentations were then used as input for both the expert system (Section 4.2.2) and supervised (Section 4.2.3) classifications.

4.2.2 Expert system classification

This section deals with the expert system classification of SAR data. The classification process is illustrated in Figure 4.10, and the full ruleset is given in Appendix A (Figures A.13, A.14, A.15).

Step one considers *Permanent waterbody* (Figure 4.10(1)). Three characteristics were used to classify this class. First, waterbodies were identified by low values for dry-season backscatter, as specular reflection of C-band microwaves occurs on water surfaces in the absence of wind (Figure A.13(1)). Second, significant changes occurred between the two dates where water surfaces experienced wind influence in the wet season and not in the dry-season (Figure A.13(2)). Third, low texture values occurred in large uniform waterbodies (Figure A.13(3)). These thresholds could only identify a small subset of features and region growing was needed to extend the classification. However, even after this operation, only the largest waterbodies could be discriminated.

Other wetland areas were identified in step two. This process was split in two, the first part (Figure 4.11(2), see rules in Figure A.14) identifying areas representing dense wetland vegetation, and the second part (Figure 4.11(3), see rules in Figure A.15) identifying the remaining areas. In the case of the dense vegetation, high backscatter values in both images identified a set of potential wetland areas and texture thresholds identified specific sites. For the remaining wetland areas (step three), intermediate levels of dry season backscatter identified potential wetland sites, while various texture and other thresholds were used to identify areas

representing wetlands and to disregard *Non-wetland* areas initially included in the potential wetland sites. Region growing was also used to extend this classification.

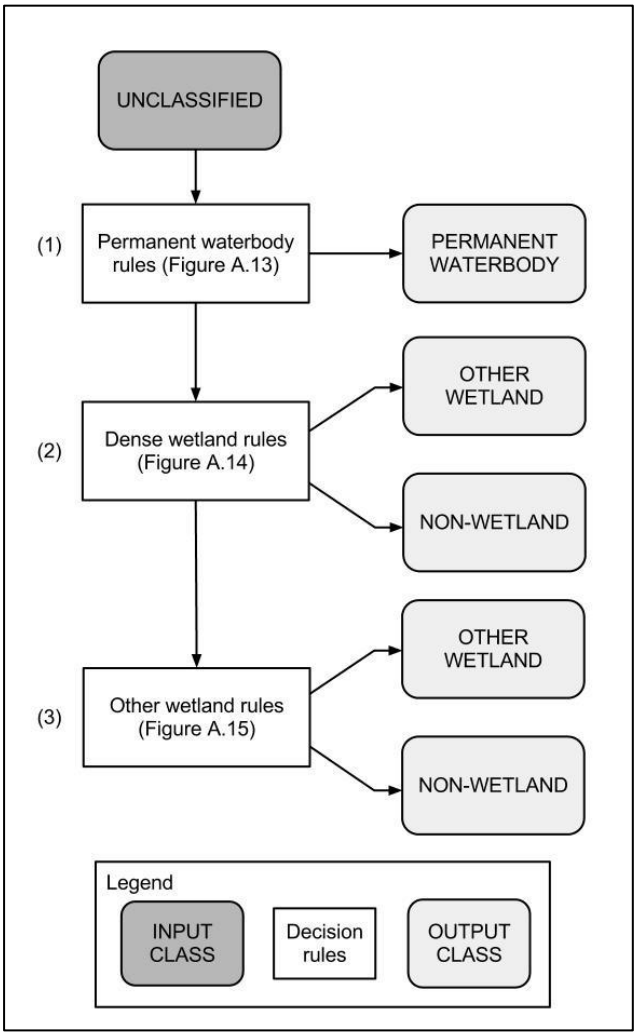

Figure 4.10: Schema for the classification of wetlands from SAR data only (see Figures A.13, A.14 and A.15)

4.2.3 Nearest-neighbour supervised classification

The supervised classification of the SAR imagery did not include an initial landcover classification phase because the images showed little potential for the identification of the landcover classes used in the SPOT-based classification. The classes used during the supervised classification of the SAR images, along with the number of samples used in each subset, are given in Table 4.6. The agricultural and upland classes, along with the *Bare ground (Non-wetland)* class, were assigned the label *Non-wetland* upon completion of the classification. The *Permanent waterbody* class was kept as is and the remaining classes were labelled *Other wetland.* Due to the nature of the different wetland sites occurring in the two subsets, slightly different strategies were again used in the two subsets regarding the classes included in the classification process.

Table 4.6: Number of samples used in the SAR-based wetlands classification

Class		Number of samples: Nuwejaars subset	Number of samples: Soetendalsvlei subset
Cultivated area		200	130
Upland vegetation	Alien	11	104
	Natural	21	
Bare ground (Non-wetland)		n/a	13
Permanent waterbody		57	23
Dense wetland vegetation		56	39
Emergent wetland vegetation		11	7
Medium wetland vegetation		47	58
Seasonal pan		22	13

As done in the SPOT-based supervised classification, the features included in the nearest-neighbour feature space were selected through the feature space optimisation tool in eCognition. Features selected for input to the tool included several object mean values, namely the backscatter from both images, the difference in backscatter between the two images, the mean of the two backscatter values and all computed Haralick texture measures for both images. The features selected by the tool are listed in Table 4.7.

Table 4.7: Features included in the classification feature space for SAR-based supervised classification

Features used: Nuwejaars subset	Features used: Soetendalsvlei subset
Feb, Sept σ_0	Feb, Sept σ_0
(Sept σ_0 – Feb σ_0)	(Sept σ_0 – Feb σ_0)
(Sept σ_0 + Feb σ_0) / 2	(Sept σ_0 + Feb σ_0) / 2
Feb, Sept contrast (11x11, 25x25)	Feb, Sept contrast (11x11, 25x25)
Feb, Sept correlation (11x11, 25x25)	Feb, Sept correlation (11x11, 25x25)
Feb, Sept dissimilarity (11x11, 25x25)	Feb, Sept dissimilarity (11x11, 25x25)
Feb GLDV entropy (11x11)	Feb, Sept GLDV entropy (11x11)
Feb inverse difference (11x11)	Feb, Sept mean (11x11, 25x25)
Feb, Sept mean (11x11, 25x25)	Feb, Sept standard deviation (11x11, 25x25)
Feb, Sept standard deviation (11x11, 25x25)	
Sept homogeneity (11x11, 25x25)	
Sept angular 2nd moment (11x11, 25x25)	
Sept entropy (11x11, 25x25)	
Sept GLDV angular 2nd moment (25x25)	

4.2.4 Accuracy assessment

Upon completion of both SAR-based classifications, statistical accuracy assessment was performed. The expert system was regarded first, followed by the supervised classification.

The error matrices (and associated accuracy measures) obtained from the expert system classification are presented in Table 4.8. Most of the measures indicate that classification results are poor. Both the producer's and the user's accuracies for *Other wetland* are particularly low, as is the user's accuracy for *Non-wetland*. The only measures attesting to reasonable results are the user's accuracy for *Permanent waterbody* (100%) and the producer's accuracy for *Non-wetland* (85%). The non-existent commission errors (0%) recorded by the former measure are offset by high omission errors (70%), indicating that *Permanent waterbody* is significantly underclassified even though the identified areas were correctly labelled. Overall accuracy is lower than considered acceptable (59%), and the kappa index value (0.38) signifies that the classification at best only moderately agrees with the reference data.

Table 4.8: Error matrix for the expert system classification of wetlands from SAR data

		Reference image			
		Permanent waterbody	*Other wetland*	*Non-wetland*	**Totals**
Classification product	*Permanent waterbody*	88	0	0	**88**
	Other wetland	26	49	22	**97**
	Non-wetland	36	101	128	**265**
	Totals	**150**	**150**	**150**	**450**

	Producer's accuracy (%)	**User's accuracy (%)**	**Omission errors (%)**	**Commission errors (%)**
Permanent waterbody	58.67	100.00	70.45	0
Other wetland	32.67	50.52	104.12	49.48
Non-wetland	85.33	48.30	8.30	51.70

Kappa index	**0.38**
Overall accuracy (%)	**58.89**

Accuracy measures for the SAR-based supervised classification are given in Table 4.9. Again, the results are unsatisfactory: the overall accuracy value of 62% is not sufficiently accurate and the kappa index value of 0.43 means that the classification only moderately agrees with the reference data. Individual user's and producer's accuracy values are poor (below 56%), except

for the user's accuracy values for *Permanent waterbody* (95%) and the producer's accuracy values for *Non-wetland* (80%). This corresponds with the results of the expert system.

Table 4.9: Error matrix for the supervised classification of wetlands from SAR data

		Reference image			
		Permanent waterbody	*Other wetland*	*Non-wetland*	**Totals**
Classification product	*Permanent waterbody*	83	3	1	**87**
	Other wetland	44	75	29	**148**
	Non-wetland	23	72	120	**215**
	Totals	**150**	**150**	**150**	**450**

	Producer's accuracy (%)	**User's accuracy (%)**	**Omission errors (%)**	**Commission errors (%)**
Permanent waterbody	55.33	95.40	77.01	4.60
Other wetland	50.00	50.68	50.68	49.32
Non-wetland	80.00	55.81	13.95	44.19

Kappa index	**0.43**
Overall accuracy (%)	**61.78**

These results confirm that classification of wetlands using only a limited number of single-band, single-polarisation SAR images is extremely challenging. This has been documented in previous research (Henderson & Lewis 2008). However, some studies have suggested that these difficulties can be overcome by using texture measures (Arzandeh & Wang 2002). This study found that acceptable accuracy levels are unachievable when wetlands are classified using only the backscatter values from two single-polarisation SAR images. The addition of texture measures does seem to improve the accuracies (initial experiments in developing a SAR-based expert system classification without them were not successful). However they remain too low to make this method worthwhile. Furthermore, the rules that were developed are highly complex and make use of very specific thresholds and region-growing methods. They are not robust and it is unlikely that they will be applicable to larger or different areas. The goal was to demonstrate that even when using such methods, accuracy levels will fall short of being acceptable. The implications of this are discussed in the final chapter. The next section concerns the combined sensor classifications.

4.3 SPOT/SAR combined classifications

This section deals with the classifications derived from a combination of the SPOT and SAR datasets. First, the expert system classification combining the two datasets is considered, then the supervised classification is discussed and finally the statistical accuracy assessments of the results are presented.

4.3.1 Expert system classification

The expert system SPOT/SAR combined classification used the SPOT-based landcover classification presented in Section 4.1.2.1 as its basis. The classes *Cultivated area* and *Roads* were set to *Non-wetland*, while the *Permanent waterbody* class was left as is. SAR-based knowledge rules were applied to the three *Natural and semi-natural vegetation* classes *(Sparse vegetation, Medium vegetation and Dense vegetation)* and the *Bare ground* class to identify the areas representing wetlands. Temporary wetland classes were used during the classification process and aggregated into the *Other wetland* class upon completion. The classification process is illustrated in Figure 4.11 and the full ruleset is given in Appendix A (Figures A.16 and A.17).

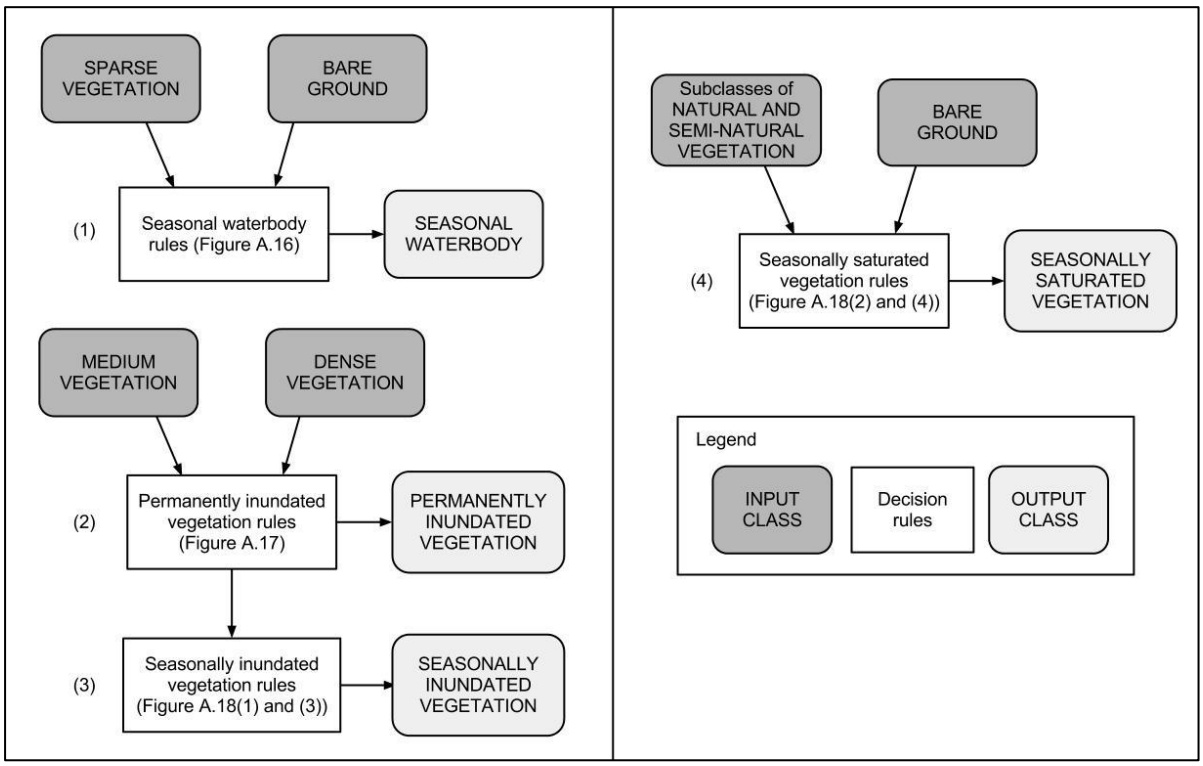

Figure 4.11: Schema for the SAR-based expert system classification of wetlands from SPOT-derived landcover classes (see Figures A.16, A.17 and A.18)

The relatively small objects used for the SPOT-based landcover classification were unsuitable for use with the lower spatial resolution SAR pixels. Consequently, the objects of the four landcover classes that possibly represent wetlands (the three *Natural and semi-natural* vegetation

classes and *Bare ground*) were separately fused using the IOF function. This created a segmentation that maintained the boundaries between neighbouring objects of different landcover classes, but fused neighbouring objects of the same landcover class according to their values in the SAR images. A threshold in the sum of the per-object standard deviations of the two σ_0 images was used to determine whether or not objects should be merged, as a low value in this variable would indicate that an object is homogenous in both σ_0 images. This threshold was set to 1. Further, the algorithm was set to fuse an object with all fitting neighbour objects.

Wetlands classification was complicated by the difficulty of identifying water surfaces in the wet season SAR image. At the time of the acquisition of this image, strong winds caused significant wave action in waterbodies. Water normally acts as a specular reflector of microwaves and can usually be identified through very low returns. This was the case in the dry season image where waterbodies were identified by having the lowest returns of any features in the image. In the wet season image the reverse is true: waves on the water surface caused very high returns, in some cases higher than any other feature. Moreover, this wind influence is inconstant over waterbodies so that rules were needed that make allowances for unaffected water areas that could be characterised by specular reflection (e.g. if they are shielded from wind by tall vegetation or other features). Combinations of scattering mechanisms in areas affected by intermediate levels of wind can make such areas indistinguishable from other classes.

Step 1 in this classification process is the identification of the *Seasonal waterbody* class (Figure 4.11(1)). This class represents seasonal pans filled with water at the time of the acquisition of the wet season SAR image, but not the dry season image (it was assumed that *Permanent waterbody* was successfully classified from the SPOT image). The rules for its identification were applied to the classes *Bare ground* and *Sparse vegetation*. These rules have to take into account the aforementioned issues regarding the identification of waterbodies on the SAR images. Hence, the rules identified areas with very high wet season backscatter, areas experiencing large decreases in backscatter between the wet and dry seasons, and areas unaffected by wind, so showing a very low wet season backscatter along with an increase in backscatter between the wet and the dry seasons.

Step 2 is the identification of *Permanently inundated vegetation* (Figure 4.11(2)). This class is identifiable through high backscatter values in both SAR images and a drop in backscatter between the wet and dry seasons. The latter is surmised to occur due to lower water levels in the dry season, which increase the influence of volume scattering and decrease the influence of double-bounce scattering. Only *Medium vegetation* and *Dense vegetation* objects were considered as candidates for this class.

Finally, the classes *Seasonally inundated vegetation* and *Seasonally saturated vegetation* were regarded in steps 3 and 4 (Figures 4.11(3) and (4)). *Seasonally inundated vegetation* was identified through high wet season backscatter or an increase in backscatter between the wet and dry seasons. *Seasonally saturated vegetation* was identified by a decrease in backscatter between the wet and dry seasons, with a lower decrease threshold needed if the dry season backscatter was very low. *Medium vegetation* and *Dense vegetation* objects were considered candidate objects for *Seasonally inundated vegetation,* while all potential wetland classes were considered candidates for *Seasonally saturated vegetation.*

After execution of the final expert system rules, the supervised classification was performed. This is discussed next.

4.3.2 Nearest-neighbour supervised classification

The supervised SPOT-SAR combined classification used the supervised SPOT-based landcover classification product described in Section 4.1.3 as input. The reclassification of the landcover classes potentially representing wetlands was done in two separate steps. In step 1 the areas identified as *Natural and semi-natural vegetation* were split into the wetland classes *Dense wetland vegetation, Emergent wetland vegetation* and *Medium wetland* vegetation, and the upland classes *Alien upland vegetation* and *Natural upland vegetation* (combined into one *Upland vegetation* class in the Soetendalsvlei subset). In step 2 the areas identified as bare ground were split into the classes *Seasonal pan* and *Bare ground (Non-wetland).*

The sample selection was done in the same iterative process described in Section 4.1.3. The number of samples used in the product is given in Table 4.10. The feature space optimisation tool was used to determine the optimal features to be included in the nearest-neighbour feature space. These are given in Table 4.11.

Statistical accuracy assessment was performed on the results of both SPOT/SAR combined classifications. This is discussed in the following subsection.

Table 4.10: Number of samples used in the combined SPOT and SAR wetlands classification

Class		Number of samples: Nuwejaars subset	Number of samples: Soetendalsvlei subset
Upland vegetation	Alien	11	115
	Natural	16	
Bare ground (Non-wetland)		10	29
Dense wetland vegetation		40	34
Emergent wetland vegetation		16	13
Medium wetland vegetation		26	46
Seasonal pan		43	20

Table 4.11: Features included in the classification feature space for SPOT/SAR combined wetlands classification

Features used: Nuwejaars subset	Features used: Soetendalsvlei subset
Green	NIR
NIR	SWIR
NDWI	EVI_2
MED (Red, 11x11)	NDTI
MPED (5x5, 11x11)	NDWI
Feb, Sept σ_0	Feb, Sept σ_0
(Sept σ_0 – Feb σ_0)	(Sept σ_0 – Feb σ_0)
Sept dissimilarity (25x25)	Sept dissimilarity (25x25)
Sept GLDV entropy (25x25)	

4.3.3 Accuracy assessment

Error matrices and associated accuracies for the SPOT/SAR combined classifications are presented in Tables 4.12 and 4.13. The results for the expert system are discussed first, followed by those of the supervised classification.

The overall accuracy of the expert system was reasonable at 77%. Furthermore, the classification of *Permanent waterbody* is highly accurate (producer's accuracy is 94% and user's accuracy is 95%) as it was taken from the same SPOT-based landcover classification used as input to the SPOT-based wetlands classification. However, the producer's accuracy for *Other wetland* (45%) is unacceptable. The user's accuracy for *Non-wetland* (63%) is also low. Moreover, the Kappa index is relatively low (0.66) showing that the classification result is relatively closer to a random classification than desired.

In the supervised classification, the combination of SPOT and SAR data achieved a slightly lower overall accuracy (82%) than the SPOT-based classification (83%). All the individual producer's and user's accuracy values exceed 72% and the kappa index value is 0.73. The producer's accuracy for *Other wetland* is 75% which is significantly better than the 45% recorded by the expert system.

This concludes the discussion of the combined-sensor classifications. The following section discusses specific classification examples to better illustrate the classification results reported in Sections 4.1, 4.2 and 4.3.

4.4 Classification examples

Six sets of maps of specific wetland areas (three in each subset) are qualitatively assessed to demonstrate the classification results obtained by the different approaches. Each set of maps shows the expert system and supervised classification results for each of the SPOT-based, SPOT-SAR combined and SAR-based classifications.

Figure 4.12 shows the southern section of Waagschaalvlei. The SPOT-based expert system produced good results in this class, with few omission errors. Notable commission errors do occur in a small stand of alien trees a short distance south of the wetland boundary. The combined-sensor expert system avoided these commission errors, but it was unsuccessful in recognising the dense reedbeds and phragmite stands characterising this wetland. The SAR-based expert system did identify some wetland areas, but could not recognise the largest pools as waterbodies. The SPOT-based supervised classification achieved relatively good results, but some errors did occur. The combined-sensor supervised classification avoided both the widespread omission errors of the combined-sensor expert system and the commission errors in the stand of alien trees which occurred when only SPOT data was used. The SAR-based supervised classification fared better than the SAR-based expert system, but this could be a result of some training area polygons that had been collected in the area shown which may have artificially improved the map.

Figure 4.13 shows wetlands and agricultural areas along the western edge of Voëlvlei. The SPOT-based and combined-sensor classifications produced comparable results, with few commission errors in agricultural areas and relatively few omission errors at the edge of the lake. However, the wetlands at the south-western corner of the map proved more difficult to classify. The SAR-based classifications were less successful, but produced relatively good results for the *Permanent waterbody* class in Voëlvlei compared to some of the smaller lakes.

Table 4.12: Error matrix for the expert system classification of wetlands from a combination of SPOT and SAR data

		Reference image			
		Permanent waterbody	*Other wetland*	*Non-wetland*	**Totals**
Classification product	*Permanent waterbody*	141	7	0	**148**
	Other wetland	4	67	10	**81**
	Non-wetland	5	76	140	**221**
	Totals	**150**	**150**	**150**	**450**

	Producer's accuracy (%)	**User's accuracy (%)**	**Omission errors (%)**	**Commission errors (%)**
Permanent waterbody	94.00	95.27	6.08	4.73
Other wetland	44.67	82.72	102.47	17.28
Non-wetland	93.33	63.35	4.52	36.65

Kappa index	**0.66**
Overall accuracy (%)	**77.33**

Table 4.13: Error matrix for the nearest-neigbour classification of wetlands from a combination of SPOT and SAR data

		Reference image			
		Permanent waterbody	*Other wetland*	*Non-wetland*	**Totals**
Classification product	*Permanent waterbody*	128	2	0	**130**
	Other wetland	20	112	22	**154**
	Non-wetland	2	36	128	**166**
	Totals	**150**	**150**	**150**	**450**

	Producer's accuracy (%)	**User's accuracy (%)**	**Omission errors (%)**	**Commission errors (%)**
Permanent waterbody	85.33	98.46	16.92	1.54
Other wetland	74.67	72.73	24.68	27.27
Non-wetland	85.33	77.11	13.25	22.89

Kappa index	**0.73**
Overall accuracy (%)	**81.78**

Figure 4.13 shows wetlands and agricultural areas along the western edge of Voëlvlei. The SPOT-based and combined-sensor classifications produced comparable results, with few commission errors in agricultural areas and relatively few omission errors at the edge of the lake. However, the wetlands at the south-western corner of the map proved more difficult to classify. The SAR-based classifications were less successful, but produced relatively good results for the *Permanent waterbody* class in Voëlvlei compared to some of the smaller lakes.

Figure 4.14 shows the results obtained in a section of the Nuwejaars river, a seasonal pan and surrounding wetlands, as well as agricultural areas. None of the classification approaches could successfully classify the centre of the pan. This is probably attributable to measurable returns from submerged vegetation or the bed of the pan when the water is sufficiently shallow. The SPOT-based expert system produced the most accurate delineation of palustrine wetlands with almost no commission errors. However, all the expert system approaches struggled to identify the denser sections of wetland occurring on the banks of the river. The supervised results were more successful along the river, but recorded some commission errors in agricultural areas. Both SAR-based approaches were relatively accurate in the palustrine wetlands along the seasonal pan, but misclassified most of the sections along the river.

Figure 4.15 shows a section of seasonal pans and palustrine wetlands north of Soetendalsvlei, surrounded by natural upland vegetation. The SPOT-based and combined-sensor expert system classifiers performed best in this area and avoided the substantial commission errors clearly visible in their supervised counterparts. However, the combined-sensor expert system shows some omission errors in the seasonal pan (along the southern edge of the map). The SAR-based expert system records few commission errors but substantial omission errors, while the SAR-based supervised classification reveals substantial omission and commission errors.

Figure 4.16 is the inflow area of the Nuwejaars River into Soetendalsvlei with the surrounding palustrine wetlands and the dense, partly inundated vegetation in the vlei itself. The SPOT-based expert system performed well, but by comparison the combined-sensor expert system is characterised by substantial omission errors. The SAR-based expert system shows widespread omission errors. The results of the SPOT-based and combined-sensor supervised classifications are comparable, with more commission errors occurring in the former than in the latter. The SAR-based supervised classification fared substantially better than its expert system equivalent.

Figure 4.17 shows the stretch of the Heuningnes River just upstream of its mouth, some surrounding seasonal pans and some coastal dune vegetation. All the classifications, bar the SAR-based expert system, show commission errors in coastal dune vegetation. Both SPOT-

based and both combined-sensor classifications classified the seasonal pan with high accuracy. The combined-sensor expert system is, however, less successful in classifying the wetlands along the river edge. The SAR-based expert system shows substantial omission errors, while its supervised equivalent has the same limitation, but it also produced substantial commission errors.

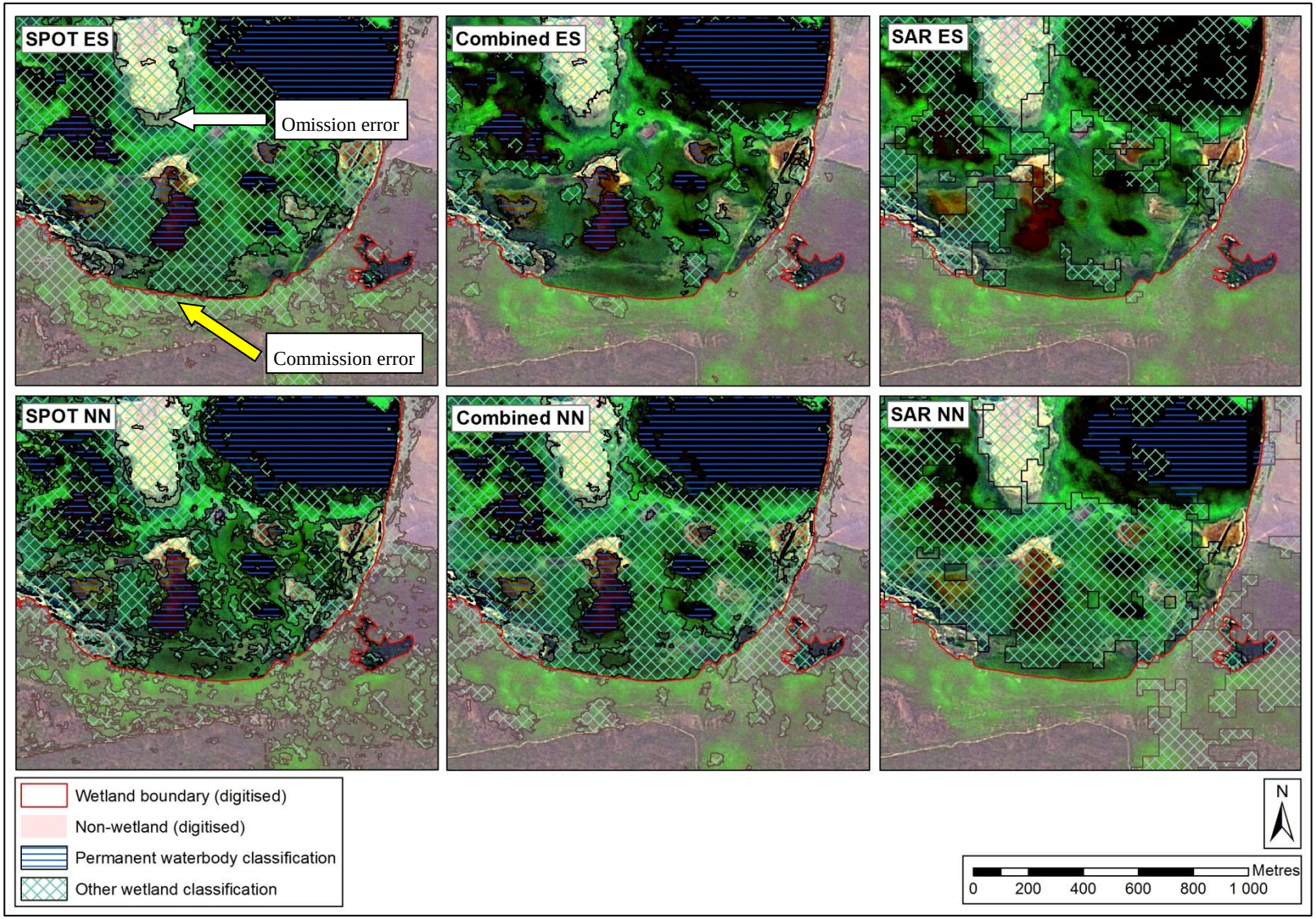

Figure 4.12: Classification results for the southern section of Waagschaalvlei

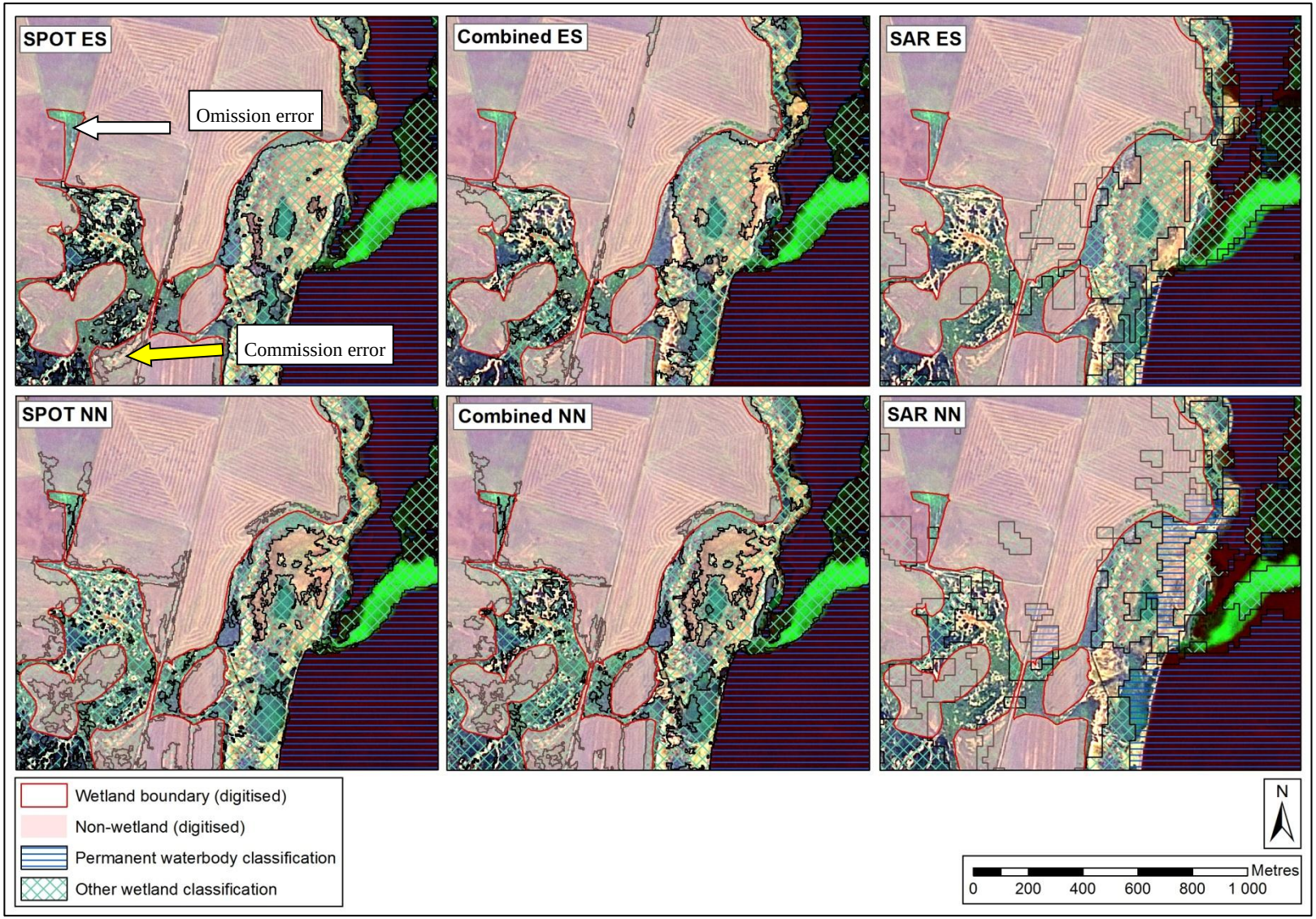

Figure 4.13: Classification results along the western edge of Voëlvlei

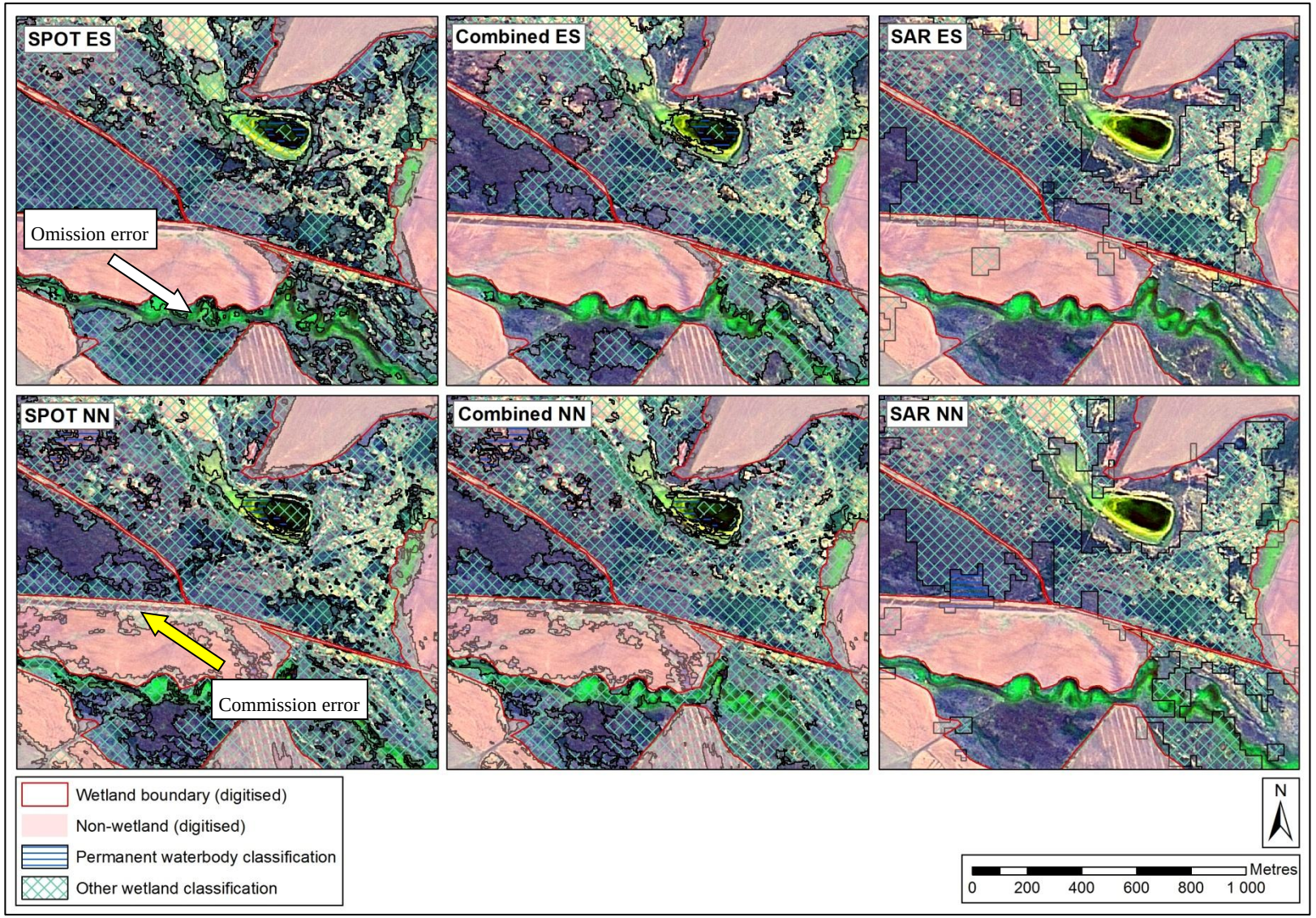

Figure 4.14: Classification results for the seasonal pan and agricultural areas in the north-eastern section of the Nuwejaars subset

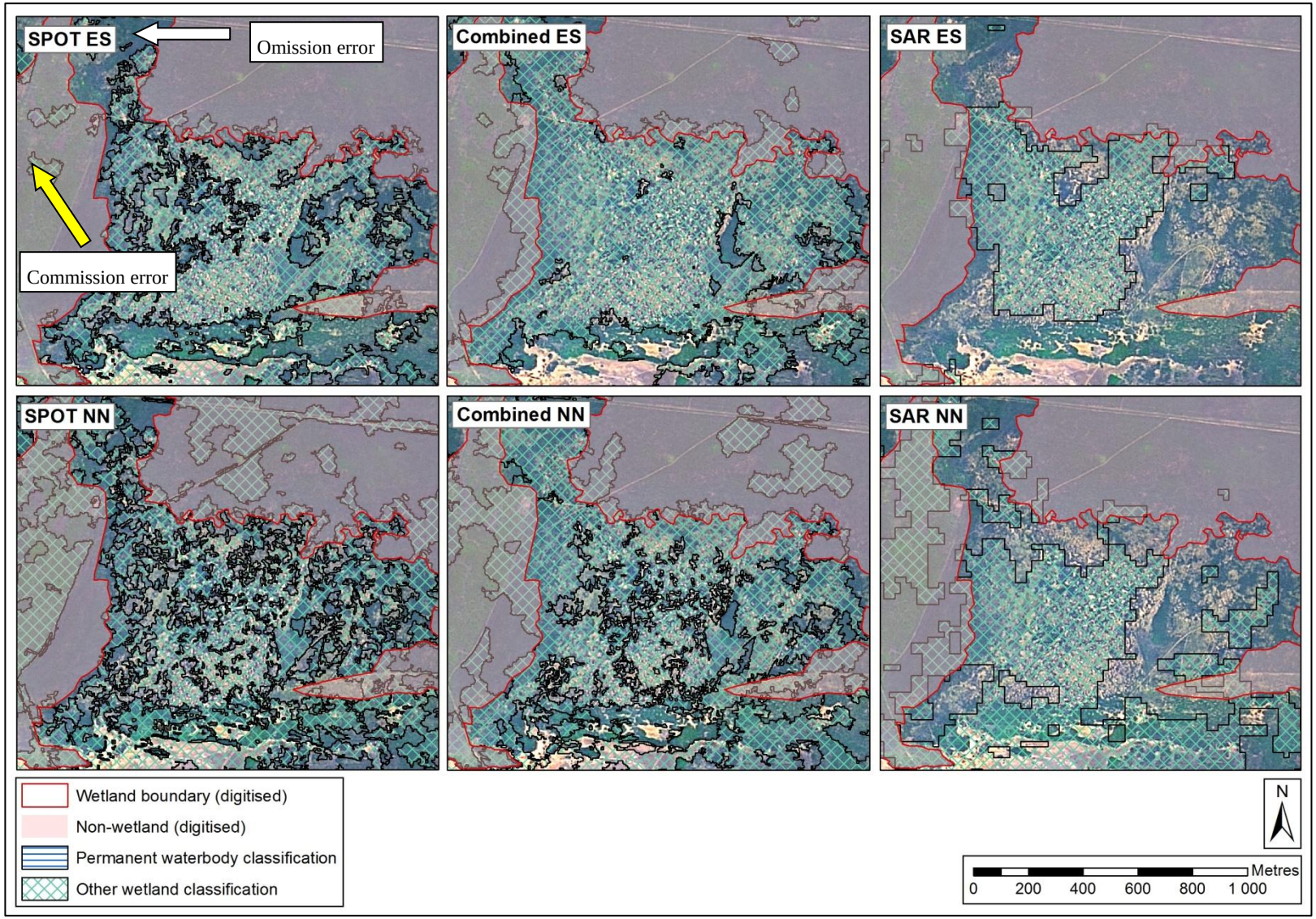

Figure 4.15: Classification results for palustrine wetlands north of Soetendalsvlei

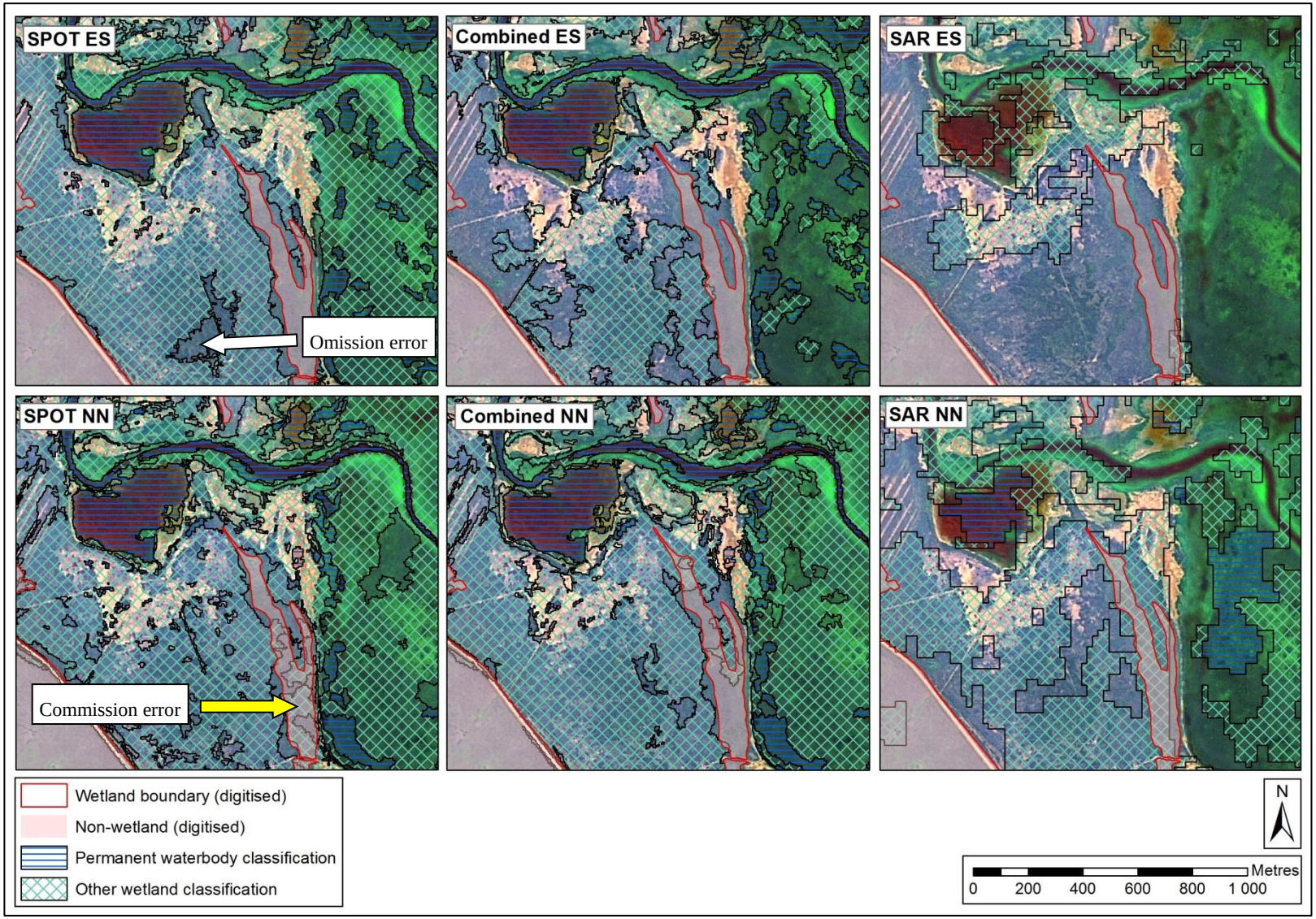

Figure 4.16: Classification results for the inlet of the Nuwejaars River into Soetendalsvlei

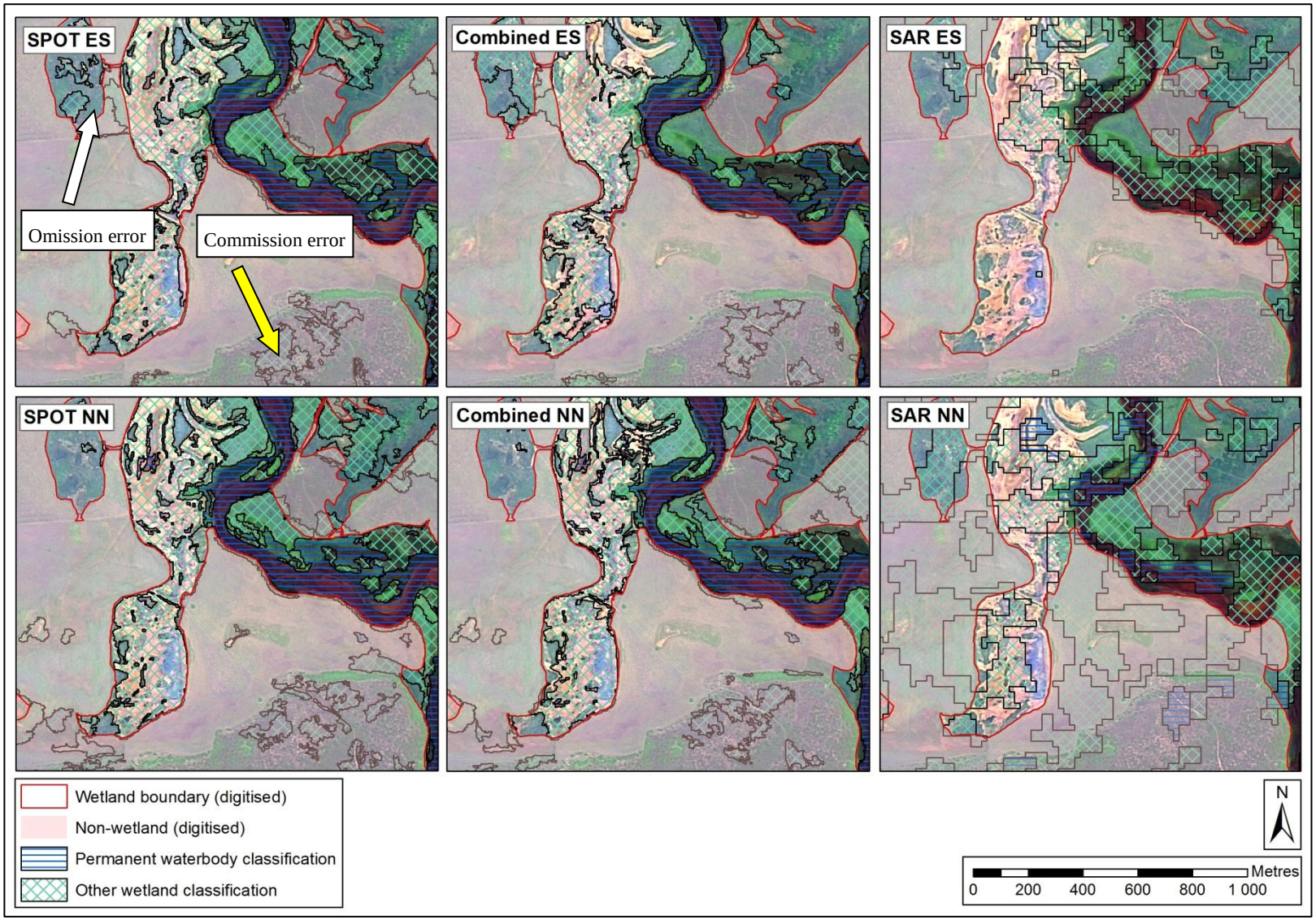

Figure 4.17: Classification results in the Heuningnes River and surrounding seasonal pans close to De Mond

This chapter has reported the classification process followed in this research and presented several examples illustrating the classification results. The influence of the different combinations of data and classifiers on the classification results will be discussed in the next and final chapter. Concluding remarks will be provided, and recommendations for future research avenues in wetlands classification will be made.

CHAPTER 5: DISCUSSION AND CONCLUSIONS

This study investigated the remotely sensed classification of wetlands on the Agulhas Plain. In this chapter, the results will be interpreted to determine which combination of the available data and classifiers best suits the research objectives. Avenues for future research will be investigated and concluding remarks will be made.

5.1 SAR and VIR sensors for Agulhas wetlands classification

This research only considered SPOT 5 and ERS2 data. Consequently the findings do not give a full picture of the use of VIR and SAR imagery in wetlands classification, as newer, more advanced sensors exist for both types of data. However, the aim of this study was to find a cost-effective method and data from those more advanced sensors is significantly more expensive.

Given this context, it is clear that two single-polarisation C-band SAR images alone do not provide enough information for accurate mapping of the Agulhas Plain's wetlands. Regardless of the classifier used, overall accuracies did not exceed 62% when this data was used, with commission and omission errors being consistently high. Although some scholars had suggested this degree of overall accuracy to be reasonable, the results cannot be regarded as acceptable for local environmental monitoring. Also, the Kappa index estimates barely exceeded the minimum threshold for the classification results to be considered as moderately in agreement with the reference data (Congalton & Green 2009) and individual user's and producer's accuracy measures were consistently poor.

Adding SAR texture parameters did seem to enhance classification results, but failed to achieve the levels of accuracy reported in previous studies. The texture parameters chosen were based on findings by Arzandeh and Wang (2002), but they had used data with a different polarisation and spatial resolution (RADARSAT-1). Therefore, it is possible that the set parameters were suboptimal for this application, and it is acknowledged that further experimentation in this regard could provide larger improvements in accuracy. However, the difficulty in relating some textural parameters to real-world features complicates their application in an expert system classifier.

Another factor influencing the SAR-based classification is the variations in backscatter caused by wind-induced waves on open water surfaces in the wet season image. It is strongly

recommended that future research on this topic avoids wind-influenced C- or X-band SAR imagery, as this significantly complicates the identification of water surfaces.

In comparison to the SAR-based classification, the accuracy achieved in the application of SPOT data was consistently higher. Overall accuracies using SPOT imagery were 83% (supervised) and 84% (expert system), while Kappa index estimates were 0.74 (supervised) and 0.75 (expert system). Accuracy for the class *Permanent waterbody* was particularly high, with producer's and user's accuracies ranging from 85 to 98%. Accuracy in the classifications of *Other wetland* was also relatively high, the only exception being the producer's accuracy for the expert system classification (65%). This indicates that significant omission errors occurred in the classification of *Other wetland*, partly because of the difficulty of separating coastal dune vegetation from several types of seasonal wetland vegetation, and *Permanent waterbody* commission errors in *Other wetland* areas in Soetendalsvlei.

The combination of SPOT and SAR data failed to significantly improve the classification of *Other wetland* areas when compared to the use of SPOT data only. In fact, it provided less accurate results with the expert system classifier and slightly less accurate results with the supervised classifier. A major failure of the SPOT/SAR combined expert system classification was again a very low producer's accuracy for *Other wetland* (45%). One factor contributing to this problem is the difficulty of recognising dense, tall wetland vegetation with C-band SAR data. In this case, dense phragmite stands in Soetendalsvlei were characterised by returns similar to those of coastal dune vegetation, which made differentiating between them problematic. Another factor that could be exacerbating this problem is the strategy of using only the SPOT data for the landcover classification, and only the SAR data for the wetlands differentiation. In the supervised classification the SPOT and the SAR data were combined in the wetlands differentiation step, and the producer's accuracy for *Other wetland* was as a result reasonably good.

5.2 Expert system vs supervised classifier

The two classifiers investigated in this research provided similar results. In terms of overall classification accuracy the supervised classifier fared slightly better in the SAR-based and combined-sensor classifications, while the expert system performed slightly better in the SPOT-based classification. However, in terms of individual accuracy measures the supervised classifier obtained more consistent results. Specifically, the producer's accuracy for *Other wetland* was

poor in the expert system but good in the supervised classification for both the SPOT-based and the combined-sensor classifications.

The choice of a classifier for a classification project is not only related to the achievable accuracy, but also to the specific needs of that project. The cost of creating an expert system ruleset will be prohibitive for many studies; in this study it took a significantly longer time to create than to perform the supervised classifications. In cases where little contextual data is available or applicable (i.e. when the focus is on spectral data only), it is expected that expert rules implementing simple thresholds will be significantly less effective than most other classifiers as such classifiers employ much more sophisticated decision boundaries between classes. However, there are applications, particularly in an OBIA environment, where contextual data will play a role. For example, in this project the *Roads* class was identified in the expert system almost entirely through contextual rules. This class was in fact not considered at all in the supervised classification. It is recommended that future research implementing supervised classifications use an integrated approach in which the supervised classifier is augmented with expert rules to identify context-related classes.

One of this study's aims was to develop the classification approach in such a way that it could be replicated with relative ease at a different time or in a different area. While this aim has not been properly tested in this study (the same imagery was used in both subsets), some recommendations can be made in this regard. If the classification is to be performed on larger areas, the cost of the supervised classification is increased significantly by the need for a larger number of training areas. In comparison, a well-defined expert system ruleset, derived from properly normalised imagery, should theoretically be applicable to imagery from other areas and other dates without modification. This seems plausible if *Permanent waterbody* areas are to be classified from SPOT data, as the SPOT-based landcover classification rules achieved similar results in both subsets. However, the SPOT-based rules for vegetated wetland discrimination that had initially been developed in the Nuwejaars subset needed substantial modification to classify both subsets accurately. This raises some questions about the application of these rules to areas where conditions are different from those in the study area. The combined sensor expert rules were transferred between the subsets without modification, but the poor producer's accuracy for *Other wetland* with this classification approach limits its applicability. It is further acknowledged that all the rulesets used in this study would require significant modification if they are to be applied to terrain including urban areas or agricultural areas different from those found in the

study area. Consequently, it cannot be stated with confidence that the expert system rules developed here will produce acceptable classifications in other areas. Further research is needed in this regard.

The ability of the developed expert system rules to monitor the same areas investigated here in different years has also not been assessed in this study, but it seems feasible. A requirement would, however, be that the imagery be sourced for dates representing conditions similar to those in this study, regarding both agricultural landcover and soil moisture. It is also recommended that such a study avoid the use of wind-influenced SAR images, although this would require a modification of the current rules.

5.3 Suggested research avenues and recommendations

5.3.1 Advanced SAR analysis

Multi-polarised SAR data, and polarimetric decomposition methods in particular, can be successfully applied in wetlands classification (Yajima et al. 2008; Touzi et al. 2009). Because this data shows great promise for wetlands studies, the topic should be further investigated.

The application of SAR interferometry to wetlands has been investigated. It is particularly useful for identifying water level changes in flooded wetlands (Hong, Wdowinski & Kim 2010).

5.3.2 Fusing SAR and VIR data

Some studies have examined fusing SAR and VIR data into a single dataset before classification (Sanli, Kuruco & Esetlili 2009). This could potentially be useful in wetlands classification.

5.3.3 Classifiers

Quite likely the results obtained here from supervised classification can be further improved through the use of more advanced classifiers. The new release of eCognition Developer coinciding with the completion of this study incorporates CART decision trees as well as SVMs, and data extracted from objects in eCognition could possibly be applied to any number of classifiers in statistical packages, notably ANNs.

5.3.4 Transferability of expert system rules

This study noted that robust expert system rules could potentially classify wetlands in imagery of other areas or different dates, but was unable to evaluate this due to data constraints. The

increased degree of classification automation potentially resulting from such rules makes this a topic worthy of further research.

5.4 Conclusions

This research set out to develop a classification approach for Cape Agulhas wetlands which is cost-effective, accurate, relatively simple to replicate for other years, and transferrable to other areas with relatively little effort. Wetland classes were originally to be distinguished on the basis of wetland hydrology, i.e. inundation or soil water saturation states of wetlands. However, a lack of appropriate field data narrowed the focus of the study to total wetland extent, as indicated by wetland-specific vegetation, waterbodies and bare seasonal pans. The only distinction within wetland areas was that between permanent waterbodies and other wetland areas.

The requirement of cost-effectiveness was met, as the imagery used was relatively inexpensive to acquire, and a limited number of images was used. The accuracy requirement was met by some of the implemented strategies, but not all. An accurate classification was not obtainable from the available SAR data only, irrespective of the classifier used. Expert system classifications from SPOT data only, as well as from a combination of SPOT and SAR data, achieved relatively high levels of accuracy throughout, but were unsupported by the low levels of producer's accuracy for non-open water wetland areas. Supervised classifications did not experience this problem, and obtained comparable or slightly higher accuracy levels in all other measures. Supervised results from the combination of SPOT and SAR data were slightly less accurate than those from SPOT data only in terms of overall accuracy, but not significantly so. Furthermore, any perceived gains of the combined approach might be offset in many applications by the additional cost of the SAR data. It is suggested that the results from the supervised classification can be significantly improved through augmenting the supervised classification with expert system rules which use object context to identify complicated classes and perform postprocessing.

The expert system rulesets should ably fulfil the requirement of the classification approach being replicable in other years, provided that the imagery used represents similar conditions. This has however not been tested in this study, and is a subject for future research. Also, whether or not the results obtainable from these expert system rules in the Soetendalsvlei area particularly are sufficiently accurate depends on the specific application. The difficulty in transferring expert system rules between two subsets within the same imagery suggests that these rules require significant modification to successfully perform classifications of other areas. This is particularly

true if such areas contain landcover classes not represented in this study area. On the other hand, the general strategy used in the supervised classification should be easy to replicate in a classification for a different year or area, but its cost is increased significantly by the need for new samples for each classification. This cost might, however, still be less than the cost of creating and modifying the expert system rules.

Both the ERS-2 sensor and its successor, Envisat, were decommissioned subsequent to the completion of this study. However, the large archive of data available for both these sensors ensures the continuing relevance of the findings of this study. Furthermore, C-band SAR data is still available from other C-band SAR sensors such as RADARSAT-2, and should shortly be available for the planned successor of ERS/Envisat, Sentinel-1.

To conclude, this research started off by noting the critical importance of the regular inventorying of the extent of sensitive wetland ecosystems, and has presented viable remote sensing-based methods to achieve this for Agulhas Plain wetlands. The classification methodology recommended is a supervised classification augmented by expert system rules. An accurate classification of total wetland extent is possible from dry season SPOT data. The addition of ERS-2 C-band SAR images from the wet and dry seasons failed to provide an increase in accuracy. Further research is needed to determine whether the expert system rules developed here can be improved to make them applicable to wetlands classification in other areas, but it is suspected that additional data will be required to make this possible.

REFERENCES

Allan DG, Seaman MT & Kaletja B 1995. The endorheic pans of South Africa. In Wetlands of South Africa [online]. Pretoria: Department of Environmental Affairs and Tourism. Available from: http://wetlands.sanbi.org/articles2/File/wetlandssa06.pdf [Accessed 2 October 2009].

Anderson JR, Hardy EE, Roach JT & Witmer RE 1976. *A land use and land cover classification system for use with remote sensor data*. Professional Paper. United States Geological Survey.

Arzandeh S & Wang J 2002. Texture evaluation of Radarsat imagery for wetland mapping. *Canadian Journal of Remote Sensing* 28: 653-666.

Baatz M & Schäpe A 2000. Multiresolution segmentation: An optimization approach for high quality multi-scale image segmentation. *Journal of Photogrammetry and Remote Sensing* 58: 12-23.

Baghdadi N, Bernier M, Gauthier R & Neeson I 2001. Evaluation of C-band SAR data for wetlands mapping. *International Journal of Remote Sensing* 22: 71-88.

Baraldi A & Parmiggiani F 1995. An investigation of the textural characteristics associated with gray level cooccurrence matrix statistical parameters. *IEEE Transactions on Geoscience and Remote Sensing* 33: 293-304.

Barbier EB, Acreman M & Knowler D 1997. Economic valuation of wetlands [online]. Gland, Switzerland: Ramsar Convention Bureau. Available from: http://www.ramsar.org/pdf/lib/lib_valuation_e.pdf [Accessed 28 May 2011].

Barnes KN 1998. Heuningnes river and estuary system. In Barnes KN (ed) *The important bird areas of Southern Africa*, 266-267. Randburg: Birdlife South Africa.

Bickerton IB 1984. Report 25: Heuningnes. In Heydoorn AEF & Grindley JR (eds) *Estuaries of the Cape Part II: Synopses of available information on individual systems*. CSIR research report No 424. Stellenbosch.

Blaschke T 2010. Object based image analysis for remote sensing. *ISPRS Journal of Photogrammetry and Remote Sensing* 65: 2-16.

Blaschke T, Lang S, Lorup E, Strobl J & Zeil P 2000. Object-oriented image processing in an integrated GIS/remote sensing environment and perspectives for environmental applications.

In Cremers A & Greve K (eds) *Environmental information for planning, politics and the public*, 555-570. Marburg: Metropolis Verlag.

Bock M, Xofis P, Mitchley J, Rossner G & Wissen M 2005. Object-oriented methods for habitat mapping at multiple scales – case studies from northern Germany and Wye Downs, UK. *Journal for Nature Conservation* 13: 75-89.

Boerner W-M 2008. Recent advances of POL-SAR, POL-IN-SAR & RP-POL-INSAR imagery for remotely sensing natural habitats: Desert and wetlands remote sensing. Paper delivered at the International Conference on Recent Advances in Microwave Theory and Applications, Jaipur, India.

Bolstad PV & Lillesand TM 1992. Rule-based classification models: Flexible integration of satellite imagery and thematic spatial data. *Photogrammetric Engineering and Remote Sensing* 58: 965-971.

Bourgeau-Chavez LL, Kasischke ES, Brunzell SM, Mudd JP, Smith KB & Frick AL 2001. Analysis of space-borne SAR data for wetland mapping in Virginia riparian ecosystems. *International Journal of Remote Sensing* 22: 3665-3687.

Boyd DS, Sanchez-Hernandez C & Foody GM 2006. Mapping a specific class for priority habitats monitoring from satellite sensor data. *International Journal of Remote Sensing* 27: 2631-2644.

Breen CM, Heeg J & Seaman M 1993. South Africa. In Whigham DF, Dykyjová D & Hejný S (eds) *Wetlands of the world i: Inventory, ecology, and management*, 79-110. Dordrecht: Kluwer Academic Publishers.

Brown de Colstoun EC, Story MH, Thompson C, Comisso K, Smith TG & Irons JR 2003. National park vegetation mapping using multitemporal Landsat 7 data and a decision tree classifier. *Remote Sensing of Environment* 85: 316-327.

Campbell JB 2002. *Introduction to remote sensing.* 3rd ed. New York: The Guildford Press.

Canty MJ 2007. *Image analysis, classification and change detection in remote sensing.* Boca Raton: Taylor & Francis Group, LLC.

Chen Y, Su W, Li J & Sun Z 2009. Hierarchical object oriented classification using very high resolution imagery and LIDAR data over urban areas. *Advances in Space Research* 43: 1101-1110.

Chuvieco E & Huete A 2010. *Fundamentals of satellite remote sensing.* Boca Raton: Taylor & Francis.

Cohen Y & Shosheny M 2002. A national knowledge-based crop recognition in Mediterranean environment. *International Journal of Applied Earth Observation and Geoinformation* 4: 75-87.

Conchedda G, Durieux L & Mayaux P 2008. An object-based method for mapping and change analysis in mangrove ecosystems. *ISPRS Journal of Photogrammetry and Remote Sensing* 63: 578-589.

Congalton RG & Green K 2009. *Assessing the accuracy of remotely sensed data: Principles and practices.* Boca Raton: Taylor & Francis.

Cowan GI 1995. South Africa and the Ramsar convention. In Wetlands of South Africa [online]. Pretoria: Department of Environmental Affairs and Tourism. Available from: http://wetlands.sanbi.org/articles2/File/wetlandssa01.pdf [Accessed 15 March 2009].

Cowan GI & Van Riet W 1998. *A directory of South African wetlands.* Pretoria: Department of Environmental Affairs and Tourism.

Davies B & Day J 1998. *Vanishing waters.* Cape Town: University of Cape Town Press.

Davranche A, Lefebvre G & Poulin B 2010. Wetland monitoring using classification trees and SPOT-5 seasonal time series. *Remote Sensing of Environment* 114: 552-562.

Dogan OK, Akyurek Z & Beklioglu M 2008. Identification and mapping of submerged plants in a shallow lake using Quickbird satellite data. *Journal of Environmental Management* 90: 2138-2143.

Drăguţ L & Blaschke T 2006. Automated classification of landform elements using object-based image analysis. *Geomorphology* 81: 330-344.

Dugan PJ (ed) 1990. *Wetland conservation: A review of current issues and required action.* Gland, Switzerland: IUCN.

ERDAS 2010. *ERDAS field guide.* Norcross, USA: ERDAS Inc.

ESA s.a.: Synthetic aperture radar: Land applications tutorial part 1: Background and theory [online]. Paris: European Space Agency. Available from: www.tiger.esa.int/training/SAR_LA1_th.pdf [Accessed 21 Oct 2011].

Euston-Brown D & Wessels E 2009. *Biodiversity assessment of the Nuwejaars Special Management Area*. Draft Report. L'Agulhas: Agulhas Biodiversity Initiative.

Frappart F, Seyler F, Martinez JM, León JG & Cazenave A 2005. Floodplain water storage in the Negro River basin estimated from microwave remote sensing of inundation area and water levels. *Remote Sensing of Environment* 99: 387-399.

Friedl MA & Brodley CE 1997. Decision tree classification of land cover from remotely sensed data. *Remote Sensing of Environment* 61: 399-402.

Fuller LM, Morgan TR & Aichele SS 2006. *Wetland delineation with IKONOS high-resolution satellite imagery, Fort Custer Training Center, Battle Creek, Michigan, 2005*. Scientific Investigations Report No 2006-5051. Reston, Virginia: U.S. Geological Survey.

Gao B-C 1996. NDWI - a normalized difference water index for remote sensing of vegetation liquid water from space. *Remote Sensing of Environment* 58: 257-266.

Geomatica 2009. *Geomatica version 10.3.* PCI Geomatics Enterprises, Inc. [Online Help].

Germishuys H 2007. Nuwejaars wetland ecosystem. *Elsenburg Journal* 2007: 9-12.

Gordon N, Adams JB & Garcia-Rodriguez F 2011. Water quality status and phytoplankton composition in Soetendalvlei, Voëlvlei and Waskraalsvlei, three shallow wetlands on the Agulhas Plain, South Africa. *African Journal of Aquatic Science* 36: 19-33.

Hahmann T, Martinis S, Twele A, Roth A & Buchroithner M 2008. Extraction of water and flood areas from SAR data. Paper delivered at the 7th European Conference on Synthetic Aperture Radar (EUSAR), Friedrichshafen, Germany

Hamilton SK, Kellndorfer J, Lehner B & Tobler M 2007. Remote sensing of floodplain geomorphology as a surrogate for biodiversity in a tropical river system (Madre de Dios, Peru). *Geomorphology* 89: 23-38.

Haralick RM, Shanmugam K & Dinstein I 1973. Textural features for image classification. *IEEE Transactions on Systems, Man and Cybernetics* 3: 610-621.

Hardin PJ 1994. Parametric and nearest-neighbor methods for hybrid classification: A comparison of pixel assignment accuracy. *Photogrammetric Engineering and Remote Sensing* 60: 1439-1448.

Hart RC 1995. South African coastal lakes. In Wetlands of South Africa [online]. Pretoria: Department of Environmental Affairs and Tourism. Available from: http://wetlands.sanbi.org/articles2/File/wetlandssa07.pdf [Accessed 15 March 2009].

Henderson FM & Lewis AJ 2008. Radar detection of wetland ecosystems: A review. *International Journal of Remote Sensing* 29: 5809-5835.

Hess LL & Melack JM 2003. Remote sensing of vegetation and flooding on Magela Creek floodplain (Northern Territory, Australia) with the SIR-C synthetic aperture radar. *Hydrobiologia* 500: 65-82.

Hess LL, Melack JM, Novo EMLM, Barbosa CCF & Gastil M 2003. Dual-season mapping of wetland inundation and vegetation for the central Amazon basin. *Remote Sensing of Environment* 87: 404-428.

Hong S-H, Wdowinski S & Kim S-W 2010. Evaluation of TerraSAR-X observations for wetland InSAR application. *IEEE Transactions on Geoscience and Remote Sensing* 48: 864-873.

Horritt MS, Mason DC & Luckman AJ 2001. Flood boundary delineation from synthetic aperture radar imagery using a statistical active contour model. *International Journal of Remote Sensing* 22: 2489-2507.

Huete AR 1988. A soil-adjusted vegetation index. *Remote Sensing of Environment* 25: 295-309.

Huete AR, Liu HQ, Batchily K & van Leeuwen W 1997. A comparison of vegetation indices over a global set of TM images for EOS-MODIS. *Remote Sensing of Environment* 59: 440-451.

Jiang Z, Huete AR, Didan K & Miura T 2008. Development of a two-band enhanced vegetation index without a blue band. *Remote Sensing of Environment* 112: 3833-3845.

Johnston RM & Barson MM 1993. Remote sensing of Australian wetlands: An evaluation of Landsat TM data for inventory and classification. *Australian Journal of Marine & Freshwater Research* 44: 235-252.

Jones K, Lanthier Y, van der Voet P, van Valkengoed E, Taylor D & Fernández-Prieto D 2009. Monitoring and assessment of wetlands using earth observation: The GlobWetland project. *Journal of Environmental Management* 90: 2154-2169.

Kasischke ES & Bourgeau-Chavez LL 1997. Monitoring South Florida wetlands using ERS-1 SAR imagery. *Photogrammetric Engineering and Remote Sensing* 63: 281-291.

Kasischke ES, Bourgeau-Chavez LL, Rober AR, Wyatt KH, Waddington JM & Turretsky MR 2009. Effects of soil moisture and water depth on ERS SAR backscatter measurements from an Alaskan wetland complex. *Remote Sensing of Environment* 113: 1868-1873.

Kasischke ES, Melack JM & Dobson MC 1997. The use of imaging radars for ecological applications: A review. *Remote Sensing of Environment* 59: 141-156.

Kasischke ES, Smith KB, Bourgeau-Chavez LL, Romanowicz EA, Brunzell S & Richardson CJ 2003. Effects of seasonal hydrologic patterns in South Florida wetlands on radar backscatter measured from ERS-2 SAR imagery. *Remote Sensing of Environment* 88: 423-441.

Kothari CR 2004. *Research methodology: Methods and techniques.* New Delhi: New Age International.

Kotze DC, Breen CM & Quinn N 1995. Wetland losses in SA. In Wetlands of South Africa [online]. Pretoria: Department of Environmental Affairs and Tourism. Available from: http://wetlands.sanbi.org/articles2/File/wetlandssa17.pdf [Accessed 15 March 2009].

Kouchi K & Yamazaki F 2007. Characteristics of tsunami-affected areas in moderate-resolution satellite images. *IEEE Transactions on Geoscience and Remote Sensing* 45: 1650-1657.

Laba M, Gregory SK, Braden J, Ogurcak D, Hill E, Fegraus E, Fiore J & DeGloria SD 2002. Conventional and fuzzy accuracy assessment of the New York Gap Analysis Project land cover map. *Remote Sensing of Environment* 81: 443-455.

Lacaux JP, Tourre YM, Vignolles CN, Ndione JA & Lafaye M 2007. Classification of ponds from high-spatial resolution remote sensing: Application to Rift Valley Fever epidemics in Senegal. *Remote Sensing of Environment* 106: 66-74.

Lang MW, Kasischke ES, Prince SD & Pittman KW 2008. Assessment of C-band synthetic aperture radar data for mapping and monitoring coastal plain forested wetlands in the Mid-Atlantic region, U.S.A. *Remote Sensing of Environment* 112: 4120–4130.

Lang S 2008. Object-based image analysis for remote sensing applications: Modelling reality - dealing with complexity. In Blaschke T, Lang S & Hay G (eds) *Object-based image analysis: Spatial concepts for knowledge-driven remote sensing applications*, 3-26. Berlin/Heidelberg: Springer Verlag.

Laur H, Bally P, Meadows P, Sanchez J, Schaettler B, Lopinto E & Esteban D 2004. *ERS SAR calibration: Derivation of the backscattering coefficient σ0 in ESA ERS SAR PRI products*. ESA Report No ES-TN-RS-PM-HL09 Issue 2 Revision 5f. ESA.

Lee J-S 1981. Refined filtering of image noise using local statistics. *Computer Graphics and Image Processing* 15: 380-389.

Lewinsky S & Bochenek Z 2008. Rule-based classification of SPOT imagery using object-oriented approach for detailed land cover mapping. Paper delivered at the 28th EARSeL Symposium "Remote Sensing for a Changing Europe," Istanbul.

Li H, Gu H, Han Y & Yang J 2010. Object-oriented classification of high-resolution remote sensing imagery based on an improved colour structure code and a support vector machine. *International Journal of Remote Sensing* 31: 1453-1470.

Lillesand TM, Kiefer RW & Chipman JW 2004. *Remote sensing and image interpretation.* 5th ed. New York: John Wiley & Sons, Inc.

Liu C, Frazier P & Kumar L 2007. Comparative assessment of the measures of thematic classification accuracy. *Remote Sensing of Environment* 107: 606-616.

Liu D & Xia F 2011. Assessing object-based classification: Advantages and limitations. *Remote Sensing Letters* 1: 187-194.

Liu X-H, Skidmore AK & Van Oosten H 2002. Integration of classification methods for improvement of land-cover map accuracy. *ISPRS Journal of Photogrammetry and Remote Sensing* 56: 257-268.

Lombard AT, Cowling RM, Pressey RL & Mustart PJ 1997. Reserve selection in a species-rich and fragmented landscape on the Agulhas Plain, South Africa. *Conservation Biology* 11: 1101-1116.

Lucas R, Rowlands A, Brown A, Keyworth S & Bunting P 2007. Rule-based classification of multi-temporal satellite imagery for habitat and agricultural land cover mapping. *ISPRS Journal of Photogrammetry and Remote Sensing* 62: 165-185.

Lück W, Mhangara P, Kleyn L & Remas H 2010. *Land cover field guide version 2.0.* Pretoria: CSIR Satellite Applications Centre: Earth Observation Service Centre.

Lunetta RS & Balogh ME 1999. Application of multi-temporal Landsat 5 TM imagery for wetland identification. *Photogrammetric Engineering and Remote Sensing* 62: 165-185.

MacAlister C & Mahaxay M 2008. Mapping wetlands in the Lower Mekong Basin for wetland resource and conservation management using Landsat ETM images and field survey data. *Journal of Environmental Management* 90: 2130-2137.

Mallinis G, Koutsias N, Tsakiri-Strati M & Karteris M 2008. Object-based classification using Quickbird imagery for delineating forest vegetation polygons in a Mediterranean test site. *ISPRS Journal of Photogrammetry and Remote Sensing* 63: 237-250.

Malthus TJ & George DG 1997. Airborne remote sensing of macrophytes in Cefni reservoir, Anglesey, UK. *Aquatic Botany* 58: 317-332.

Mangnall MJ & Crowe TM 2002. Population dynamics and the physical and financial impacts to cereal crops of the Egyptian goose *Alopochen aegyptiacus* on the Agulhas Plain, Western Cape, South Africa. *Agriculture, Ecosystems and Environment* 90: 231-246.

Mansourpour M, Rajabi MA & Blais JAR 2006. Effects and performance of speckle noise reduction filters on active radar and SAR images. Paper delivered at the ISPRS Workshop on Topographic Mapping from Space (with Special Emphasis on Small Satellites), Ankara, Turkey.

Marcus WA & Fonstad MA 2007. Optical remote mapping of rivers at sub-meter resolutions and watershed extents. *Earth Surface Processes and Landforms* 33: 4-24.

Masocha M & Skidmore AK 2011. Integrating conventional classifiers with a GIS expert system to increase the accuracy of invasive species mapping. *International Journal of Applied Earth Observation and Geoinformation* 13: 487-494.

Mather PM 2004. *Computer processing of remotely-sensed images.* 3rd ed. Chicester, West Sussex: Wiley.

McFeeters SK 1996. The use of the normalized difference water index (NDWI) in the delineation of open water features. *international Journal of Remote Sensing* 17: 1425-1432.

Michelson DB, Liljeberg BM & Pilesjö P 2000. Comparison of algorithms for classifying Swedish landcover using Landsat TM and ERS-1 SAR data. *Remote Sensing of Environment* 71: 1-15.

Mori S, Takeuchi W & Sawada H 2009. Estimation of land surface water coverage (LSWC) with AMSR-E and MODIS. Paper delivered at the Joint Student Seminar on Civil Infrastructures, Thailand.

Mountrakis G, Im J & Ogole C 2011. Support vector machines in remote sensing: A review. *ISPRS Journal of Photogrammetry and Remote Sensing* 66: 247-259.

Mouton J 2001. *How to succeed in your master's and doctoral studies: A South African guide and resource book.* Pretoria: Van Schaik Publishers.

Nagler PL, Glenn EP & Huete AR 2001. Assessment of spectral vegetation indices for riparian vegetation in the Colorado River delta, Mexico. *Journal of Arid Environments* 49: 91-110.

Nangendo G, Skidmore AK & van Oosten H 2007. Mapping East African tropical forests and woodlands - a comparison of classifiers. *ISPRS Journal of Photogrammetry and Remote Sensing* 61: 393-404.

NEST 2010. *Next ESA SAR toolbox version 4a-1.5.* Array Systems Computing Inc. [Online Help].

Noble RG & Hemens J 1978. *Inland water ecosystems in South Africa - a review of research needs*. South African National Scientific Programmes Report No 34. Pretoria: Cooperative Scientific Programmes, Council for Scientific and Industrial Research.

Nuwejaars Wetland SMA 2011. *Towards a sustainable Agulhas Plain: How the Nuwejaars Wetland Special Management Area was born: 2002 – 2011*. Nuwejaars Wetland SMA Project Report. Bredasdorp, South Africa: Nuwejaars Wetland Land Owners' Association.

Ordoyne C & Friedl MA 2008. Using MODIS data to characterize seasonal inundation patterns in the Florida Everglades. *Remote Sensing of Environment* 112: 4107-4141.

Ormsby JP, Blanchard BJ & Blanchard AJ 1985. Detection of lowland flooding using active microwave systems. *Photogrammetric Engineering and Remote Sensing* 51: 317-328.

Ozesmi SL & Bauer ME 2002. Satellite remote sensing of wetlands. *Wetlands Ecology and Management* 10: 381-402.

Pence GQK, Botha MA & Turpie JK 2003. Evaluating combinations of on-and off-reserve conservation strategies for the Agulhas Plain, South Africa: A financial perspective. *Biological Conservation* 112: 253-273.

Platt RV & Rapoza L 2008. An evaluation of an object-oriented paradigm for land use/land cover classification. *The Professional Geographer* 60: 87-100.

Podest E & Saatchi S 2002. Application of multiscale texture in classifying JERS-1 radar data over tropical vegetation. *International Journal of Remote Sensing* 23: 1487-1506.

Pope KO, Rejmankova E, Paris JF & Woodruff R 1997. Detecting seasonal flooding cycles in marshes of the Yucatan Peninsula with SIR-C polarimetric radar imagery. *Remote Sensing of Environment* 59: 157-166.

Qi J, Chehbouni A, Huete AR, Kerr YH & Sorooshian S 1994. A modified soil-adjusted vegetation index. *Remote Sensing of Environment* 48: 119-126.

Raitala J & Lampinen J 1986. Generalization of Landsat MSS interpretations of aquatic areas in southwestern Finland. *Earth, Moon & Planets* 36: 63-88.

Raitala J, Rantunen H & Hellsten S 1984. A Landsat assisted study of the aquatic areas of the Lake Kemijarvi region, northern Finland. *Earth, Moon & Planets* 31: 183-216.

Rocchini D, Chiarucci A & Loiselle SA 2004. Testing the spectral variation hypothesis by using satellite multispectral images. *Acta Oecologica* 26: 117-120.

Rogan J, Franklin J & Rogers DA 2002. A comparison of methods for monitoring multitemporal vegetation change using Thematic Mapper imagery. *Remote Sensing of Environment* 80: 143-156.

Rouget M 2003. Measuring conservation value at fine and broad scales: Implications for a diverse and fragmented region, the Agulhas Plain. *Biological Conservation* 112: 217-232.

Russel IA & Impson ND 2006. Aquatic systems in and adjacent to Agulhas National Park with particular reference to the fish fauna. *Koedoe* [online], 49(2): 45-57. Available from: http://koedoe.co.za/index.php/koedoe/article/viewArticle/120 [Accessed 26 May 2011].

Sader SA, Ahl D & Liou W-S 1995. Accuracy of Landsat-TM and GIS rule-based methods for forest wetland classification in Maine. *Remote Sensing of Environment* 53: 133-144.

SANBI 2010. *Draft rehabilitation plan: Agulhas*. SANBI Report No 5262/105782. Pretoria: South African National Biodiversity Institute. Prepared by Franci Gresse, Aurecon South Africa (Pty) Ltd as part of the planning phase for the Working for Wetlands Rehabilitation Programme.

Sanli F, Kuruco Y & Esetlili M 2009. Determining land use changes by radar-optic fused images and monitoring its environmental impacts in Edremit region of western Turkey. *Environmetal Monitoring and Assessment* 151: 45-58.

SANParks 2008. *Agulhas National Park park management plan.* L'Agulhas: Agulhas National Park.

Sarmap 2009. Synthetic aperture radar and SARScape. Available from: http://www.sarmap.ch/pdf/SAR-Guidebook.pdf [Accessed 21 October 2011].

Sawaya KE, Olmanson LG, Heinert NJ, Brezonik PL & Bauer ME 2003. Extending satellite remote sensing to local scales: Land and water resource monitoring using high-resolution imagery. *Remote Sensing of Environment* 88: 144-156.

Schiewe J 2002. Segmentation of high-resolution remotely sensed data - concepts, applications and problems. Paper delivered at the Joint ISPRS Commission IV Symposium: Geospatial Theory, Processing and Applications, Ottawa.

Schmitt A, Brisco B, Kaya S & Murnaghan K 2010. Polarimetric change detection for wetlands. Paper delivered at the Remote Sensing and Hydrology Symposium, Jackson Hole, Wyoming, USA.

Schowengerdt RA 1997. *Remote sensing: Models and methods for image processing.* 2nd ed. San Diego: Academic Press.

Shanmugam R, Ahn Y-H & Sanjeevi S 2006. A comparison of the classification of wetland characteristics by linear spectral mixture modelling and traditional hard classifiers on multispectral remotely sensed imagery in southern India. *Ecological Modelling* 194: 379-394.

Shouten L, Leeuwen & Twongo T 2000. Satellite remote sensing for environmental monitoring: Case studies on water hyacinth detection and wetlands inventory. Paper delivered at the International Conference on Lake Victoria 2000: a New Beginning, Jinja, Uganda.

Silva TSF, Costa MPF, Melack JM & Novo EMLM 2008. Remote sensing of aquatic vegetation: Theory and applications. *Environmetal Monitoring and Assessment* 140: 131-135.

Skidmore AK 1989. An expert system classifies eucalypt forest types using Thematic Mapper data and a digital terrain model. *Photogrammetric Engineering and Remote Sensing* 55: 1449-1461.

Skidmore AK, Watford F, Luckananurug P & Ryan PJ 1996. An operational GIS expert system for mapping forest soils. *Photogrammetric Engineering and Remote Sensing* 62: 501-511.

South Africa 1986. *South Africa 1:50 000 sheet 3420 CA&CC Bredasdorp.* Third edition. (Map). Cape Town: Chief Directorate of National Geospatial Information.

South Africa 2002. *South Africa 1:50 000 sheet 3419 DB&DD Elim.* Fourth edition. (Map). Cape Town: Chief Directorate of National Geospatial Information.

Story M & Congalton RG 1986. Accuracy assessment: A user's perspective. *Photogrammetric Engineering and Remote Sensing* 52: 97-399.

Straatsma MW & Baptist MJ 2008. Floodplain roughness parameterization using airborne laser scanning and spectral remote sensing. *Remote Sensing of Environment* 112: 1062-1080.

Takeuchi W & Yasuoka Y 2004. Development of normalized vegetation, soil and water indices derived from satellite remote sensing data. *Journal of the Japan Society of Photogrammetry and Remote Sensing* 43: 7-19.

Touzi R, Deschamps A, Demers AM & Rother G 2009. The Touzi decomposition for wetland classification using polarimetric C-band SAR. Paper delivered at the 4th International Workshop on Science and Applications of SAR Polarimetry and Polarimetric Interferometry: PolInSAR, Frascati, Italy.

Töyrä J & Pietroniro A 2005. Towards operational monitoring of a northern wetland using geomatics-based techniques. *Remote Sensing of Environment* 97: 174-191.

Töyrä J, Pietroniro A & Martz LW 2001. Multisensor hydrologic assessment of a freshwater wetland. *Remote Sensing of Environment* 75: 162-173.

Trimble 2011a. *eCognition Developer 8.64.1 reference book.* München: Trimble Germany GmbH.

Trimble 2011b. *eCognition Developer 8.64.1 user guide.* München: Trimble Germany GmbH.

Tsatsoulis C 1993. Expert systems in remote sensing applications. *IEEE Geoscience and Remote Sensing Newsletter* June: 7-15.

Tseng M-H, Chen S-J, Hwang G-H & Shen M-Y 2008. A genetic algorithm rule-based approach for land-cover classification. *ISPRS Journal of Photogrammetry and Remote Sensing* 63: 202-212.

United Nations 2003. *Project document: Agulhas Biodiversity Initiative (ABI).* New York: United Nations Development Programme Global Environmental Facility.

Van der Sande CJ, de Jong SM & de Roo APJ 2003. A segmentation and classification approach of IKONOS-2 imagery for land cover mapping to assist flood risk and flood damage assessment. *International Journal of Applied Earth Observation and Geoinformation* 4: 217-229.

Wang Y, Hess LL, Filoso F & Melack JM 1995. Understanding the radar backscattering from flooded and nonflooded Amazonian forests: Results from canopy backscatter modeling. *Remote Sensing of Environment* 54: 324-332.

Watanachaturaporn P, Arora MK & Varshney PK 2008. Multisource classification using support vector machines: An empirical comparison with decision tree and neural network classifiers. *Photogrammetric Engineering and Remote Sensing* 74: 239-246.

Whiteside T & Ahmad W 2005. A comparison of object-oriented and pixel-based classification methods for mapping landcover in northern Australia. Paper delivered at the SSC2005 Spatial intelligence, innovation and praxis: The national biennial Conference of the Spatial Sciences Institute, Melbourne.

Wilkinson GG, Kanellopoulos I, Kontoes C & Mégier J 1992. A comparison of neural network and expert system methods for analysis of remotely sensed imagery. Paper delivered at the International Geoscience and Remote Sensing Symposium (IGARSS), Houston, Texas.

Woodhouse IF 2006. *Introduction to microwave remote sensing.* Boca Raton: Taylor & Francis.

Wright C & Gallant A 2007. Improved wetland remote sensing in yellowstone national park using classification trees to combine TM imagery and ancillary environmental data. *Remote Sensing of Environment* 107: 582-605.

Xu H 2006. Modification of normalised difference water index (NDWI) to enhance open water features in remotely sensed imagery. *International Journal of Remote Sensing* 27: 3025-3033.

Yajima Y, Yamaguchi Y, Sato R, Yamada H & Boerner W-M 2008. POLSAR image analysis of wetlands using a modified four-component scattering power decomposition. *IEEE Transactions on Geoscience and Remote Sensing* 46: 1667-1673.

Yamaguchi T, Kishida K, Nunohiro E, Park JG, Mackin KJ, Hara K, Matsushita K & Harada I 2010. Artificial neural networks paddy-field classifier using spatiotemporal remote sensing data. *Artificial Life and Robotics* 15: 221-224.

Yamaguchi Y 2007. Polarimetric radar remote sensing. Paper delivered at the International Symposium on Antennas and Propagation, Niigata, Japan.

Yuan L & Zhang LQ 2008. Mapping large-scale distribution of submerged aquatic vegetation coverage using remote sensing. *Ecological Informatics* 3: 245-251.

Zhang Y 2004. Understanding image fusion. *Photogrammetric Engineering and Remote Sensing* 70: 657-661.

PERSONAL COMMUNICATIONS

Ambrose T 2010. Project Manager, Nuwejaars Special Management Area. Bredasdorp. Interview on 5 November 2010 about the Nuwejaars Wetland SMA and its associated wetlands.

Lu J (junlu@array.ca) 2010. RE: Calibration problem. E-mail to Theo Pauw (theopauw@gmail.com) (21 April-14 June).

Padayachee P (ppadayachee@sansa.org.za) 2011. RE: SPOT 5. E-mail to Theo Pauw (theopauw@gmail.com) (1 September).

APPENDIX A: EXPERT SYSTEM RULESETS

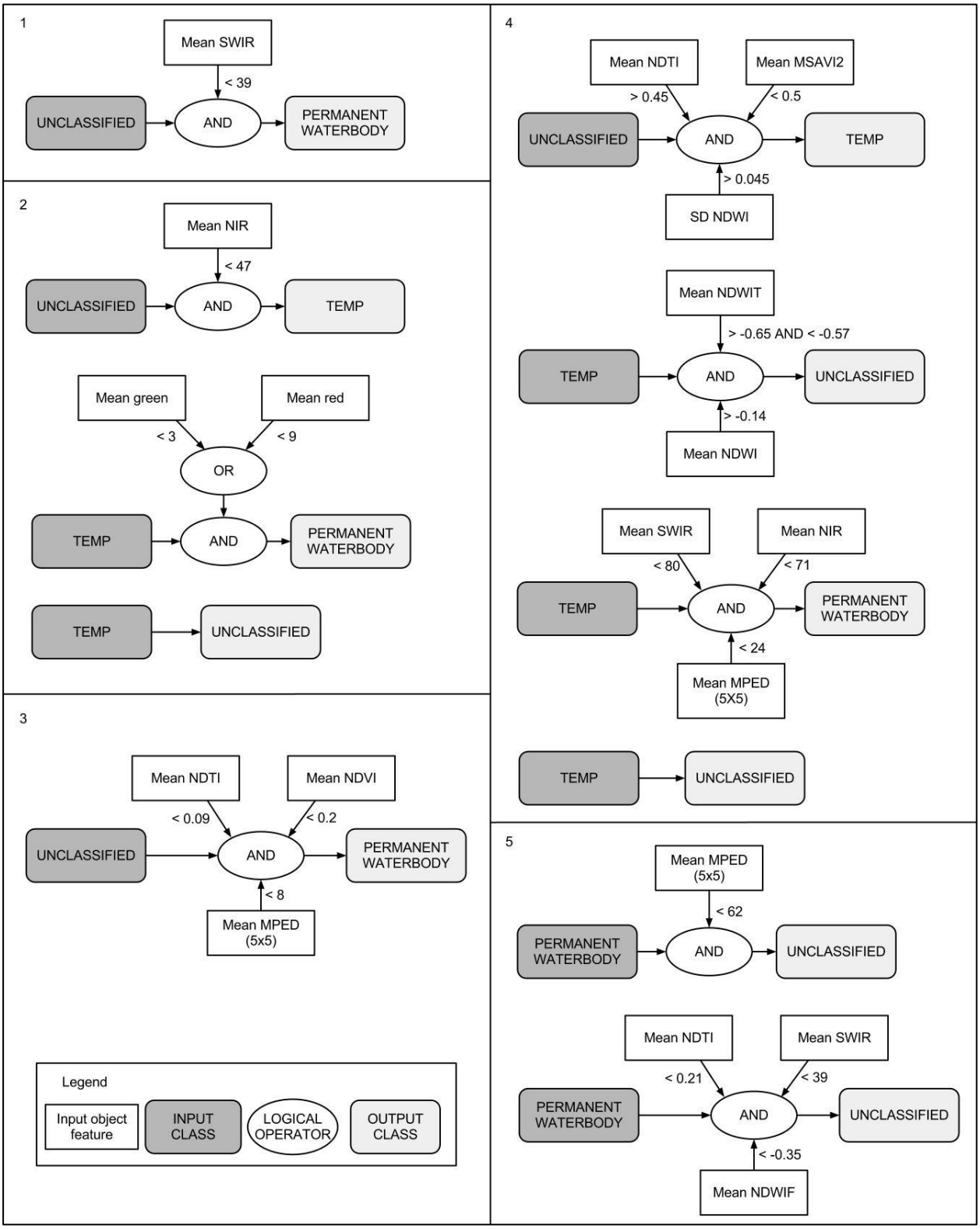

Figure A.1: Rules for the classification of *Permanent waterbody* (see Figure 4.2)

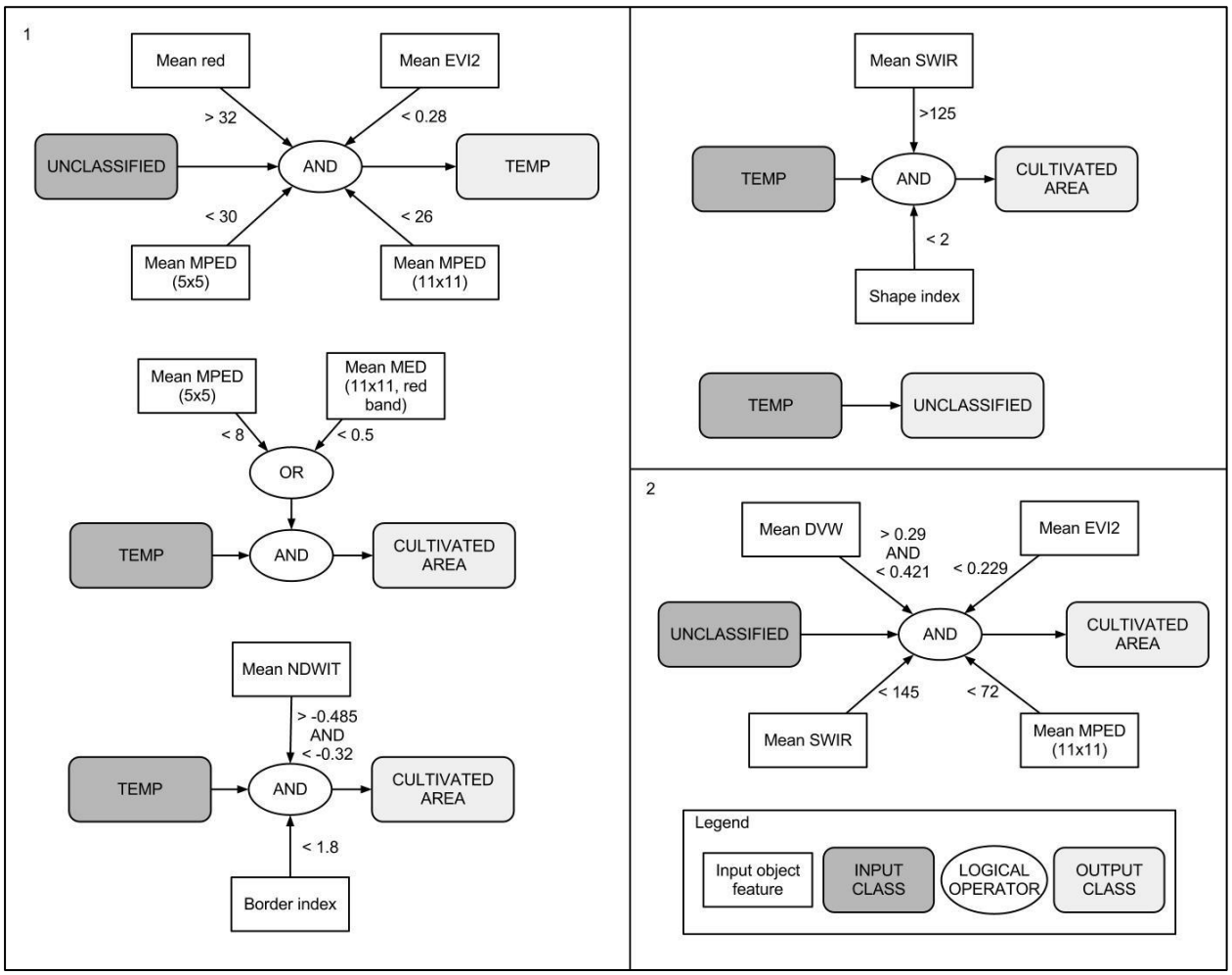

Figure A.2: Rules for the classification of *Cultivated area* (see Figure 4.3)

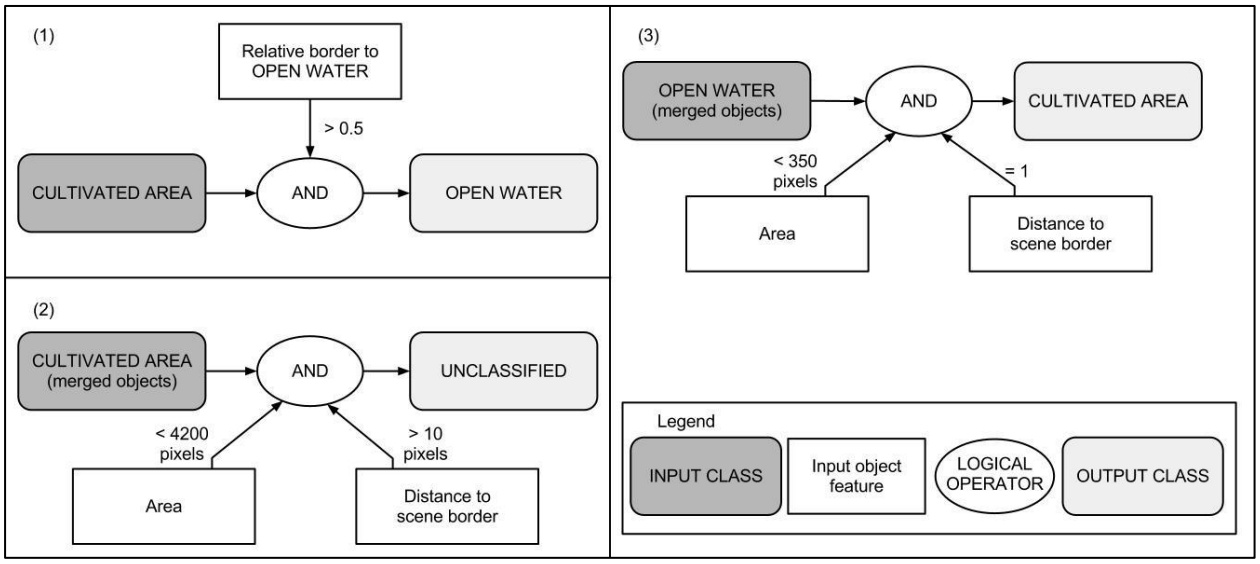

Figure A.3: Rules for the post-processing of *Cultivated area* and *Permanent waterbody* (see Figure 4.4)

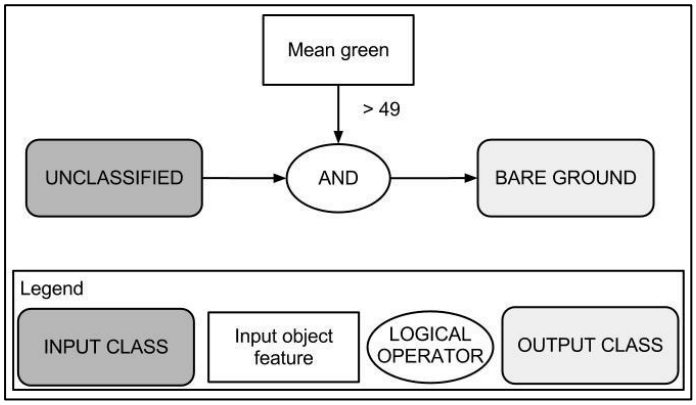

Figure A.4: Rule for the classification of *Bare ground* (see Step 1 in Figure 4.5)

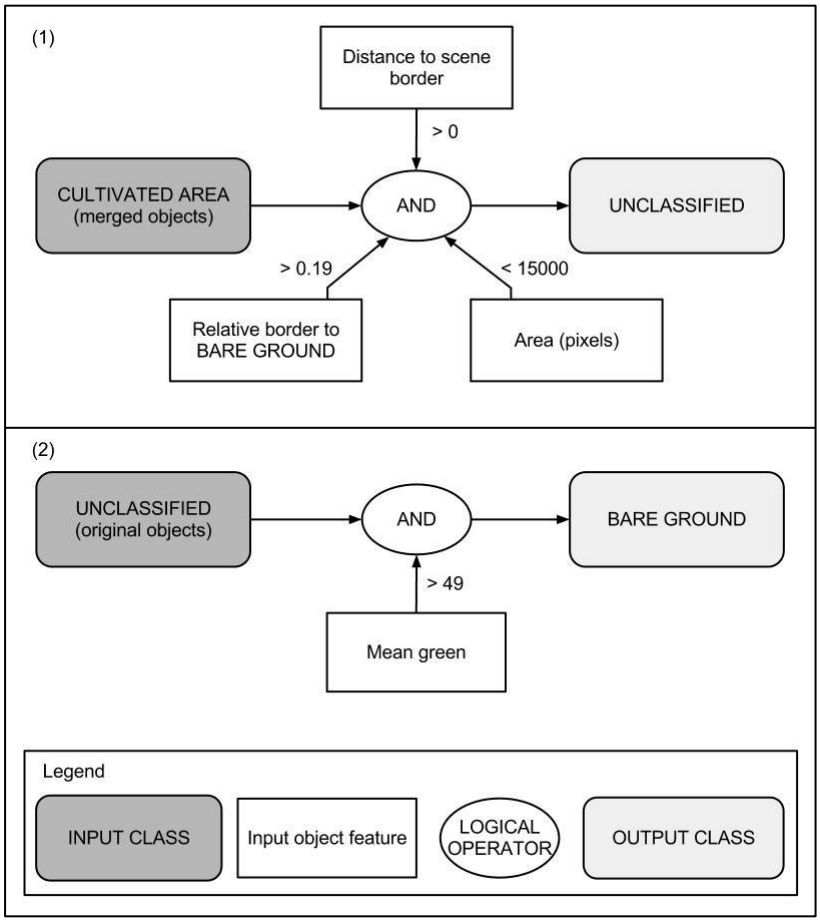

Figure A.5: Rules for the post-processing of *Cultivated area* and *Bare ground* (see Step 2 in Figure 4.5)

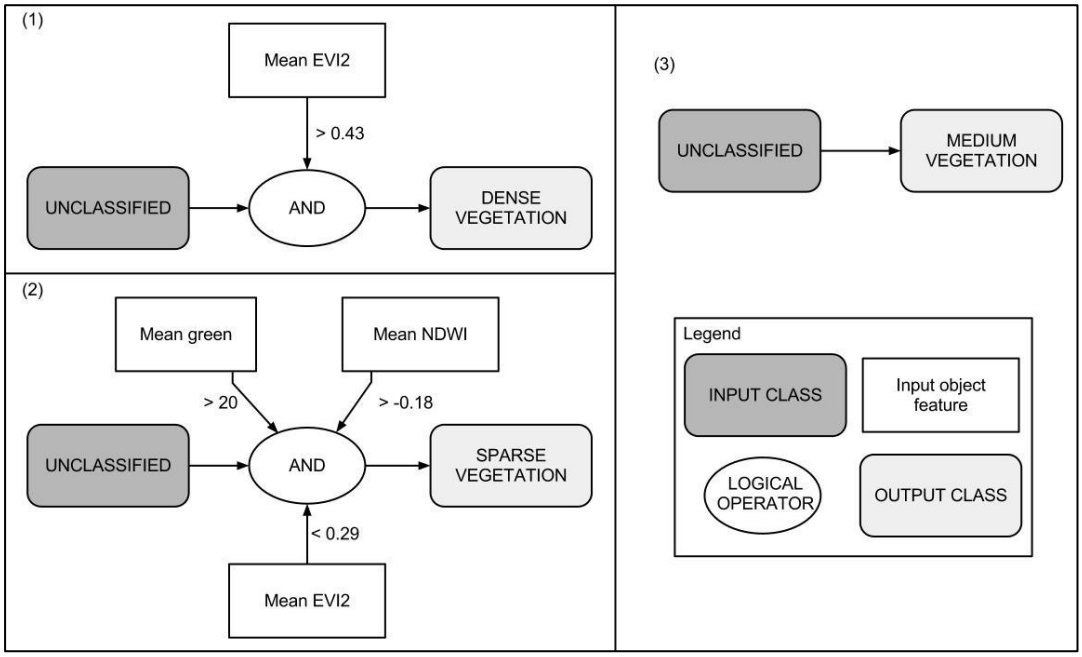

Figure A.6: Rules for the classification of *Natural and semi-natural vegetation* (see Figure 4.6)

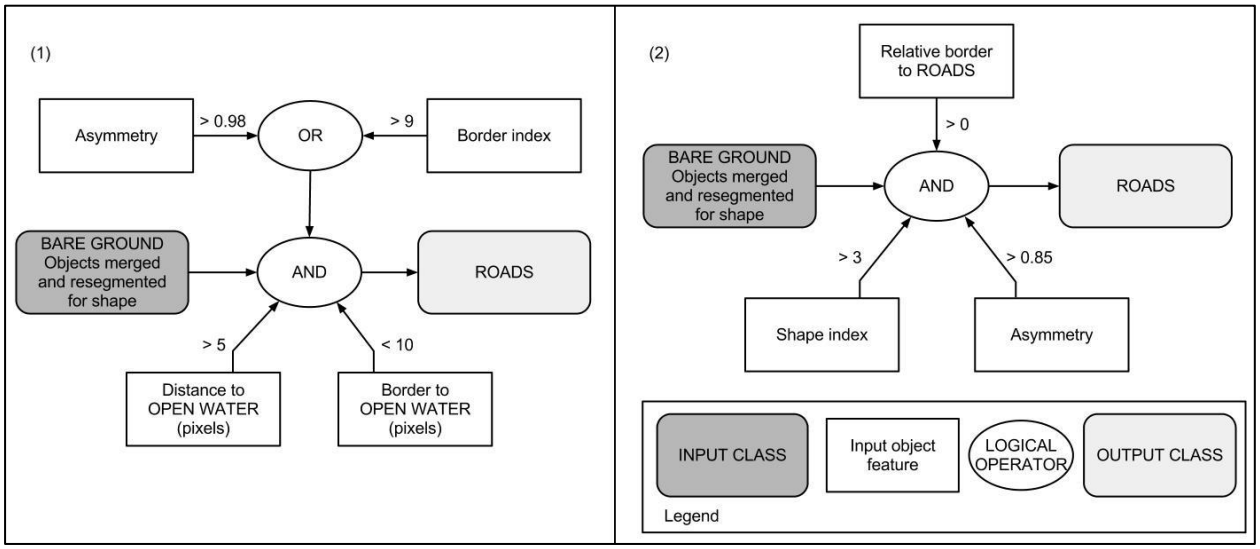

Figure A.7: Rules for the classification of *Roads* (see Figure 4.7)

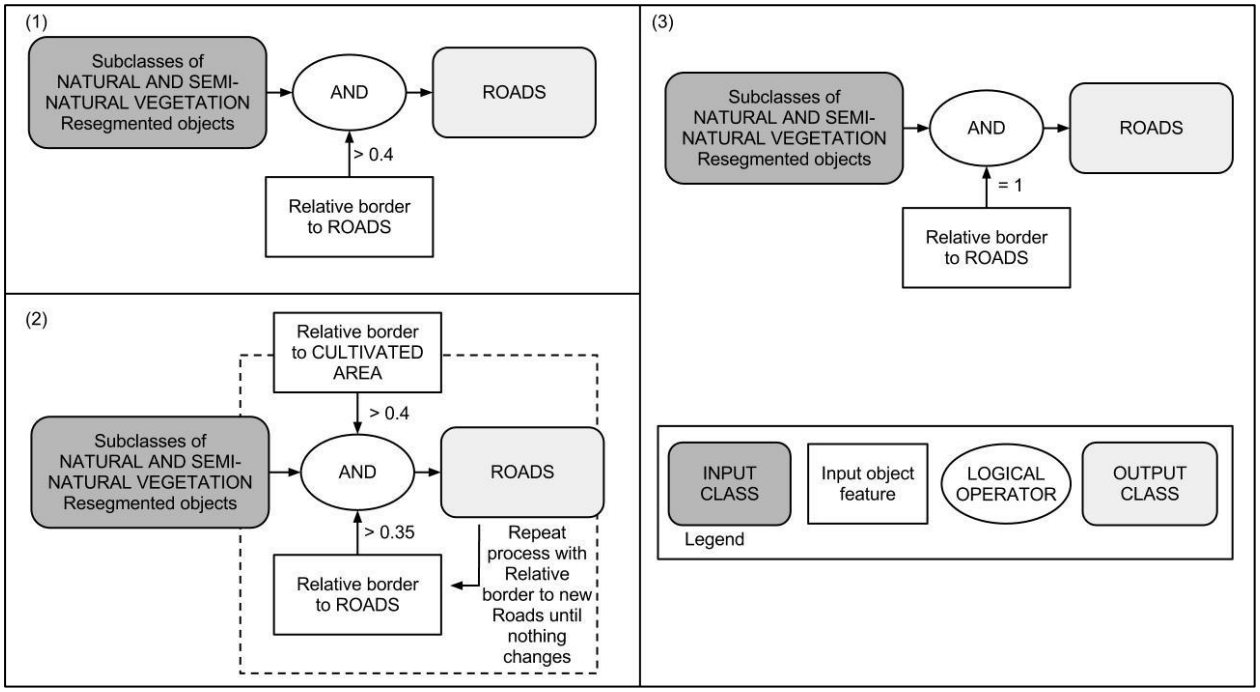

Figure A.8: Rules assigning vegetated roadside verges to *Roads* (see Figure 4.7)

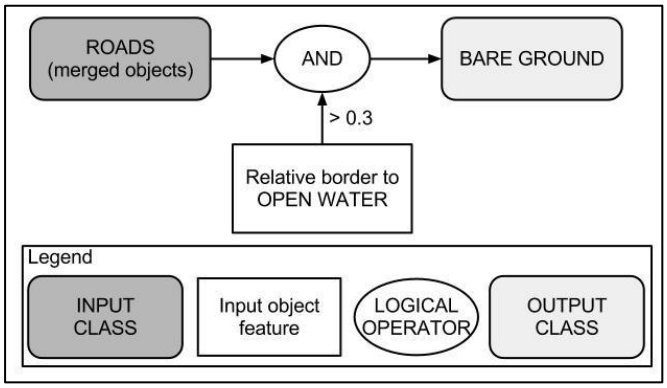

Figure A.9: Rule for the post-processing of *Roads* (see Figure 4.7)

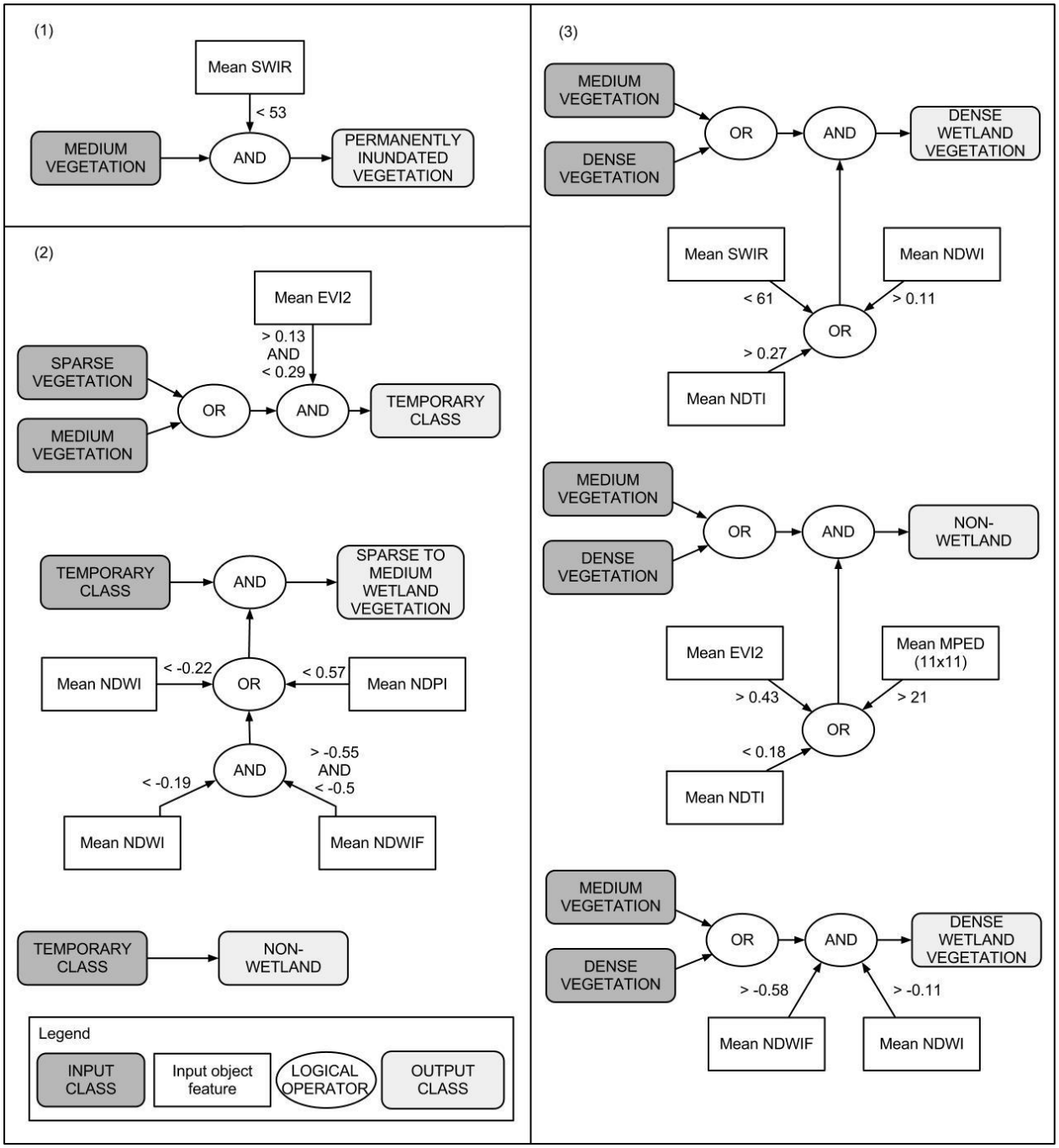

Figure A.10: SPOT-based rules for conversion of SPOT-based landcover classes to wetland classes (see Figure 4.8 Steps 1-3)

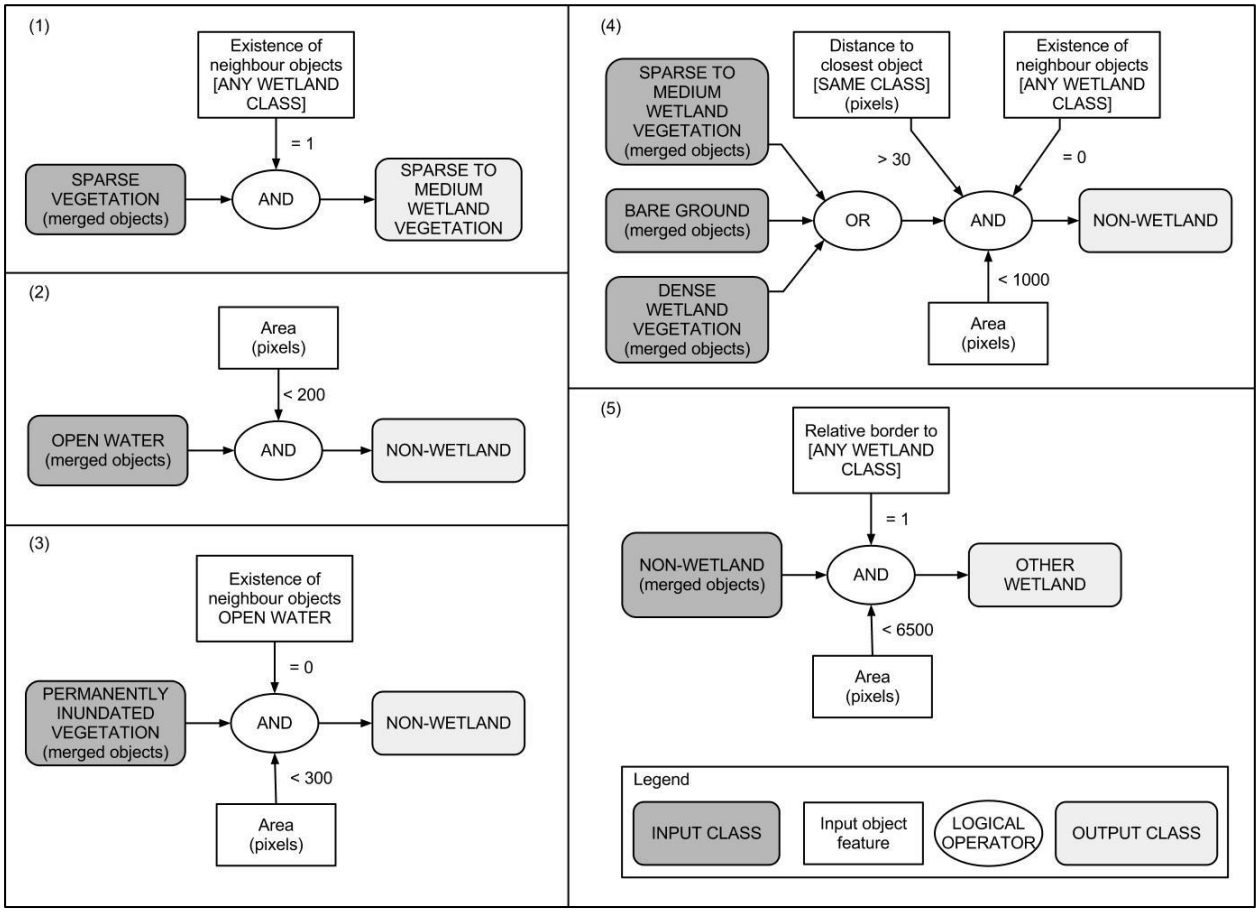

Figure A.11: Rules for the post-processing of SPOT-derived wetlands classes (see Figure 4.8 Steps 4-6)

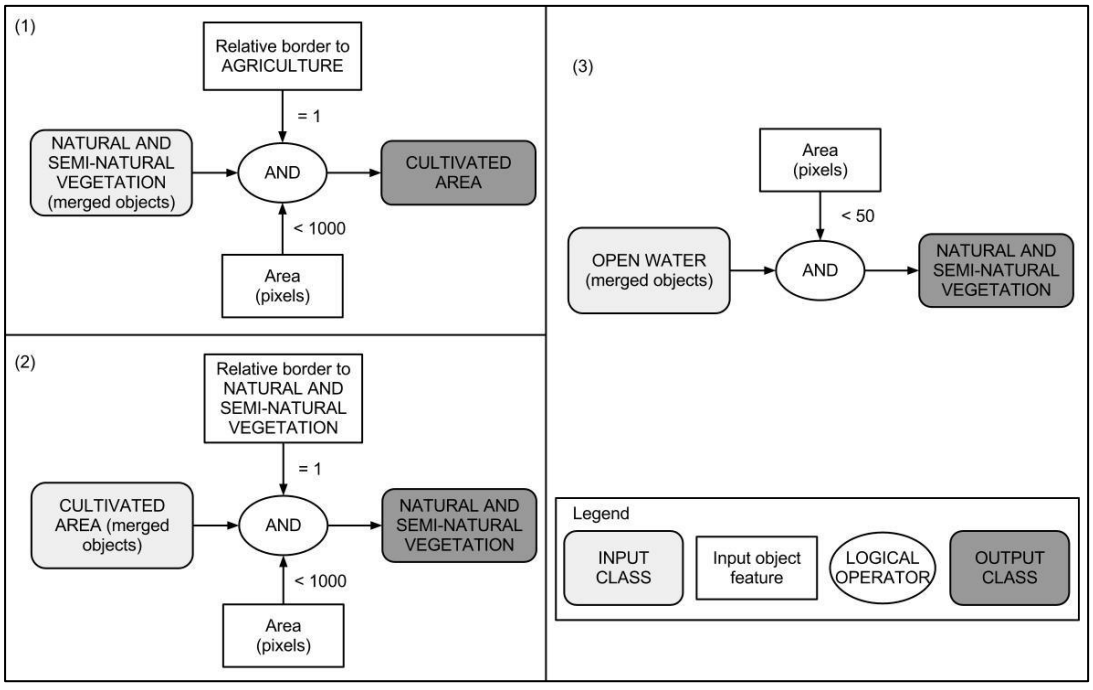

Figure A.12: Rules for the post-processing of supervised landcover classes (see Figure 4.9)

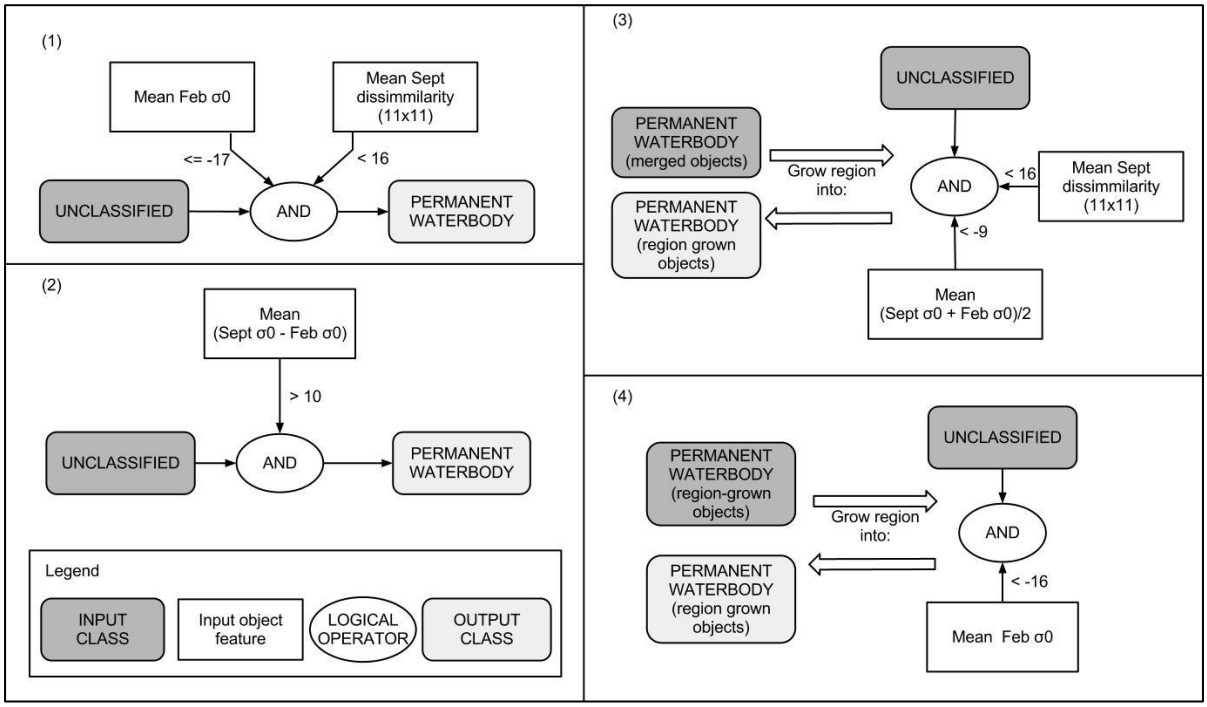

Figure A.13: SAR-based rules for the classification of *Permanent waterbody* (see Step 1 in Figure 4.10)

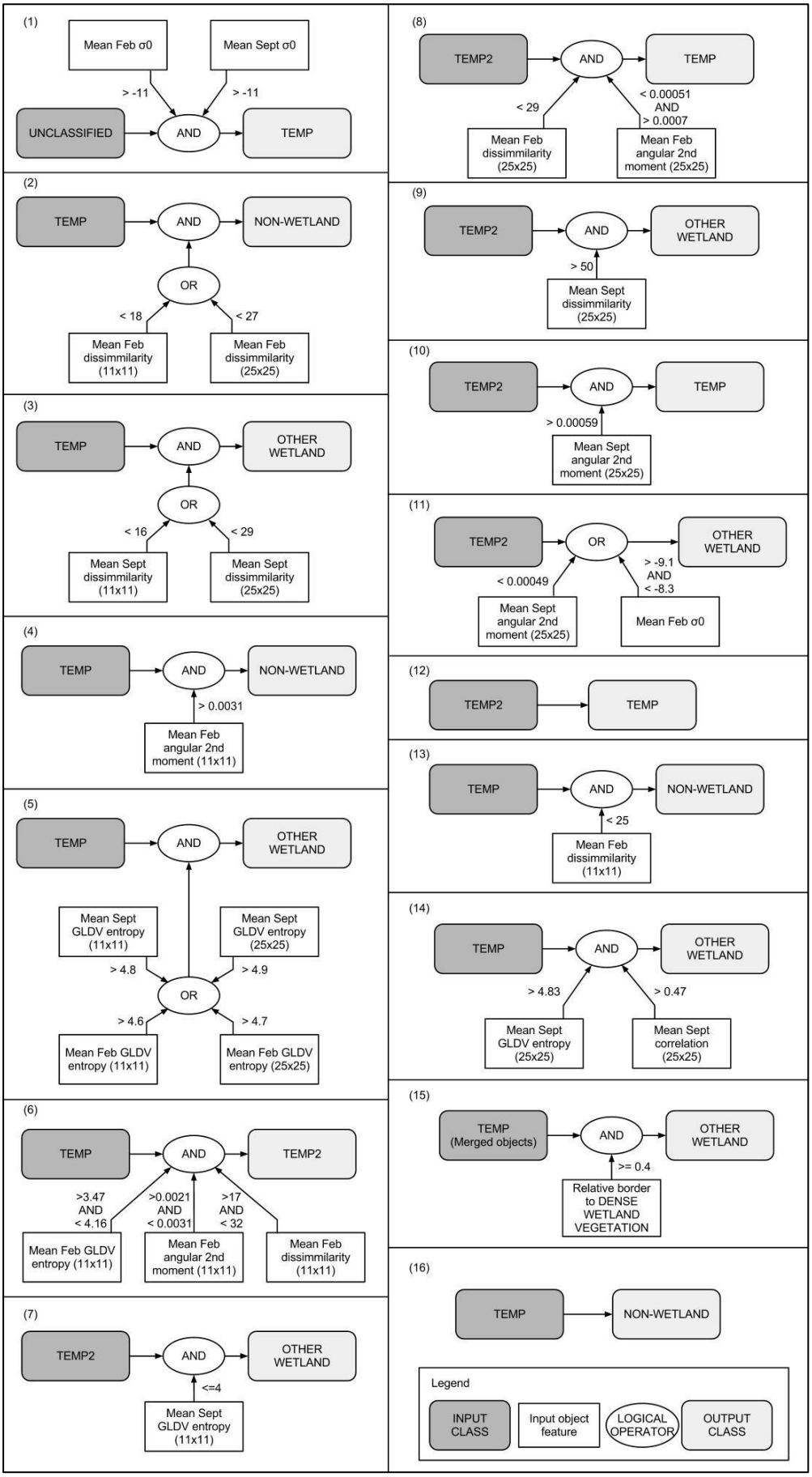

Figure A.14: SAR-based rules for the classification of *Other wetland* objects representing dense wetland vegetation (see Step 2 in Figure 4.10)

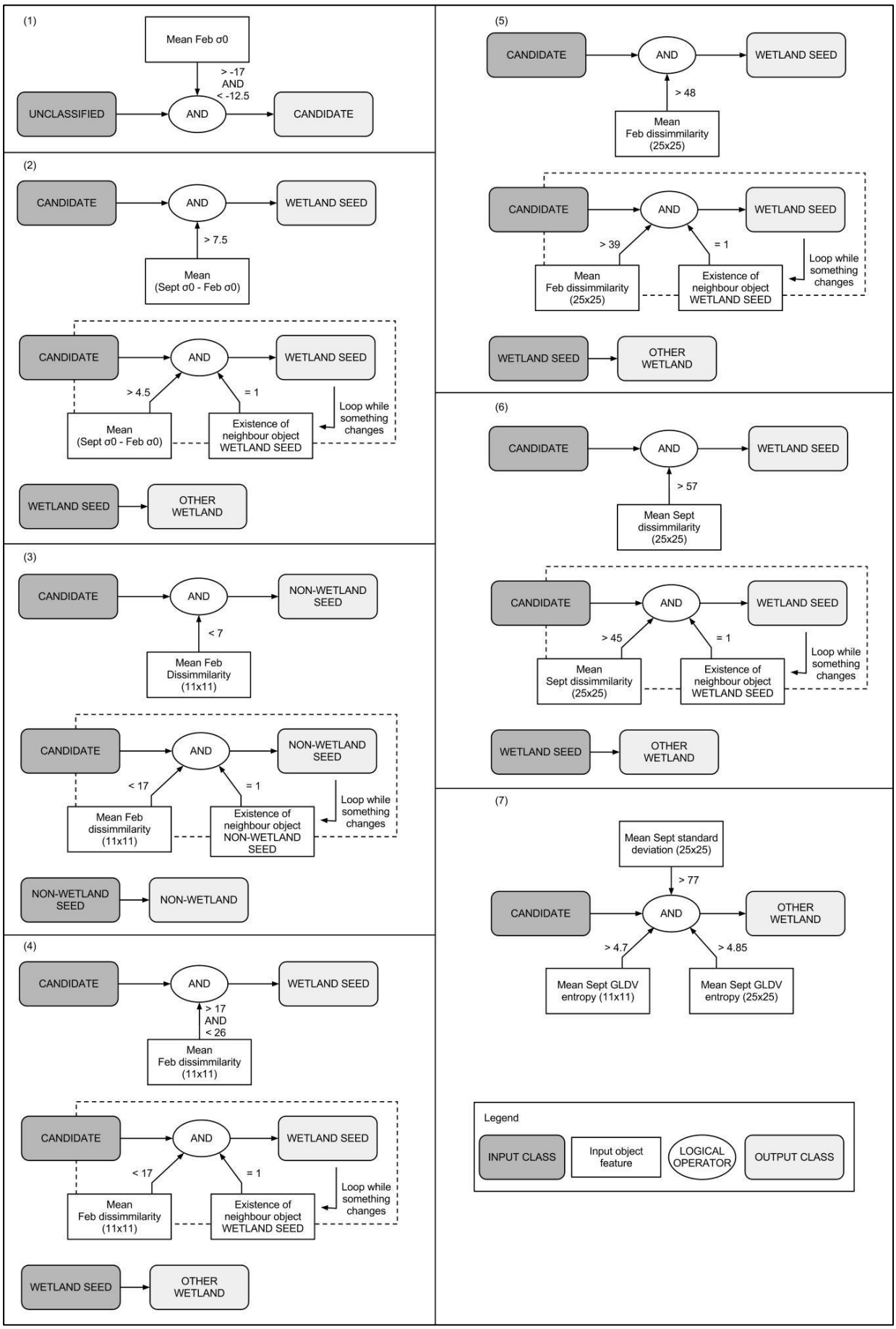

Figure A.15: SAR-based classification of remaining *Other wetland* objects (see Step 3 in Figure 4.10)

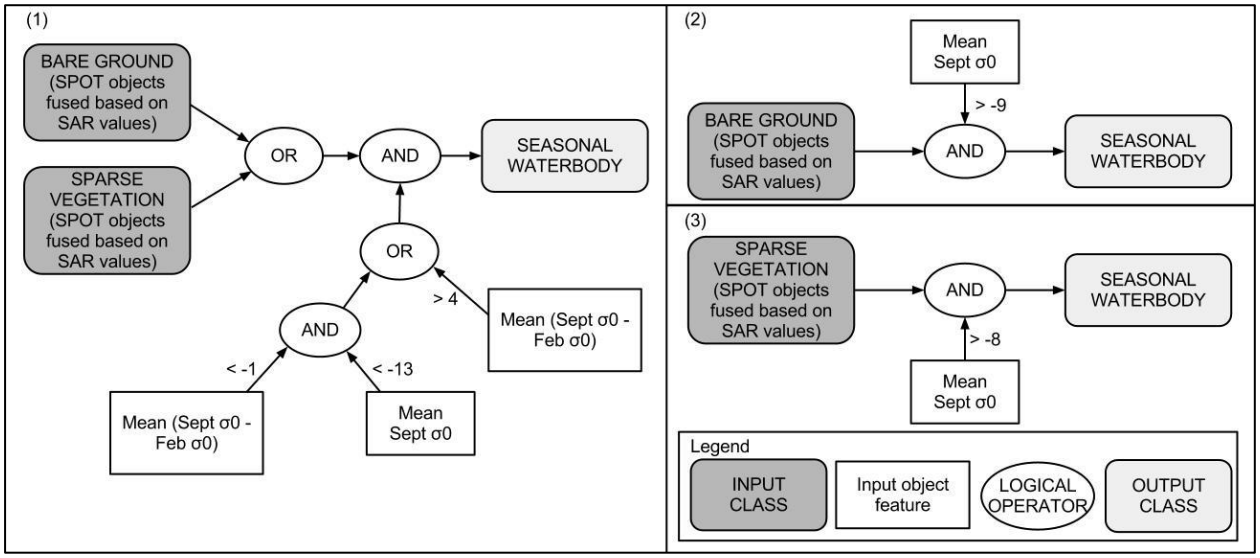

Figure A.16: SAR-based rules classifying *Seasonal waterbody* from SPOT-derived landcover classes (see Step 1 in Figure 4.11)

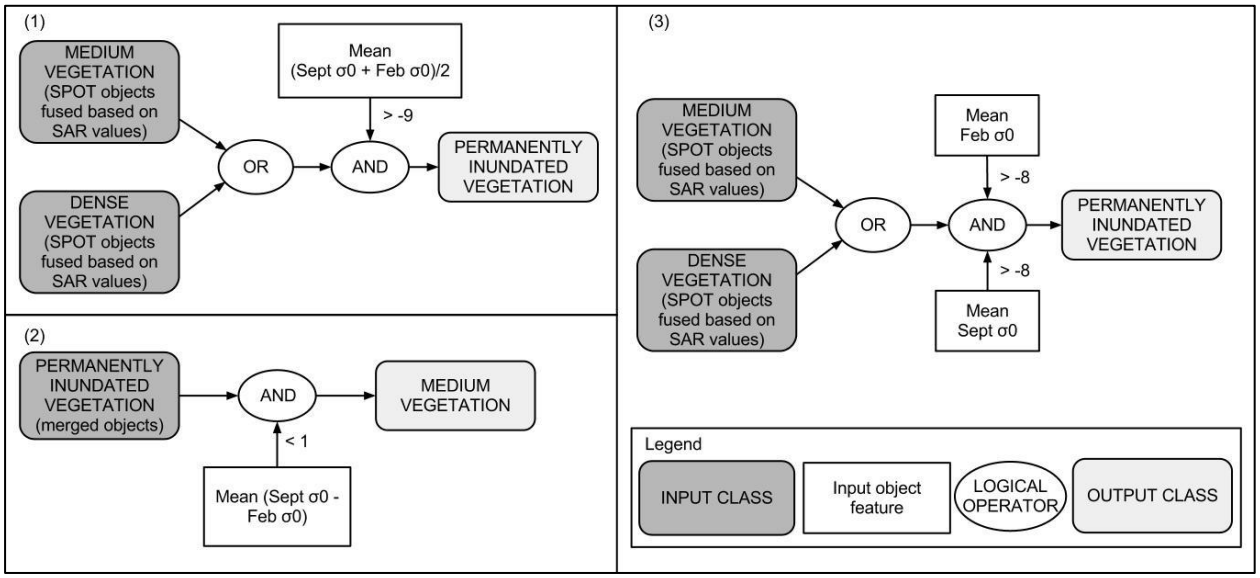

Figure A.17: SAR-based rules classifying *Permanently inundated vegetation* from SPOT-derived landcover classes (see Step 1 in Figure 4.11)

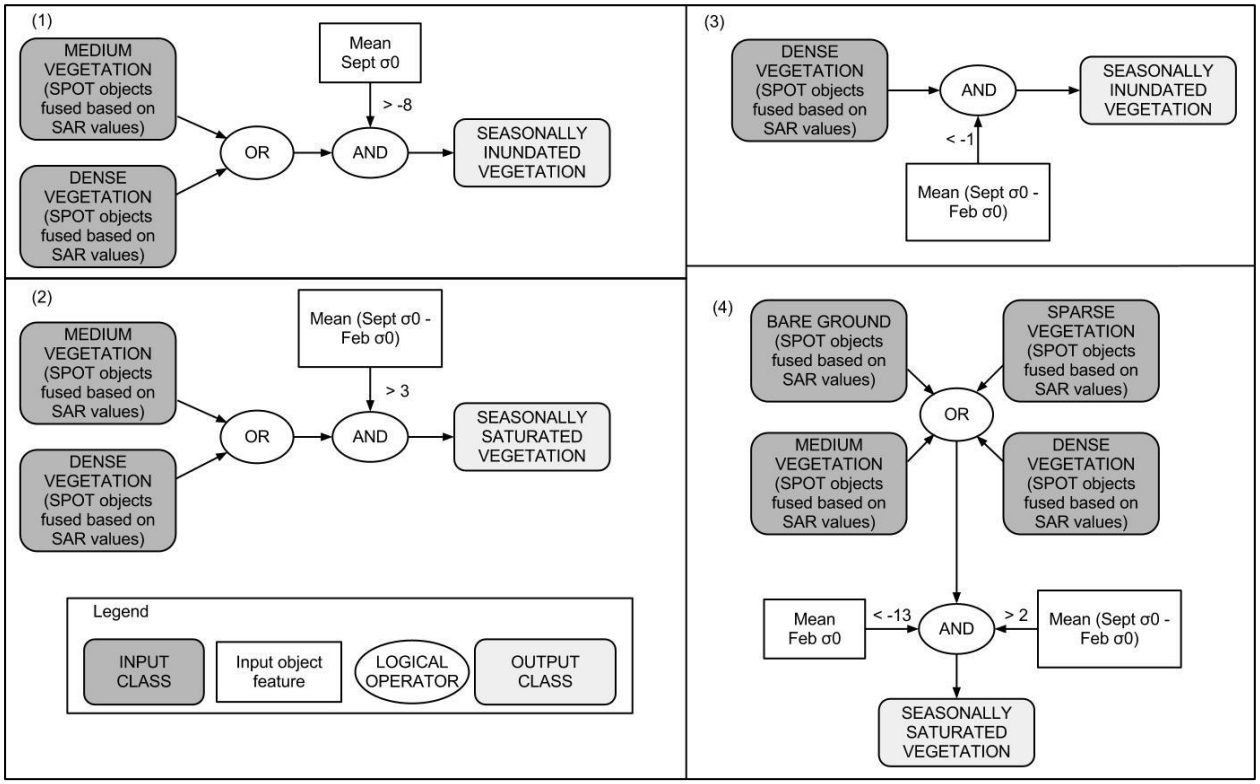

Figure A.18: SAR-based rules classifying vegetated wetland classes from SPOT-derived landcover classes (see Steps 2, 3 and 4 in Figure 4.11)